의학박사 학위논문

호흡기 상피세포의 상피-간엽 전이가 코 폴립 형성에 미치는 영향에 대한 연구

Study about the mesenchymal transition of upper airway epithelial cells in nasal polyp formation

2020년 2월

서울대학교 대학원

의과학과 약리학 전공

이 민 규

A thesis of the Degree of Doctor of Philosophy

Study about the mesenchymal transition of upper airway epithelial cells in nasal polyp formation

호흡기 상피세포의 상피-간엽 전이가 코 폴립 형성에 미치는 영향에 대한 연구

February 2020

The Department of Biomedical Science,

Seoul National University

College of Medicine

Pharmacology Major

Mingyu Lee

ABSTRACT

Nasal polyps (NPs) imply a refractory clinical course in chronic rhinosinusitis (CRS). Previous research showed that hypoxia-inducible factor (HIF)-1 could mediate nasal polypogenesis via epithelial-to-mesenchymal transition (EMT). Although several HIF-1 inhibitors were introduced for the treatment of hypoxia-related diseases, most were developed as anti-cancer drugs, and thus were cytotoxic. Sirtuin1 (SIRT1), a histone deacetylase, reportedly suppresses the transcriptional activity of HIF-1. Thus, I hypothesized that SIRT1 attenuates nasal polyposis by inhibiting HIF-1-induced EMT. SIRT1 transgenic (TG) mice had presented reduced mucosal lesions with epithelial disruption and fewer nasal polyps than wild-type (WT) mice. In addition, resveratrol (RSV), a polyphenolic SIRT1 activator, treatment suppressed nasal polypogenesis in WT mice; however, sirtinol (a SIRT1 inhibitor) administration increased the polyp burden in SIRT1 TG mice. In CRS sino-nasal specimens, SIRT1 was downregulated in the mucosa from patients with polyps as compared with patients without polyps. SIRT1 overexpression or activation reversed hypoxia-induced EMT in human nasal epithelial cells (hNECs). The intranasal transfection of a sh-SIRT1 lentiviral vector induced more nasal polypoid lesions in SIRT1 TG mice. Importantly, mucosal extracts from CRS without nasal polyps increased SIRT1 expression in nasal epithelial cells, and those from CRS with nasal polyps did not. RSV has been shown to effectively suppresses CRSwNP in a mouse model; however, when locally administered to the sino-nasal cavity, bolus RSV is limited by low drug bioavailability owing to its low aqueous solubility and relatively rapid clearance from the administration site. To address this limitation, I proposed muco-adhesive nanostructured micro-particles (PLGA/PEG NM) as a potential carrier for the sino-nasal delivery of RSV. PLGA/PEG NM released RSV in a sustained manner. Owing to the enlarged specific surface area of the nanostructures, PLGA/PEG NM had synergistically enhanced muco-adhesiveness and thus showed improved *in vivo* retention properties in the sino-nasal cavity. Therefore, RSV encapsulated with PLGA/PEG NM treatment mitigated nasal polyp formation and restored epithelial integrity better than the control treatments in a NP murine model. The therapeutic effect was

similar at half the dose of PLGA/PEG NM, suggesting improved local bioavailability of RSV in the sino-nasal cavity. Taken together, SIRT1 and RSV treatment efficiently suppressed nasal polyp formation, possibly due to inhibition of HIF-1-induced EMT, and thus indicating that SIRT1 may be a therapeutic target for nasal polyps. Therefore, RSV encapsulated with PLGA/PEG NM, potential material for delivering RSV, can be utilized for treating NPs.

KEYWORDS: SIRT1, HIF-1, resveratrol, nasal polyp, acetylation, epithelial-to-mesenchymal transition, PLGA/PEG NM, mucoadhesiveness, nanostructure, microparticle

STUDENT NUMBER: 2014-22013

Parts of these thesis were previously published in J Clin Immunol 2016; 137(1):87-98. e7 and Sci Reports 2017; 10;7:40249.

TABLE OF CONTENTS

ABSTRACT ····· **i**

TABLE OF CONTENTS ····· **iii**

LIST OF FIGURES AND TABLES ····· **v**

LIST OF ABBREVIATIONS ····· **viii**

GENERAL BACKGROUND ····· **1**

MATERIAL AND METHODS ····· **5**

CHAPTER

1. SIRT1 attenuates nasal polypogenesis by suppressing epithelial-to-mesenchymal transition ····· **18**

1.1 INTRODUCTION ····· **19**

1.2 RESULTS ····· **21**

1.2.1. Reduced polyp burden in SIRT1 TG mice ····· **21**

1.2.2. Reciprocal expression of SIRT1 and HIF-1α in chronic rhinosinusitis tissues ···· **21**

1.2.3. Effects of a SIRT1 activator and/or inhibitor on polyp formation in a murine NP model ····· **22**

1.2.4. SIRT1 attenuates HIF-1α activity via de-acetylation in nasal epithelial cells ····· **22**

1.2.5. Tissue-specific SIRT1 knockdown restores polyp formation in SIRT1 TG mice ·· **23**

1.2.6. SIRT1 expression is enhanced by mucosal extracts from CRS patients, but not by

extracts from NPs ····· 23

1.3 DISCUSSION ····· 45

2. Sinonasal Delivery of Resveratrol via Mucoadhesive Nanostructured Micro-particles in a Nasal Polyp Mouse Model ····· 49

2.1 INTRODUCTION ····· 50

2.2 RESULTS ····· 52

2.2.1. Micro-particle characterization ····· 52

2.2.2. *In vitro* release profile of RSV ····· 52

2.2.3. *In vivo* sino-nasal retention properties ····· 53

2.2.4. *In vivo* effects on nasal polyps and epithelial disruptions ····· 55

2.2.5. *In vivo* evaluation of inflammatory surrogates ····· 55

2.2.6. *In vivo* efficacy on E-cadherin restoration ····· 56

2.2.7. Biocompatibility evaluation ····· 57

2.3 DISCUSSION ····· 76

REFERENCES ····· 78

ABSTRACT IN KOREAN ····· 100

LIST OF FIGURES AND TABLES

Chapter 1

Figure 1. Establishment of the SIRT1 transgenic mouse. ·····25

Figure 2. Polyp burden is reduced in sirtuin (SIRT)1 transgenic (TG) mice. ·····26

Figure 3. Immuno-histochemical staining of SIRT1, HIF-1α and E-cadherin in Control-UP, CRSsNP-UP, CRSwNP-UP, and NP tissues. ·····27

Figure 4. Reciprocal expression of SIRT1 and hypoxia-inducible factor (HIF)-1α in chronic rhinosinusitis with or without nasal polyps. ·····28

Figure 5. Schematic illustration of nasal polyp murine model. ·····29

Figure 6. Effect of a SIRT1 activator or inhibitor on polyp formation in mice. ·····30

Figure 7. SIRT1 suppresses hypoxia-induced epithelial-to-mesenchymal transition (EMT).·····32

Figure 8. Effect of different inflammatory cytokines on SIRT1 and HIF-1α expression in nasal epithelial cells. ·····33

Figure 9. The effect of resveratrol on HIF-1α–induced EMT. ·····34

Figure 10. Resveratrol suppresses hypoxia-induced epithelial-to-mesenchymal transition (EMT) by de-acetylating HIF-1α.·····35

Figure 11. Effect of SIRT1 on HIF-1α de-acetylation. ·····36

Figure 12. Tissue-specific knockdown of SIRT1 restores polyp formation in SIRT1 TG mice.·····37

Figure 13. Tissue-specific knockdown of SIRT1 restores the number of epithelial disruptions and polyp formation in SIRT1 TG mice. ·····38

Figure 14. Increased expression of SIRT1 in nasal epithelial cells treated with mucosal extracts from CRSsNP, but not those from CRSwNP. ·····39

Figure 15. Attenuation of HIF-1α activity by the treatment of mucosal extracts from CRSsNP, but not those from CRSwNP. ·····40

Figure 16. Comparison of SIRT1, HIF-1α, and E-cadherin (E-Cad) expression between ENPs and NENPs of patients with CRS. ·····41

Figure 17. Schematic illustration of the role of SIRT1 in chronic rhinosinusitis with nasal polyps. ··42

Table 1. Patient cahracteristics and methodologies used ····· 43

Table 2. List of antibodies used in this project ·····44

Chapter 2

Figure 18. Representative scanning electron micrographs. ·····59

Figure 19. Size distribution profiles of PLGA/PEG MS (blue) and PLGA/PEG NM (red). ·····60

Figure 20. Powder X-ray diffraction (PXRD) patterns of intact PLGA, intact PEG, intact RSV and RSV loaded PLGA/PEG NM. ·····61

Figure 21. *In vitro* release profiles of RSV from the micro-particles. ·····62

Figure 22. *In vitro* release profiles of RSV from the PLGA/PEG NM obtained with pH 5.5 simulated nasal electrolyte solution containing 1% w/v Tween 20. ·····63

Figure 23. *In vivo* sino-nasal retention profiles of micro-particles. ·····64

Figure 24. *In vivo* effects on nasal polyps and epithelial disruption. ·····66

Figure 25. *In vivo* evaluation of inflammatory markers. ·····67

Figure 26. Representative photographs of sino-nasal tissues. ·····68

Figure 27. *In vivo* efficacy of attenuating HIF-1α activity. ·····70

Figure 28. Evaluation of cytotoxicity of RSV, RSV-loaded PLGA/PEG NM and blank PLGA/PEG NM in cells. ·····71

Figure 29. Evaluation of the biocompatibility of RSV-loaded PLGA/PEG NM. ·····72

Table 3. Properties of the DTTCI-loaded micro-particles used in this work ····· 73

Table 4. Properties of the RSV-loaded micro-particles used in this work ····· 74

Table 5. Half-lives of micro-particles administered to the sino-nasal cavity ····· 75

LIST OF ABBREVIATIONS

CRSwNP: Chronic rhinosinusitis with nasal polyps

CRSsNP: Chronic rhinosinusitis without nasal polyps

DTTCI: Diethylthiatricarbocyanine iodide

ERK: extracellular signal-regulated kinase

ENP: Eosinophilic nasal polyps

EMT: Epithelial-to-mesenchymal transition

HIF: Hypoxia-inducible factor

HPF: High power field

H-NMR: H-nuclear magnetic resonance

hNEC: human nasal epithelial cell

IHC: Immunohistochemistry

IVIS: *In vivo* imaging system

IFN-γ: Interferon gamma

MS: Microsphere

MP: Microparticle

MT: Masson's Trichrome

MAPK: Mitogen-activated protein kinase

NF-κB: Nuclear factor κB

NENP: Non-eosinophilic nasal polyps

NM: Nano-structured microparticle

OVA: Ovalbumin

PDK1: Pyruvate dehydrogenase lipoamide kinase isozyme 1

PLGA: poly lactic-co-glycolic acid

PEG: polyethylene glycol

PXRD: Powder X-ray diffraction

PAS: Periodic Acid-Schiff

RSV: Resveratrol

SIRT1: Sirtuin 1

SEB: Staphylococcus aureus enterotoxin B

TG: transgenic

TGF-β: Transforming growth factor β

UP: Uncinate process

GENERAL BACKGROUND

Chronic rhinosinusitis (CRS) is a heterogeneous disease characterized by inflammation of the paranasal sinuses and nose, and is clinically associated with two or more symptoms, one of which always includes either nasal discharge or nasal obstruction/blockage persisting for more than 12 weeks without complete resolution.[1] Other accompanying symptoms can include sinus pressure/pain and/or decreased sense of smell.[2] The prevalence of CRS ranges from 7% in south Korea to 14% in north America (10.9% of the EU adult population, 14% in the North American population, and 7% in South Korea), causing decreased life quality, attenuated productivity, and lost time at work, consequently leading to more than a million annual surgical interventions worldwide.[3-5] CRS is commonly divided into two clinical phenotypes: CRS without nasal polyps (CRSsNP) and CRS with nasal polyps (CRSwNP), based on nasal endoscopy.[1, 6, 7] CRSsNP is two to three times more prevalent than CRSwNP, and is less likely to be managed by surgical dissection.[8] Although CRSwNP is less common, its patients are relatively recalcitrant to medical treatment and usually continue treatment for a longer period, and usually recurred in nasal mucosa after endoscopic sinus surgery (ESS).[9, 10] In addition, CRSwNP has high management costs and is frequently associated with the morbidity of asthma.[11-13] Therefore, identifying the factors and underlying mechanisms that drive the development of nasal polyps (NPs) may have significant clinical implications.

Some of the histo-morphological features of NPs include the accumulation of inflammatory cells in sub-epithelial regions, frequent epithelial loss or disruptions, basement membrane thickening, glandular cell hyperplasia, and edematous stroma.[14, 15] Based on the presence of tissue eosinophilia, CRS with or without NP may also be divided into eosinophilic (E-NP) and non-eosinophilic (NE-NP) subtypes.[16-18] However, the criteria for distinguishing between E-NP and NE-NP have been controversial. Eosinophilic CRS with or without NPs has been previously diagnosed using tissue eosinophil count per high-power field (HPF), with variable minimum thresholds for diagnosis reported including five [19, 20], ten [21, 22], twenty [23], and even more than one hundred eosinophils [24, 25] per HPF. The

percentage of eosinophils in tissue-infiltrated inflammatory cells has also been used for diagnosis with reported thresholds of 5% [26], 10% [18], or 15% [27]. Additionally, if more than 20 neutrophils per HPF are detected, a high-neutrophil group is designated.[28] E-NP is more prevalent in the west compared to other regions and typically linked to T2 inflammatory disease. Patients typically present with pronounced eosinophilia and high levels of T2 cytokines such as interleukin (IL)-4, IL-5, and IL-13.[9, 29, 30] However, the tissue eosinophilia in CRS patients shows notable geographic and ethnic predisposition.[31-33] NP patients in Asia including China, Japan, and Korea typically present with a mixed inflammatory pattern (Th1/Th2/Th17) linked to neutrophils rather than to potent eosinophilia infiltration.[18, 34]

Epithelial dysfunction and innate/adaptive inflammatory response are potential pathogenesis of CRS, and can be further sub-divided depending on the underlying mechanisms.[9, 35, 36] One such mechanism and prominent feature of CRSwNP is epithelial remodeling induced by epithelial dysfunction, that is a dynamic procedure involving a structural reorganization of tissues.[37] Emerging evidence shows that airway epithelium may participate in airway remodeling following an environmental challenge through the epithelial-to-mesenchymal transition (EMT) process.[38, 39] EMT is a reversible process in which epithelial cells lose their properties (such as cell polarity and cell-to-cell adhesion) and undergo multiple biochemical changes and trans-differentiation into mesenchymal cells.[40, 41] During EMT, epithelial cells lose their plasma membrane proteins or junctions (e.g. E-cadherin and occludin), reorganize their cytoskeleton and reprogram their gene expression, that can increase cell motility. This leads to excessive cell proliferation and remodeling of the sino-nasal epithelium.[42] Actually, epithelial cells from NP patients have been reported to show a mesenchymal phenotype and epithelial hyperplasia.[43, 44] Previous research showed that hypoxia-inducible factor 1 (HIF-1) contributes to NP formation through the EMT process.[45] In addition, the vascular endothelial growth factor (VEGF) which has been known to HIF-1α-regulated protein is responsible for epithelial hyperplastic growth and mucosal edema in NPs. HIF-1α inhibitors have been effectively suppressed VEGF induction.[46] This was possible because various types of inflammatory cells and their products

promote inflammatory status in the sino-nasal cavity leading to HIF-1α expression via hypoxia-independent mechanisms.[47, 48] As a result, HIF-1α can be viewed as a therapeutic target in the development of NPs. Several HIF-1 inhibitors have already been used for the treatment of hypoxia-related diseases, whereas most HIF-1 targeting drugs have been established as anti-cancer drugs due to their cytotoxicity. [49, 50] Because CRSwNP disease is not associated with the mortality of patients, application of these potent HIF-1 modulating drugs could potentially have safety-related implications.

Sirtuin (Sir2) is a highly conserved class-III histone deacetylase, first identified in yeast, Drosophila and *Caenorhabditis elegans*.[51] Siruin consumes one molecule of nicotinamide adenine dinucleotide (NAD^+) during each deacetylation cycle to regulate lifespan in lower organisms[31] and is involved in a broad range of physiological functions such as inflammation, metabolism, and aging.[52, 53] There are seven reported sirtuin homologs of which SIRT1-7, and SIRT1 are the closest paralogues of Sir2.[54] SIRT1, the most studied sirtuin, not only deacetylates histones to affect gene expression via epigenetic mechanisms but also deacetylates specific transcription factors and enzymes to control the aging process and suppress inflammation.[55] The anti-aging functions of Sir2 are particularly highly conserved.[56, 57] SIRT1 deacetylates a continuously growing list of key histone residues as well as diverse non-histone transcription factors as substrates. The list comprises of histone H3 lysine 9 (H3-K9), H4-K16, and H1-K26, p53 (tumor suppressor protein), members of the FoxO family (forkhead box factors regulated by insulin/Akt), HES1 (hairy and enhancer of split 1), HEY2 (hairy/enhancer-of-split related with YRPW motif 2), PPARγ (peroxisome proliferator-activated receptor gamma), CTIP2 [chicken ovalbumin upstream promoter transcription factor (COUPTF)- interacting protein 2], p300, PGC-1α (PPARγ coactivator), and NF-κB (nuclear factor kappa B).[52, 58, 59] Above all, SIRT1 has been reported to fine-tune cellular responses to hypoxia by deacetylating HIF-1α and HIF-2α.[60] HIF-1α transcriptional activity is attenuated due to the p300 separation from the C-terminal transactivation domain (CAD) of HIF-1α because of SIRT1-mediated deacetylation.[60, 61] Most importantly, there is a diverse range of readily available drugs and/or chemicals that can stimulate or block the activity of

SIRT1.[62] It is therefore a plausible hypothesis that regulation of HIF-1α activity by using SIRT1 targeting drugs can be useful to reduce HIF-1α-mediated NP formation.

Trans-resveratrol (*trans*-RSV), a naturally occurring phytoalexin highly abundant in the peels of red grapes and blueberries, has received great attention for its anti-carcinogenic, anti-inflammatory and anti-oxidant properties.[63-65] RSV functions as an activator of SIRT1—one of the main forms of Sir2 family[66] —and therefore is speculated to have benefits against diseases caused by abnormal metabolic control, cell cycle defects, and inflammation.[67] RSV has therefore attracted attention from the pharmaceutical, cosmetic, and food industries, having also been shown to have chemo-preventive and chemo-therapeutic effects on multiple types of cancers and NP, hence making it a promising anti-NP agent.[68, 69] Several reports indicate that although RSV efficiently reduces the NP count in mouse models, it has limited bioavailability when locally administered to the nasal spaces in solutions or suspensions.[68, 70, 71] In vivo application of RSV to the nasal cavity is limited due to its low bioavailability as a consequence of its low aqueous solubility, limited stability, and susceptibility to rapid clearance from the nasal cavity.[72] Repeated intranasal treatments are often needed to achieve a therapeutic effect for a sustained period.

Micro-particles composed of poly(lactic-co-glycolic acid) (PLGA) and polyethylene glycol (PEG) allow the sustained delivery of RSV[73, 74] and improve muco-adhesion to nasal epithelium respectively.[75, 76] For PLGA/PEG micro-particles fabricated in nano-structured surfaces[77], the carrier has potential to provide an enlarged specific surface area, thus leading to synergistic enhancement of residence time in the nasal cavity. Utilizing RSV-loaded PLGA/PEG micro-particles could therefore allow better adhesion to the mucous layer on the nasal epithelium, thus sustaining the delivery of RSV, enhancing its bioavailability, and yielding a high potential for resolving refractory clinical problems.

Thus, I attempted to elucidate the effects of SIRT1 and RSV in terms of nasal polyposis, and speculated that these might be a therapeutic target for the treatment of nasal polyps via blocking HIF-1-induced tissue remodeling.

MATERIALS AND METHODS

1. Human Subjects

The diagnosis of CRS with or without nasal polyps (NPs) was based on history, nasal endoscopy, clinical examination and radiographic criteria.[1] NPs were confirmed by nasal endoscopic findings and signs of persistent bilateral and diffuse paranasal sinus mucosal thickening in computed tomographic (CT) scans. Endoscopic sinus surgery was performed when patient's symptoms and radiographic findings did not resolve at least 6 weeks after patients were treated with antibiotics, topical corticosteroids, decongestants, and/or mucolytic agents. Antibiotics and topical steroids were discontinued two weeks prior to surgery. No patients took oral corticosteroids at the time of their surgery. Patients with acute infection were excluded in this study. The patients with deviated nasal septum (DNS) were considered as the control group. Demographic findings of patients are summarized in Table 1. Mucosal extracts from patients with DNS only, CRSsNP and CRSwNP were isolated and used for in vitro studies. NPs were classified as eosinophilic ones when percent eosinophils among all immune cells in tissues exceeded 10 %, which was chosen as the cutoff in previous report.[18]

2. Culture of epithelial cell lines

Normal human nasal epithelial cells (hNECs) were purchased from PromoCell (Heidelberg, Germany). The RPMI2650 cell line, which originated from upper airway epithelial cell, was obtained from the Korean Cell Line Bank (Seoul, South Korea). hNECs were cultured in airway epithelial cell growth media from PromoCell (Heidelberg, Germany). RPMI 2650 cells were cultured in RPMI 1640 media supplemented with 10 % heat inactivated fetal bovine serum, 100 units/ml of penicillin, and 100

μg/ml of streptomycin, respectively. hNECs were used for analysis within five passages after purchase. All cells were grown in 5% CO_2/20% O_2 (normoxic) or in 5% CO_2/1% O_2 (hypoxic).

3. Immunoblotting and Immunoprecipitation

Proteins were separated on SDS-polyacrylamide gels (8-12%), and transferred to Immobilon-P membranes (Millipore, MA, USA). Membranes were incubated sequentially with primary antibodies. The antibodies used in this study were summarized in Table 2. Membranes were incubated with HRP-conjugated secondary antibodies (1:5000) for 1 hour at room temperature, and visualized by ECL Plus or ECL Select detection reagents (GE Healthcare, CA, USA). Immunoblotting for β-tubulin served as a protein loading control. For immunoprecipitation, cell lysates were incubated sequentially with 1 μg of antibodies and 20 μl protein A/G sepharose beads for 4 hours at 4℃ (Santa Cruz). Then, immuno-precipitates were eluted with a sample buffer (1% SDS, 100mM DTT, 50mM Tris, pH 7.5), and then subjected to immunoblotting.

4. Plasmid DNA and shRNA lentiviral vector transfection

Cells at 60% confluence were transfected with Myc-His-SIRT1 plasmid using lipofectamine 2000 reagent (Invitrogen, CA, USA) or siRNAs using RNAi-MAX reagent (Invitrogen, CA, USA). The Myc-His-SIRT1 plasmid was kindly given by Dr. Junjie Chen (University of Texas). For gene silencing, the pLKO.1-puro vector was purchased from Sigma-Aldrich and oligonucleotides targeting the green fluorescent protein (control small hairpin RNA) or SIRT1 were inserted into the vector using AgeI and EcoRI restriction enzymes. For SIRT1, Two oligos, 5'-CCGGAAGTACAAACTTCTAGGAATGCTCGAGCATTCCTAGAAGTTTGTACTTTTTTT-3' and 5'-AATTAAAAAAAGTACAAACTTCTAGGAATGCTCGAGCATTCCTAGAAGTTTGTACTT-3' were annealed and ligated into pLKO.1-puro vector to generate sh-SIRT1 RNA according to the

manufacturer's instructions. The construct was confirmed by sequencing. The viral vector was co-transfected with pMD2-VSVG, pRSV-RRE, and pMDLg/pRRE helper DNA into HEK293T cells, and the viral supernatant was collected.

5. Immunohistochemistry

SIRT1, HIF-1α, Ki-67 and E-cadherin were immuno-stained in paraffin sections (4 μm) of sino-nasal tissues. Sino-nasal tissues were fixed in 4% PFA at 4℃ for 24 hours, and then in ethanol and sequentially xylene before embedding them in paraffin. Paraffin sections (4 μm) of sino-nasal tissues were mounted on slide glasses and dried at room temperature for 24 hours. The sections were rehydrated, and autoclaved at 121℃ for 10 minutes in 100 mM citrate buffer (pH 6.0; Dako, CA, USA) to retrieve antigens. After treated with 3% hydrogen peroxide which diluted in methanol for 10 minutes, the sections were incubated in 2% bovine serum at room temperatures for 1 hours to block nonspecific signals. They were incubated with antibodies which were delineated in Table 2. Biotinylated secondary antibodies (Vector laboratories, CA, USA) were used for staining HIF-1α (1:200), SIRT1 (1:200), E-cadherin (1:500), Ki-67 (1:500). The immune complexes were visualized using the Vectastatin ABC kit (Vector Laboratories, CA, USA). Negative controls were performed using IgG isotype antibodies (eBioscience, CA, USA). All immune-stained sections were lightly counterstained with Mayer's hematoxylin (Sigma Aldrich, Mo, USA). The slides were evaluated with a bright-field microscope (BX-51; Olympus, Tokyo, Japan) equipped with a camera (DP70; Olympus, Tokyo, Japan) and a micrograph field of view of the entire stained section. To score the expression levels of E-cadherin, I observed 3 separated high-power fields (HPFs) per slide. Detailed method was described previously.[45] Shortly, three different spots were randomly selected in every HPFs, and two independent examiners blinded to the experimental group determined whether E-cadherin was expressed in each spot or not. In case that >30 of E-cadherin positive epithelial cells exist continuously, the area was defined as a positive spot.

The final score of each sample is presented as the average of scores from three HPFs. If the examiners had a disagreement, a consensus was reached by reviewing the specimen at a multi-head microscope by our research team. Then, the expression level was presented as the mean values of positive spots per HPFs. When it comes to the expression of HIF-1α, and SIRT1, the numbers of HIF-1α or SIRT1-positive cells were counted in at least 3 different high-power fields (x400) and presented as mean values of them.

6. Generation of SIRT1 transgenic mice

Transgenic mice overexpressing human SIRT1 were produced by using modified pcDNA3.1 vector containing the myc-tagged SIRT1 with the ubiquitously expressed CMV promoter. Purified transgenic construct DNA was micro-injected into the fertilized eggs collected from the superovulated C57BL/6 females. Genotyping was performed by PCR analysis of genomic DNAs obtained from the tails of founder mice at 3 weeks of age and protein expression was confirmed by immunoblotting with anti-SIRT1 and anti-His (Figure 1). Each different founder was bred in the hemizygous state, and transgenic and non-transgenic littermates were assigned into pair-matched groups for all experiments. Mice were fed a normal condition in the Institute for Experimental Animals of Seoul National University College of Medicine under specific pathogen-free conditions.

7. A murine nasal polyp model

C57BL/6J mice (5 weeks old) were purchased from Central Laboratory Animal (Seoul, South Korea), and kept in specific pathogen-free rooms. SIRT1 transgenic mice were established using Myc-His tagged SIRT1 plasmid with a CMV promoter. Detailed information was described in Figure 1. All experimental protocols complied with the Guidelines of the National Institute of Health and the Declaration of Helsinki, and were approved by the Committee on the Use and Care of Animals. A

murine NP model was generated from allergic rhiniosinusitis model, in mice with minor modification, as described previously.[71] Briefly, mice were immunized with an intraperitoneal injection of 25 μg of ovalbumin (OVA; Sigma Aldrich, Mo, USA) in 2 mg of aluminum hydroxide gel on days 0 and 5, followed by a daily intranasal instillation from days 12-19 with 6% OVA diluted in PBS. Thereafter, prolonged continuous inflammation was maintained in the experimental mice by the subsequent nasal exposure of mice to 6% OVA three times a week for 12 consecutive weeks. In addition to 6% OVA, all groups of mice were challenged three times a week with 10 ng of Staphylococcus aureus enterotoxin B (SEB; List Biological laboratories, CA, USA) from the 8th week through the 14th week after OVA instillation. The control groups were designated as follows: instillation with phosphate buffered saline (PBS) only (negative control); and instillation with 6% OVA (ovalbumin) + 10 ng of SEB (staphylococcus enterotoxin B) + vehicle (nasal polyp control). The experimental groups were designated as follows: instillation with 6% OVA + SEB + chemicals (1 μg of resveratrol or sirtinol) or lentiviral vectors (sh-tGFP or sh-SIRT1) (see corresponding figures for detailed schedule, Figure 2, 5 and 12). For the sino-nasal delivery of RSV, I utilized the animal nasal polyp model using 4-week old BALB/c mice from Central Laboratory Animal (Seoul, South Korea), according to a slightly modified version of the protocol reported in previous study.[71] In this work, I prepared a total of 34 animals and divided them into 6 distinct groups, A – F, according to the type of treatment. Group A consisted of animals without nasal polyps (i.e., no administration of OVA or SEB). I prepared 5 different treatment formulations: PBS vehicle without RSV, a bolus RSV solution, and 3 distinct suspensions of PLGA/PEG NM in PBS. The formulations were intra-nasally administered 1 day after the OVA and SEB administration, which were scheduled 3 times per week. At each administration, 20 μl of the same formulation was applied to both nostrils; hence, a total of 40 μl was administered to each mouse. The 6 animal groups and treatment formulations were as follows:

(Group A) PBS; n = 3; RSV dose = 0;

(Group B) PBS; n = 7; RSV dose = 0;

(Group C) RSV solution; n = 6; RSV dose = 0.44 μg per nostril;

(Group D) RSV-loaded PLGA/PEG NM; n = 7; RSV dose = 0.44 μg per nostril;

(Group E) Half dose of RSV-loaded PLGA/PEG NM; n = 5; RSV dose = 0.22 μg per nostril;

(Group F) Blank PLGA/PEG NM; n = 6, RSV dose = 0.

To prepare the RSV solution for Group C, 10 μg of RSV was dissolved in 1 μl of DMSO and was then added to 450 μl of PBS (pH 7.4). To prepare the micro-particle suspensions for Groups D and E, 0.83 mg of PLGA/PEG NM with and without RSV were suspended in 40 μl of PBS at pH 7.4 and containing 0.02% w/v Tween 80 as a dispersing agent. For Group E, a half portion (0.415 mg) of PLGA/PEG NM loaded with RSV was suspended in 40 μl of PBS.

8. Histologic analysis of animal study

The mice were euthanized and decapitated. The tissue specimens were fixed in 4% paraformaldehyde at 4℃ for 1 day and decalcified in 5% nitric acid at 4℃ for 3 days. The specimens were excised from the second palatal ridge to the first upper molar teeth. The tissue was dehydrated and processed according to standard paraffin-embedding procedures. The tissue was cut in coronal sections with a thickness of 4 μm. The tissues were stained with hematoxylin and eosin (H&E), Sirius red, Giemsa, Masson's trichrome and PAS to assess overall inflammation, eosinophils, mast cells, collagen deposition and goblet cell hyperplasia, respectively. An atlas of normal murine sino-nasal anatomy was used to standardize the anatomic locations being examined. Three coronal sections that were similar to the sinus cavity were chosen for evaluation. The sections were examined under a light microscope (x400, HPF; BX-51; Olympus, Tokyo, Japan) equipped with a camera (DP70, Olympus, Tokyo, Japan) by 2 independent examiners who were blinded to the experimental groups; the examiners determined the numbers of inflammatory cells, secretory cells, sub-epithelial collagen thickness, nasal polyp numbers

and epithelial disruptions. I defined a polypoid lesion as a distinct mucosal elevation with eosinophilic infiltration and micro-cavities following previous report.[45, 71] Epithelial disruptions were only counted if the pieces of epithelium were more than 50 μm in length and were stripped off of the epithelial regions or split from adjacent epithelial cells. I reviewed three consecutive slides to rule out processing errors and confirm mucosal lesions. Polyp formation and epithelial disruption were counted microscopically from three coronal sections, and expressed as a total number. Inflammatory cells, secretory cells, and sub-epithelial collagen thickness were counted or measured in mucosal samples in 10 high-power fields (HPFs). The numbers of inflammatory and secretory cells were expressed as cells per HPF. Sub-epithelial collagen thickness was quantified using ImageJ software (National Institutes of Health, MD, USA). In case of disagreement (the 2 counts differ by >10%), a consensus was reached by reviewing the specimen at a multi-head microscope by our research team.

9. ELISA for mouse IgE and OVA-specific IgE

Blood was collected via cardiac puncture and was then centrifuged at 1,300 RCF for 20 min. The obtained sera were stored at –70℃ until measurement. Mice serum levels of IgE and OVA-specific IgE were quantified using the LEGEND MAX ELISA kit from Biolegend (CA, USA) and the LEGEND MAX™ ELISA kit provided by Biolegend (CA, USA) according to the manufacturer's instructions respectively. Each assay was performed in triplicate.

10. Human tissue extracts

Freshly obtained tissue specimens were weighed, and all of the tissue volumes are determined equally 110 μl. 1 mL of PBS supplemented with 0.05% Tween 20 (Sigma-Aldrich, Mo, USA) and 1 % protease inhibitor cocktails (P8340; Sigma-Aldrich, Mo, USA) was added for each tissues. The tissue was then homogenized with a Bullet Blender Blue (Next Advance; Averill Park, NY, USA) at setting 7

for 8 minutes at 48℃. After homogenization, the suspension was centrifuged at 4000 rpm for 20 minutes at 48℃, and the supernatants were stored at -70℃ until analysis. The total protein concentrations in each of the extracts were measured using Bradford assay. Then, I used the extract at the adequate protein concentration (20 μg/ml).

11. Materials

Poly (lactic-co-glycolic acid) (PLGA; glycolic acid:lactic acid = 1:1, i. v. = 0.43 dl/g) and polyethylene glycol (PEG; MW = 6 kDa) were provided by Evonik Industries (Essen, Germany) and Acros Organics (NJ, USA), respectively. Resveratrol (RSV), polyvinyl alcohol (PVA; 87–89% hydrolyzed; MW = 31–50 kDa), Mucin from porcine stomach (Type III), Calcium chloride dehydrate, Tween 20, Tween 80, Type III Mucin, and dimethyl sulfoxide (DMSO) were obtained from Sigma-Aldrich (Mo, USA) and diethylthiatricarbocyanine iodide (DTTCI) was purchased from Alfa Aesar (MA, USA). Dimethylformamide (DMF), dichloromethane (DCM), and tetrahydrofuran (THF) were obtained from Mallinckrodt (MO, USA), J. T. Baker (NJ, USA), and Daejung (Seoul, South Korea), respectively. Potassium phosphate monobasic (KH_2PO_4), sodium hydroxide pellets (NaOH), Sodium Chloride (NaCl), and Potassium chloride (KCl) were purchased from Daejung (Seoul, South Korea), and acetonitrile (ACN) was obtained from J.T. Baker (NJ, USA). Phosphate buffered saline (pH 7.4) was obtained from the Seoul National University Biomedical Research Institute. Ovalbumin (OVA, grade V; Sigma-Aldrich, Mo, USA) were used to sensitize and challenge experimental mice. Staphylococcus aureus enterotoxin B (SEB; List Biological laboratories, CA, USA) was used to induce nasal polyp in sino-nasal cavity.

12. Micro-particle preparation

Four distinct types of micro-particles, namely PLGA MS, PLGA/PEG MS, PLGA NM and PLGA/PEG NM, were prepared according to a previously reported protocol with slight modifications.[77, 78] The micro-particles were loaded with a drug, RSV, to examine their efficacy as sino-nasal drug delivery carriers. Alternatively, a fluorescent dye, DTTCI, was loaded to evaluate the *in vivo* retention of micro-particles in the sino-nasal cavity. To prepare the spherical micro-particles, i.e., PLGA MS or PLGA/PEG MS, 1,000 mg of PLGA or a blend of 1,000 mg of PLGA and 250 mg of PEG was dissolved in 10 ml of dichloromethane (DCM), respectively, into which 3 mg of resveratrol (RSV) or 10 mg of diethylthiatricarbocyanine iodide (DTTCI) was dissolved. The prepared polymer solution was then added to 50 ml of a polyvinyl alcohol (PVA) solution (1% w/v) and agitated vigorously at 1,000 rpm for 2 min for emulsification. The resulting emulsion was added to 50 ml of a PVA solution (1% w/v), which was then stirred at 200 rpm for 30 min under vacuum (-12.5 psi) for solvent evaporation. A 100 μm-pore metallic mesh (C8.20047; Seoul, South Korea) was used to filter the resulting micro-particles, which were then thoroughly washed with deionized (DI) water and freeze-dried.

To prepare nanostructured micro-particles, i.e., PLGA NM or PLGA/PEG NM, 1,000 mg of PLGA or a mixture of 1,000 mg of PLGA and 100 mg of PEG, respectively, were dissolved in 3.35 ml of a solvent mixture of DCM, tetrahydrofuran (THF) and dimethylformamide (DMF) (3:1:1, v/v/v) in which either 1 mg of RSV or 8.5 mg of DTTCI had been dissolved. The solution was then electro-spun for 1 h under the following conditions (Nano NC, Seoul, South Korea): applied voltage, 20 kV; tip-to-collector distance, 10 cm; collector rotation speed, 100 rpm; needle gauge, 26 G; and flow rate, 2.0 $ml \cdot h^{-1}$. The resulting nano-fibrous sheets were then freeze-milled at -196℃ for 30 min (6770 Freezer Mill, Spex, Metuchen, NJ, USA) and then filtered through a 100 μm-pore metallic mesh.

13. HPLC measurement

The RSV concentration was measured with high-performance liquid chromatography (HPLC; Agilent 1260 series; Agilent Technologies, CA, USA) using a Diamonsil C18 column (150 × 4.6 mm,

5 μm pore; Dikma Technologies, CA, USA). A mobile phase was prepared by mixing 20 mM phosphate-buffered saline (pH 2.5) and acetonitrile (60:40, v/v). The flow rate and injection volume were 1 ml/min and 30 μl, respectively. The column temperature was maintained at 37 °C, and UV absorbance was measured at 333 nm.

14. Micro-particle characterization

The micro-particles were imaged under a scanning electron microscope (SEM; 7401F, JEOL, Japan). The size distribution of micro-particles was assessed using a Coulter counter (Multisizer 4; Beckman Coulter, CA, USA), and at least 10,000 micro-particles were counted for each sample type. The amount of PEG that was present in micro-particles was determined using a proton ^{1}H - nuclear magnetic resonance (^{1}H NMR) spectrometer (Bruker spectra spin 500 MHz; Leipzig, Germany).[77, 78] The specific surface areas of the micro-particles were measured using a surface area and porosity analyzer (TriStar II 3020; Micromeritics, GA, USA).[77, 78] Approximately 5–10 mg of micro-particles was completely dissolved in DMF, and a spectrophotometer (UV-1800; Shimadzu, Japan) was used at 770 nm or 340 nm to measure the amounts of loaded DTTCI or RSV, respectively. The *in vitro* drug release experiments were performed with RSV-loaded micro-particles in 1.5 ml of PBS (pH 7.4) or simulated nasal electrolyte solution (SNES, pH 5.5) containing 1% w/v Tween 20 at 37℃. At scheduled times, the release medium was collected and assessed via high-performance liquid chromatography (HPLC; Agilent 1260 series, Agilent Technologies, CA, USA).

An in vitro assay was performed to evaluate the muco-adhesiveness of PLGA NM and PLGA/PEG NM. For this, either 8 mg PLGA NM or PLGA/PEG NM was suspended in 2 ml of 1 mg/ml mucin solution (mucin from porcine stomach, Type III), which was incubated at 37°C for 30 min. After centrifugation at 10,000 × g for 10 min, the amount of free mucin left in the supernatant was measured spectrophotometrically using the periodic acid/Schiff staining method,[79] and the amount of measured mucin was subtracted from the original amount of mucin in order to calculate the amount of mucin

absorbed to micro-particles.

15. Evaluation of cytotoxicity

The cytotoxicity of the RSV solution, the RSV-loaded PLGA/PEG NM and the blank PLGA/PEG NM was evaluated with RPMI 2650 (nasal septum-derived squamous cell carcinoma) and hNECs (human nasal epithelial cells) using a methyl thiazolyl tetrazolium (MTT) viability assay. The cells were seeded in 96-well culture plates at a density of $1x10^4$ cells per well in 200 μl of culture medium. The RPMI 2650 cells were cultured in RPMI 1640 medium supplemented with 10% FBS, 100 units/ml of penicillin and 100 μg/ml streptomycin. The hNECs were cultured in airway epithelial cell growth medium from PromoCell (Heidelberg, Germany). The cells were grown at 37°C in a 5% CO_2 humidified environment. After 12 h, the culture medium from each well was completely removed, and then 160 μl of fresh culture medium and 40 μl of the test medium was added. I employed 4 distinct testing media, namely RSV solution (0.88 μg RSV), RSV-loaded PLGA/PEG NM suspension (0.83 mg particles), blank PLGA/PEG NM suspension (0.83 mg particles) and a mixture of DMSO and PBS (1:450, v/v) (i.e., PBS+DMSO vehicle without RSV or PLGA/PEG NM). For explore concentration dependent experiments, I prepared 2.4 μg RSV (50 μM) for RSV solution, RSV-loaded PLGA/PEG NM suspension (2.26 mg particles), blank PLGA/PEG NM suspension (2.26 mg particles) and 4.8 μg RSV (100 μM) for RSV solution, RSV-loaded PLGA/PEG NM suspension (4.5 mg particles), blank PLGA/PEG NM suspension (4.5 mg particles). The RSV solution was prepared by dissolving 10 μg of RSV in a solution consisting of 1 μl of DMSO and 450 μl of PBS containing 0.02% v/v Tween 80. The micro-particle suspensions were prepared in PBS containing 0.02% v/v Tween 80. After 12, 24, 36 and 48 h of incubation, the cells were washed twice and incubated in fresh culture medium mixed with MTT (1 mg/ml) for 3 h at 37°C. Finally, the MTT solution was removed, and the cells were re-suspended in 100 μl of 2-propanol to lyse the cells and completely dissolve the dye. The absorbance was measured

at a wavelength of 570 nm using a Vmax microplate reader (Molecular Devices, MD, USA). Triplicate experiments were conducted for each test medium and time. The cell viability was expressed as a percentage of the control (measured at 0 h).

16. In vivo sino-nasal retention of micro-particles

This protocol complied with the NIH *Guide for "The Care and Use of Laboratory Animals".* Male BALB/c nude mice (4 weeks old, Orient Bio, Seongnam, South Korea) were used to assess the *in vivo* sino-nasal retention of the micro-particles. The mice were housed in standard cages in a well-controlled environment (temperature, 22℃ ± 2℃; humidity, 50% ± 10%, ventilation, 12–18 times/h) with free access to food and water.

For this experiment, I used suspensions of DTTCI-loaded micro-particles, which were sino-nasally administered.[80] To prepare the suspensions, 1 mg of DTTCI-loaded micro-particles were added to 40 μl of pH 7.4 PBS containing Tween 80 (0.02% v/v) as a dispersing agent, thus yielding a 25 mg/ml micro-particle suspension. For each of the micro-particle types, 20 μl of suspension was administered into each of the 2 nasal cavities in each mouse (i.e., a total of 40 μl for each mouse)[71, 81]. Immediately after administration, the mouse was placed under anesthesia using isoflurane and the whole head of each mouse was imaged using an IVIS (Caliper Life Sciences, CA, USA) equipped with indocyanine green filters (excitation, 748–789 nm; emission, 814–851 nm) under the following conditions: exposure time, 1 s; binning factor, medium; f-stop, 4; and field of view, 10 × 10 cm. The intensity of the fluorescence signal from the nasal cavity at each time point was measured in the selected region of interest and was normalized to the maximum intensity (obtained at 2 h after administration). For each micro-particle type, 3 animals were tested for statistical analysis.

17. Statistical analyses

The mean fraction of micro-particles remaining in the sinonasal cavity was analyzed using analysis of variance (ANOVA) with $\alpha = 0.05$, where pairwise comparisons were made using Tukey's post hoc test. For the other statistical analyses, Mann-Whitney *U* with 2-tailed test for unpaired comparisons, Wilcoxon signed rank test, Pearson's correlation test and linear regression were performed using IBM SPSS 21 (SPSS, Inc., Chicago, IL). Figures were generated with GraphPad Prism software 6.0 (GraphPad Software Inc., La Jolla, CA). Pearson's correlations were used to determine variable relationships. If not normally distributed, Spearman's correlation coefficient was selected. All statistical tests were two-sided, and significance was considered when *P* is <0.05.

18. Study approval

All human subjects studied were enrolled after providing written informed consent under the internal review board of SNUH Boramae Medical Center–approved protocol (IRB No. 06-2012-109). Animal experiments were performed under an animal protocol approved by the Institutional Animal Care and Use Committee (IACUC) of the Biomedical Research Institute at the Seoul National University hospital (13-0277-C3A2) and Seoul National University (SNU-120313-10-1 and SNU-150311-1).

Chapter 1

SIRT1 attenuates nasal polypogenesis by suppressing epithelial-to-mesenchymal transition

1.1 INTRODUCTION

Chronic rhinosinusitis (CRS) is characterized by chronic inflammation of the nasal and paranasal sinus mucosa, and is related to mucosal alterations ranging from inflammatory thickening to nasal polyp formation.[82, 83] CRS is frequently divided into two groups based on the absence or presence of nasal polyps (NPs): CRS with nasal polyps (CRSwNP) and CRS without nasal polyps (CRSsNP).[84] Histo-morphological features of nasal polyps include: the sub-epithelial accumulation of inflammatory cells with a prominent rate of eosinophils, frequent epithelial damage, and a thickened basement membrane.[14] The formation of NPs, which is associated with T helper cell (T_H)2-skewed inflammation, particularly in Western countries, implies a greater burden of illness with refractory clinical features.[85, 86] However, the mechanisms underlying mucosal remodeling and polyp formation in patients with CRSwNP are unclear.

A hypoxic environment affects mucosal inflammation and epithelial remodeling, and promotes the development of nasal polyps.[45, 46, 87] A previous research reported that hypoxia-inducible factor (HIF)-1 mediated nasal polypogenesis by inducing epithelial-to-mesenchymal transition (EMT), and suggested that HIF-1α be viewed as a therapeutic target for nasal polyposis.[45] HIF-1 expression and stabilization in cells can be triggered by hypoxic stress, but also by other factors related to pathological stress such as inflammation and infectious microorganisms.[48] Actually, HIF-1 induction has also been presented in non-hypoxic conditions (e.g. rheumatoid arthritis and diabetes).[88, 89] Several stimuli that promote HIF-1 expression in normoxic conditions are known to activate transcription factor such as NF-kB.[90] Considering that CRS with or without NPs were associated with bacteria, fungi and various type of inflammatory cytokines[9], these may lead to the HIF-1 stabilization via hypoxia-independent mechanisms, and thus finally contribute to nasal polyp formation.

In addition, hypoxia-induced vascular endothelial growth factor (VEGF) production contributed to mucosal edema in nasal polyps; HIF-1α inhibitors effectively suppressed VEGF secretion.[46] It was

also suggested that HIF-1α regulated VEGF to perpetuate the hyperplastic epithelial growth observed in CRSwNP.[43] Although several HIF-1 inhibitors were introduced for the treatment of hypoxia-related diseases, most were developed as anti-cancer drugs, and thus were cytotoxic.[49] Given that CRSwNP is not life threatening, application of these potent HIF-1 modulating drugs could lead to safety issues.

Sirtuin (Sir2), which is reportedly involved in gene silencing and lifespan extension, was originally identified in yeast and *Drosophila.*[91] SIRT1 reportedly fine-tuned cellular responses to hypoxia by de-acetylating HIF-1α and HIF-2α.[60] Among the seven known mammalian Sir2 homologs (SIRT 1–7), SIRT1 is considered to be the prototypical sirtuin because it is most homologous to Sir2.[92] SIRT1 functions to remove the acetyl group from acetylated lysine residues in both histones and non-histone proteins. As a consequence of SIRT1-mediated de-acetylation, HIF-1α transcriptional activity is suppressed due to p300 dissociation from the C-terminal transactivation domain (CAD) of HIF-1α.[60, 61] In addition, diverse drugs and/or chemicals activate or inhibit the activity of SIRT1 and are readily available.[93] Thus, I speculated that SIRT1 might be a therapeutic target for the treatment of nasal polyposis by inhibiting HIF-1-induced tissue remodeling.

1.2 RESULTS

1.2.1. Reduced polyp burden in SIRT1 TG mice

I firstly investigated the effect of SIRT1 overexpression on nasal polyp formation using a previously established murine nasal polyp model.[71] As shown in Figure 2A, C57BL/6 wild type (WT) and SIRT1 transgenic (TG) mice were treated with ovalbumin (OVA) and *Staphylococcus aureus* enterotoxin B (SEB) to induce nasal polyp formation (see Methods for a detailed explanation). Interestingly, OVA and SEB treatment did not induce any marked mucosal changes in TG mice, but led to prominent polypoid lesions in WT mice (Figure 2B). Mucosal polyp number in the nasal cavities and epithelium disruptions were significantly reduced in SIRT1 TG mice compared to WT mice (Figures 2C and 2D).

1.2.2. Reciprocal expression of SIRT1 and HIF-1α in chronic rhinosinusitis tissues.

I previously found that HIF-1α-induced epithelial (E)-cadherin loss in NP epithelial cells.[45] To verify the relationship between SIRT1 and HIF-1α, both proteins were analyzed using immunohistochemistry. In uncinate process (UP) specimens from patients with deviated nasal septa (Control) or CRSsNP, marked E-cadherin-positive staining was observed in the mucosal epithelia, whereas HIF-1α was weakly detected. However, E-cadherin expression was downregulated and nuclear HIF-1α expression was upregulated in both UP and NP tissues harvested from CRSwNP patients (Figure 3 and Figures 4B, 4C). More SIRT1-positive nuclei were detected in CRSsNP-UP than in Control-UP; SIRT1-positive nuclei were markedly reduced in CRSwNP-NP (Figure 3 and Figure 4A). Further, nuclear SIRT1 levels were positively correlated with E-cadherin expression (Figure 4D). These findings imply that SIRT1 and HIF-1α were reciprocally expressed, and that SIRT1 could contribute to the repression of HIF-1α-mediated E-cadherin loss.

1.2.3. Effects of a SIRT1 activator or inhibitor on polyp formation in a murine model.

I next evaluated the effects of SIRT1 on polypogenesis in WT and SIRT1 TG mice via intranasal treatment with a SIRT1 activator (resveratrol) and inhibitor (sirtinol), respectively. All mice were treated with OVA and SEB to induce nasal polyps according to a previously described protocol. Additionally, 1 μg of each drug was instilled three times per week from beginning on day 47 until the end of the experiment, as shown in Figure 5. Resveratrol instillation in WT mice significantly suppressed polyp formation (Figure 6A), and also reduced the number of mucosal goblet cells (Figure 6B). On the contrary, sirtinol intranasal treatment in SIRT1 TG mice increased polyp formation (Figure 6A) and the number of goblet cells (Figure 6B). Total immunoglobulin (Ig)E levels were decreased following resveratrol treatment in WT mice, and elevated by sirtinol administration in SIRT1 TG mice (Figure 6C). Thus, polypoid changes induced by OVA and SEB in mice were affected by intranasal treatment with SIRT1 modulators.

1.2.4. SIRT1 attenuates HIF-1α activity via de-acetylation in nasal epithelial cells.

I then investigated the molecular mechanism underlying the suppressive effect of SIRT1 on polypogenesis *in vitro*. When cultured under hypoxic conditions (1% O_2), human nasal epithelial RPMI 2650 cells underwent EMT, as evidenced by a decrease in epithelial markers (E-cadherin and β-catenin) and an increase in mesenchymal markers (alpha smooth muscle actin [α-SMA] and vimentin) and known EMT-inducing factors (TWIST, ZEB and SNAIL) (Figure 7A). SIRT1 overexpression reversed this hypoxia-induced EMT in RPMI 2650 cells (Figure 7A). Similarly, resveratrol, a SIRT1 activator, inhibited hypoxia-induced EMT in both RPMI 2650 cells and hNECs (Figure 7B). In addition, hNEC cellular morphology was restored following resveratrol treatment (Figure 7C). Previously, HIF-1α could mediate hypoxic EMT in human nasal epithelial cells.[45] Interestingly, HIF-1α and its well-known

downstream target, pyruvate dehydrogenase lipoamide kinase isozyme 1 (PDK1), were suppressed by SIRT1 upregulation (Figures 7A and 7B). Therefore, I questioned whether HIF-1α could be inhibited by SIRT1 activation in hypoxia-independent condition. When HIF-1α was upregulated by the direct transfection or the interferon (IFN)-γ treatment (Figures 8 A-C), resveratrol could downregulate HIF-1α and EMT in RPMI 2650 cells (Figure 9). Considering that SIRT1 inhibited HIF-1α via its de-acetylation,[60] I examined the influence of SIRT1 activity on HIF-1 acetylation in RPMI 2650 cells. Using a previously developed antibody against K674-acetylated HIF-1α,[61] I confirmed that HIF-1α acetylation was diminished by activating SIRT1 both in normoxic and hypoxic conditions (Figures 10A, B and Figures 11A, B). These data suggested that SIRT1 could inhibit HIF-1α-treated EMT in human nasal epithelial cells by suppressing HIF-1α expression and transcriptional activity.

1.2.5. Tissue-specific SIRT1 knockdown restores polyp formation in SIRT1 TG mice

To avoid the effects of whole body SIRT1 expression in TG mice, I manipulated SIRT1 in a tissue-specific manner using lentiviral vectors in murine polyp model (Figure 12A). As expected, SIRT1 TG mice bore less inflammatory mucosal changes than WT mice, but the intranasal administration of sh-SIRT1 lentiviral vectors in SIRT1 TG mice restored distinct mucosal inflammation with multiple polypoid lesions (Figure 12B). The change in SIRT1 expression was confirmed by performing immunohistochemistry against SIRT1 (Figure 12C). The number of epithelial disruptions and nasal polyps was also reversed by the nasal mucosa-specific knockdown of SIRT1 in TG mice (Figures 13A and 13B).

1.2.6. SIRT1 expression is enhanced by mucosal extracts from CRS patients, but not by extracts from NPs

Finally, I examined the effect of mucosal extracts from CRS patients with or without NPs on SIRT1 expression in nasal epithelial cells. As SIRT1 was highly expressed in epithelium from CRS patients and lost in NPs (Figure 3 and Figure 4A), I hypothesized that features of the mucosal environmental could differentially affect the epithelial SIRT1 level, possibly contributing to hypoxia-induced EMT and epithelial remodeling, such as polyp formation. The detailed protocol and concentrations used were described in the Methods section. First, RPMI 2650 cells were treated with different mucosal extracts, and then SIRT1 expression was measured (Figure 14A). Surprisingly, the CRSsNP mucosal extract treatment upregulated the SIRT1 level, but the NP extract treatment did not. Furthermore, the non-eosinophilic nasal polyp (NENP) mucosal extract suppressed the SIRT1 level, contrary to the eosinophilic nasal polyp (ENP) extract (Figure 14A). Next, I determined if this extract-induced SIRT1 expression could modulate HIF-1 expression and function in primary human nasal epithelial cells (Figure 14B). Under hypoxic incubation conditions, CRSsNP mucosal extract treatment enhanced the SIRT1 level, which suppressed the expression of HIF-1α and PDK1. On the contrary, the NP extract-treated cells had a much lower SIRT1 level than CRSsNP-treated cells. Specifically, cells treated with NENP extract had a minimal detectable SIRT1 level and prominent HIF-1α and PDK1 expression. Interestingly, the levels of SIRT1 and HIF-1α were negatively correlated. In fact, hypoxic incubation with CRSsNP extract did not induce any mesenchymal morphology in hNECs, compared to the other types of extract-treated cells with EMT features (Figure 14C). Finally, I measured the transcriptional activity of HIF-1α with Epo-luciferase reporter plasmids in RPMI 2650 cells under normoxic or hypoxic conditions following treatment with diverse tissue extracts. Similar to HIF-1α and PDK1 expression, luciferase activity was lower in the CRSsNP extract condition than in control mucosa or in NP extract treatment groups (Figure 15A, left). Mutated Epo-luciferase activity was not significantly different among the conditions (Figure 15B, right). Taken together, my findings suggest that the inflammatory milieu of CRSsNP induces SIRT1, a suppressor of HIF-1α-mediated epithelial remodeling, but that the NP mucosal environment is not conducive to SIRT1 induction.

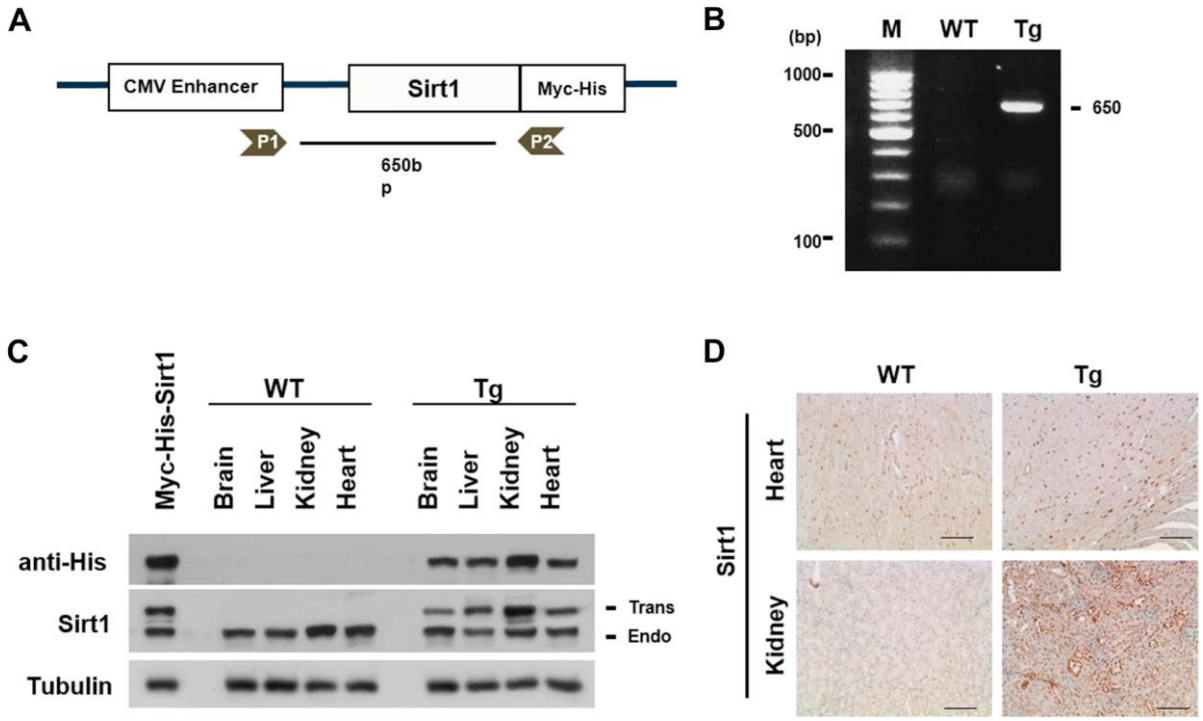

Figure 1. Establishment of the SIRT1 transgenic mouse. (A) Structure of the Myc/His-tagged SIRT1 expression vector introduced into transgenic mice. Gene expression was driven under the control of a cytomegalovirus (CMV) promoter. **(B)** The presence of the SIRT1 vector in transgenic mouse was verified by using PCR. **(C)** Expression of endogenous SIRT1 (Endo) and transgenic Myc/His-tagged SIRT1 (transgenic [Tg]) in WT and SIRT1 transgenic mice. Tissue homogenates were prepared from the brain, liver, kidney and heart and analyzed by means of immunoblotting with anti-His and anti-SIRT1 antibodies. **(D)** Paraffin sections of hearts (top panel) and kidneys (bottom panel) from WT and SIRT1 transgenic mice were subjected to immuno-histochemical analyses with anti-SIRT1 antibody. Scale bars, 100 μm.

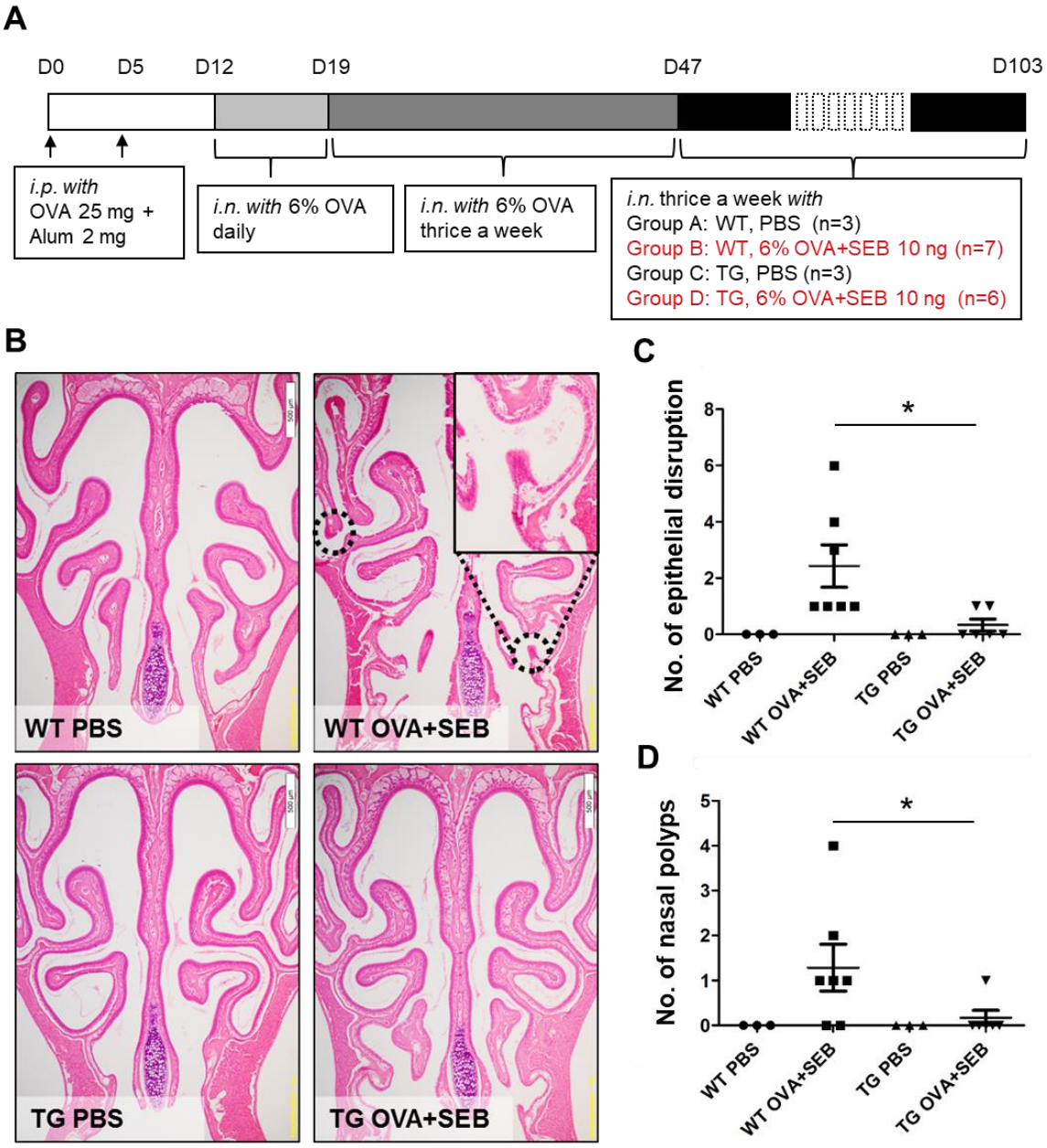

Figure 2. Polyp burden is reduced in sirtuin (SIRT)1 transgenic (TG) mice. (A) Protocol for the murine nasal polyp (NP) model. Wild-type (WT) and SIRT1 TG mice were treated with ovalbumin (OVA) and *Staphylococcus aureus* enterotoxin B (SEB). *i.p.*, intraperitoneal; *i.n.*, intranasal. **(B)** Photographs of representative sinonasal spaces and polypoid lesions stained with hematoxylin and eosin (H&E). The criteria for NP are described in the Methods section, and dotted circles indicate polypoid lesions. **(C, D)** Numbers of epithelial disruptions and polyps were expressed as a total number per a coronal section. * denote $P < 0.05$, the Mann-Whitney U-test was used.

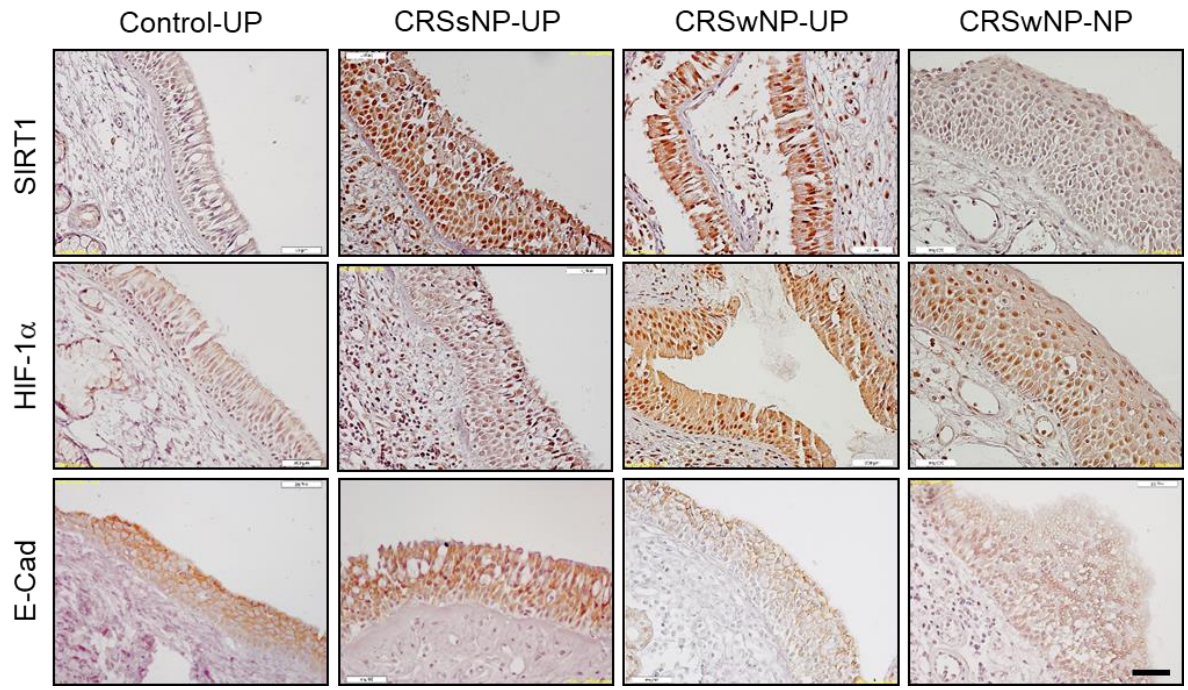

Figure 3. Immuno-histochemical staining of SIRT1, HIF-1α and E-cadherin in Control-UP, CRSsNP-UP, CRSwNP-UP, and NP tissues. Control uncinate process (UP) mucosa from patients without nasal disease, UPs from patients with chronic rhinosinusitis without polyps (CRSsNP), and both UP and NP tissues from chronic rhinosinusitis with nasal polyps (CRSwNP) were immuno-stained with SIRT1, HIF-1α and epithelial (E)-cadherin (E-Cad) antibodies. Scale bar represents 100 μm.

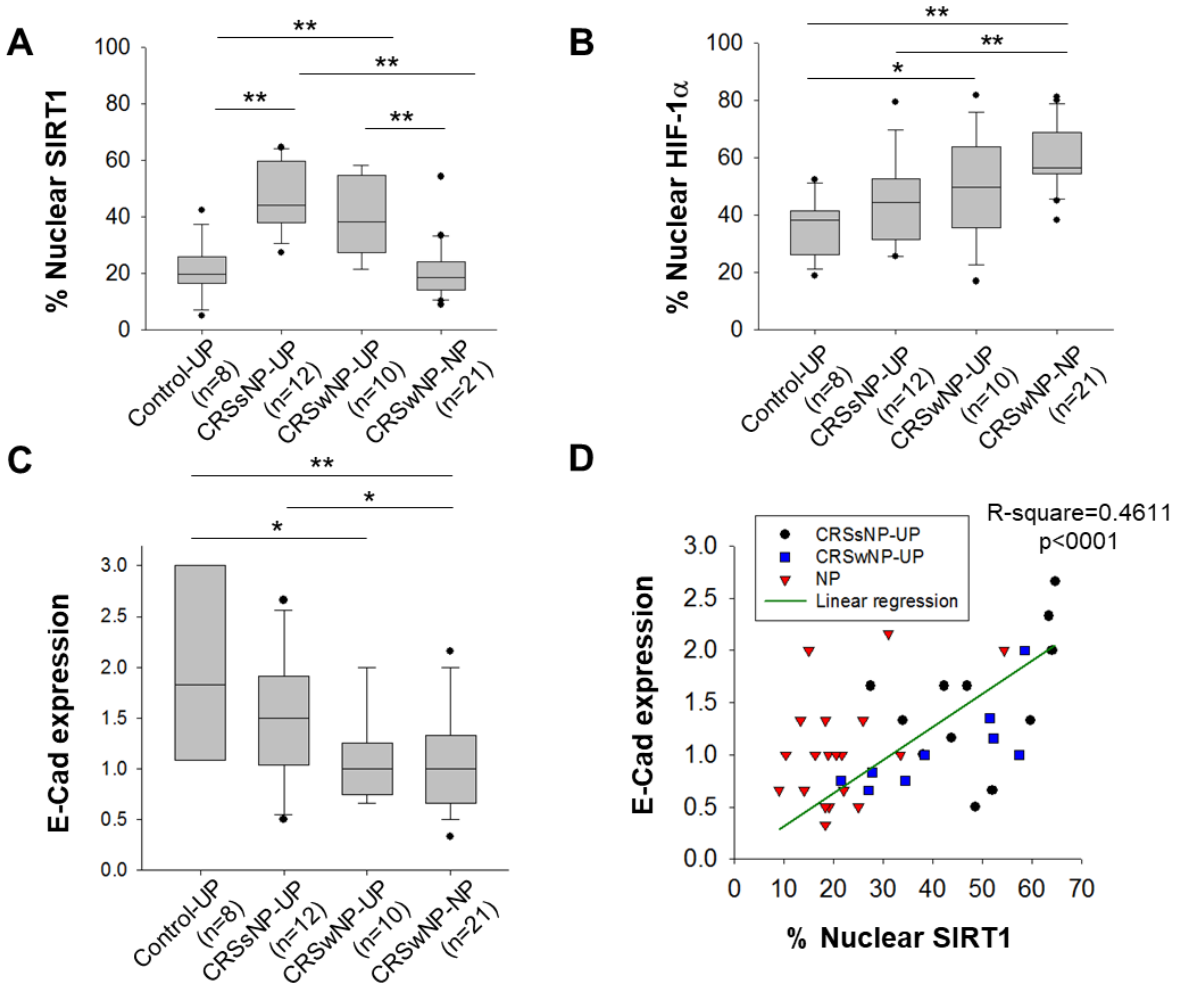

Figure 4. Reciprocal expression of SIRT1 and hypoxia-inducible factor (HIF)-1α in chronic rhinosinusitis with or without nasal polyps. (A-C) Comparison of nuclear HIF-1α, SIRT1, and E-cadherin expression in Control-UP, CRSsNP-UP, CRSwNP-UP, and NP. The detailed criteria for scoring are described in the repository Methods section. * and ** denote $P < 0.05$ and $P < 0.01$, respectively, as determined using the Mann–Whitney U-test. **(D)** Relationship between nuclear SIRT1 and E-cadherin expression. The Pearson correlation test was used, and R-square represents the coefficient of determination.

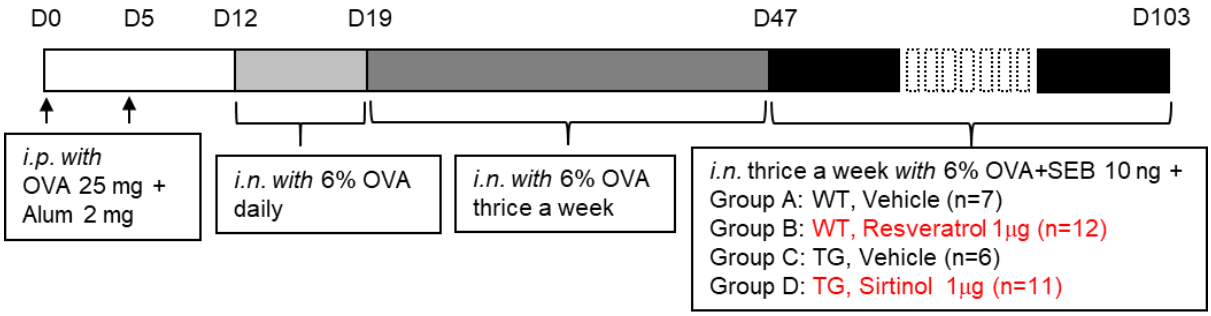

Figure 5. Schematic illustration of nasal polyp murine model. Protocol for the murine nasal polyp model. *i.p.*, intraperitoneal; *i.n.*, intranasal.

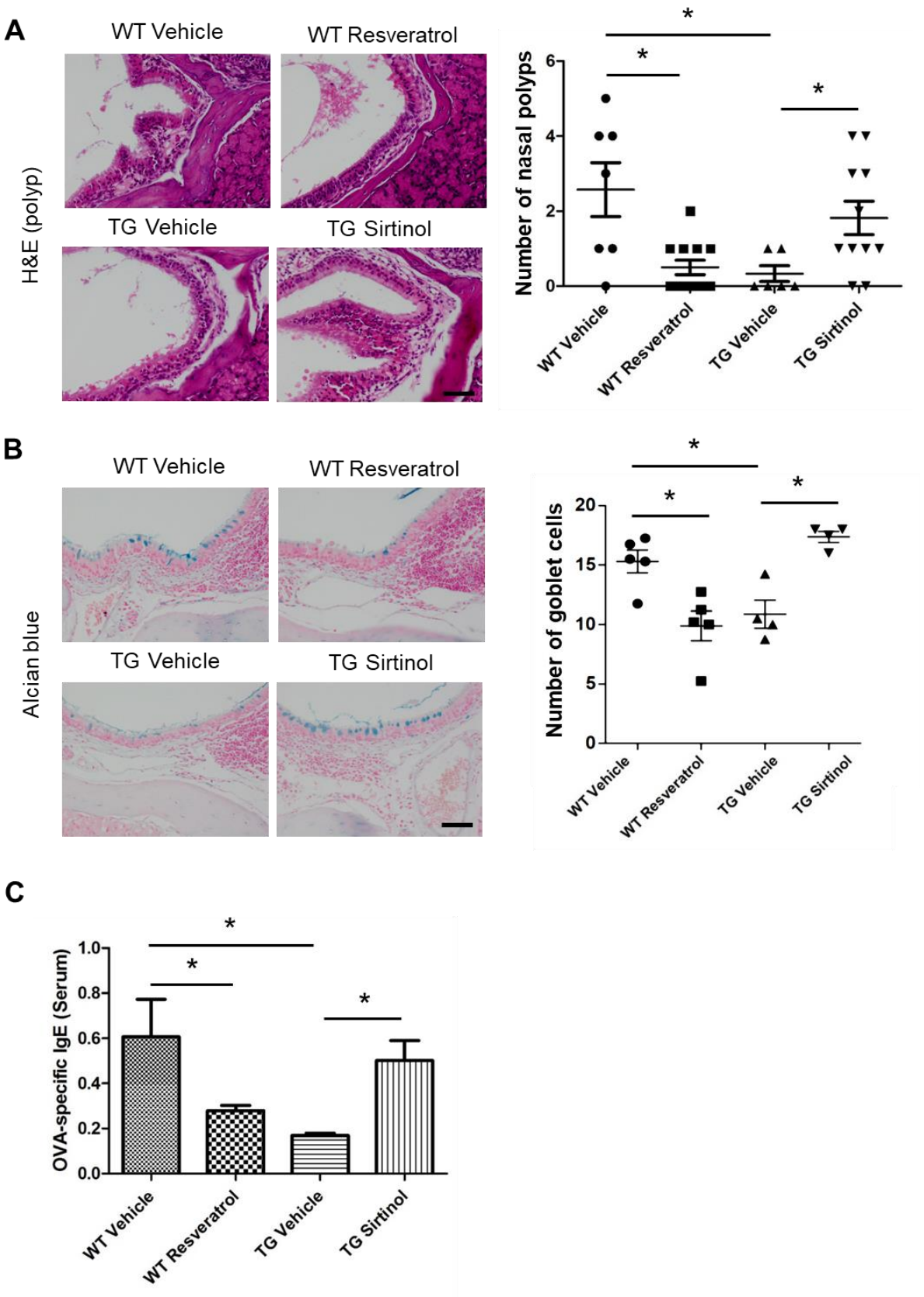

Figure 6. Effect of a SIRT1 activator or inhibitor on polyp formation in mice. (A) Representative

photographs and numbers of polypoid lesions stained with H&E. NP criteria are described in the Methods section. **(B)** Representative photographs and numbers of goblet cells stained with alcian blue. **(C)** OVA-specific immunoglobulin (Ig)E levels in mouse serum. * denotes $P < 0.05$ as determined using the Mann–Whitney U-test. Scale bar represents 50 μm.

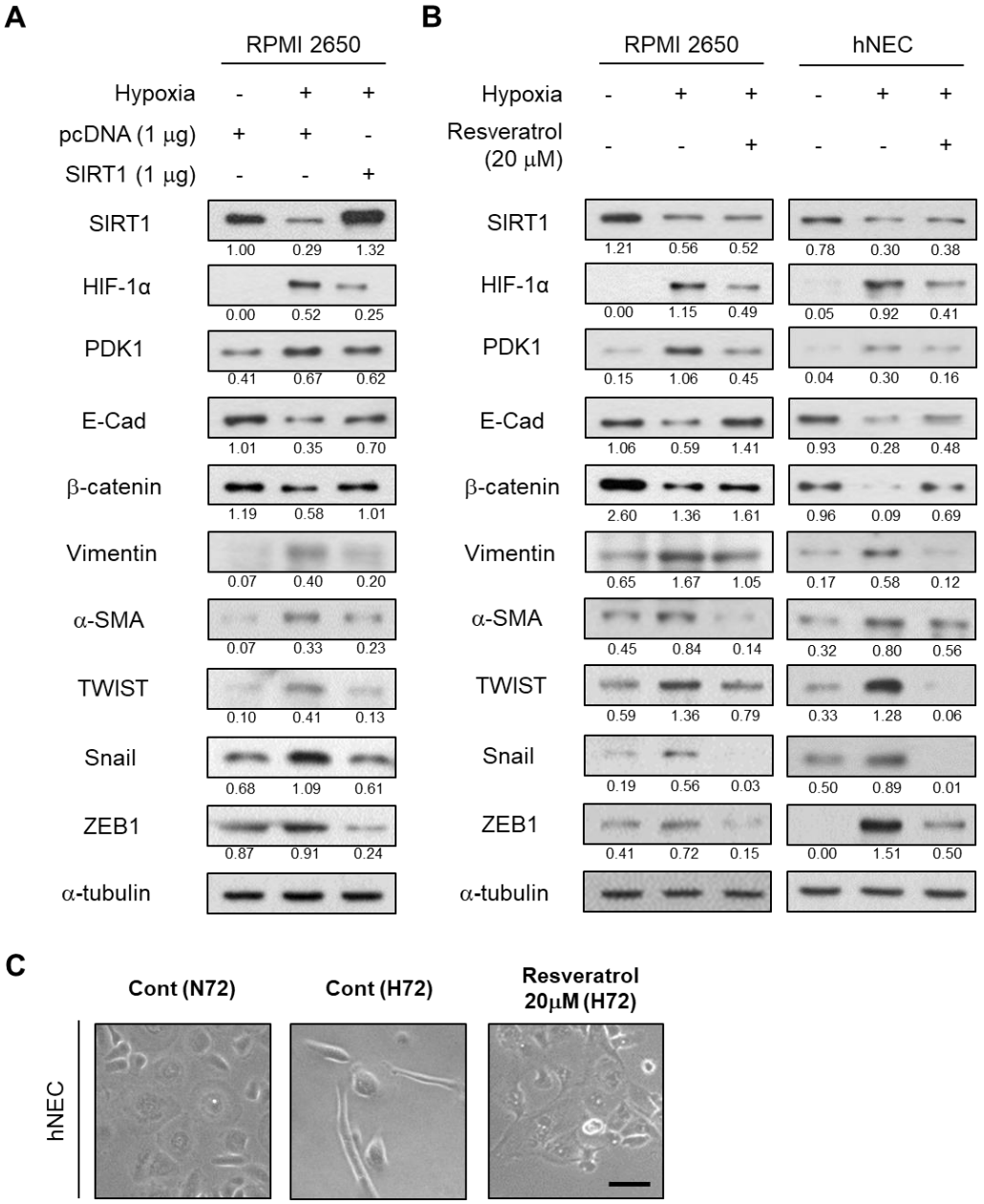

Figure 7. SIRT1 suppresses hypoxia-induced epithelial-to-mesenchymal transition (EMT). (A) RPMI 2650 cells were transfected with 1 μg of pcDNA or SIRT1 plasmid and incubated under normoxic (N) or hypoxic (H) conditions for 72 h. EMT markers were immunoblotted. The intensity values of bands were normalized by α-tubulin expression. **(B, C)** RPMI 2650 and hNECs were treated with resveratrol or vehicle, and incubated under N or H conditions for 72 h. EMT markers were immunoblotted**,** and phase-contrast images of human nasal epithelial cells (hNECs) were acquired. Scale bar represents 100 μm.

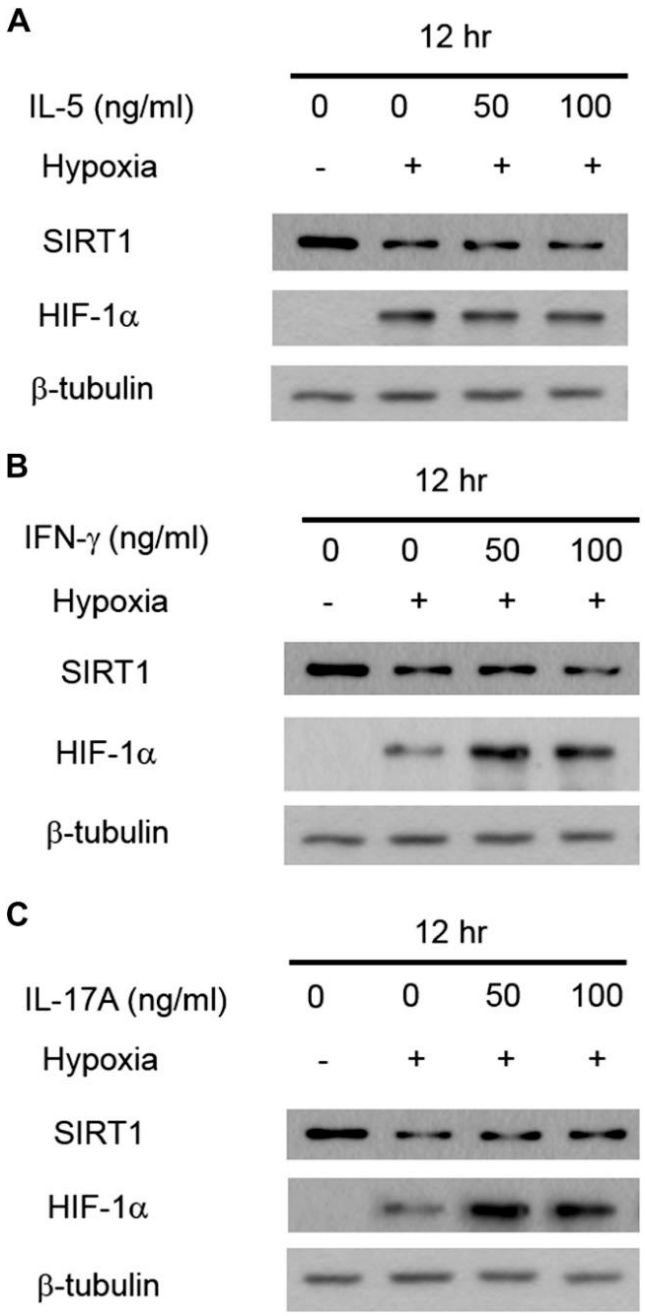

Figure 8. Effect of different inflammatory cytokines on SIRT1 and HIF-1α expression in nasal epithelial cells. RPMI 2650 cells were cultured under normoxic or hypoxic conditions for 12 hours with the indicated cytokines: **A,** IL-5; **B,** IFN-γ; and **C,** IL-17A. Cell lysates were prepared for immunoblotting with the indicated antibodies.

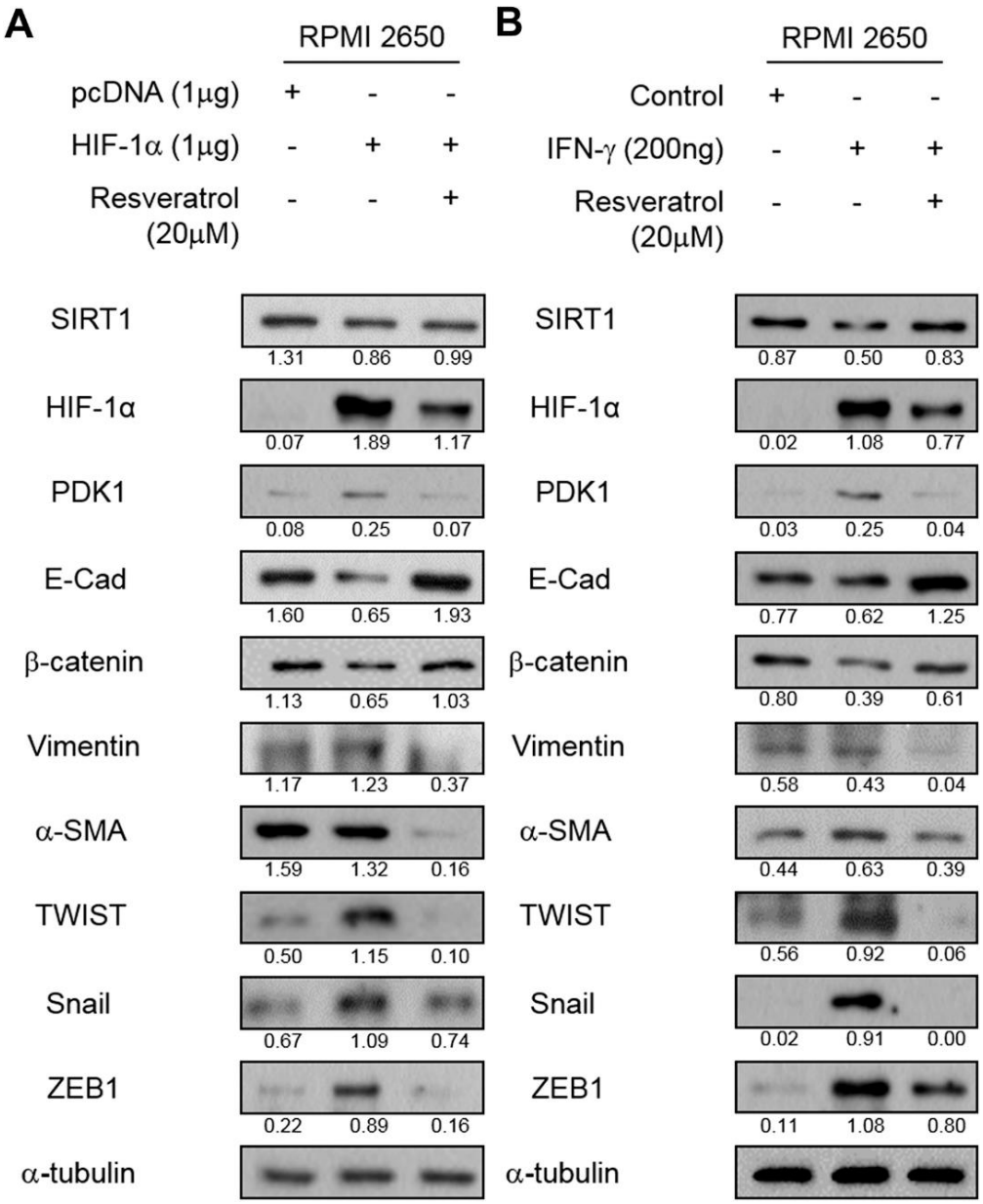

Figure 9. The effect of resveratrol on HIF-1α–induced EMT. (A) HIF-1α was induced by the transfection of HIF-1α plasmid in RPMI2650 cells, and EMT-related markers were traced after resveratrol treatment. **(B)** IFN-γ was treated to RPMI 2650 cells and the effects of resveratrol on EMT-related markers were investigated.

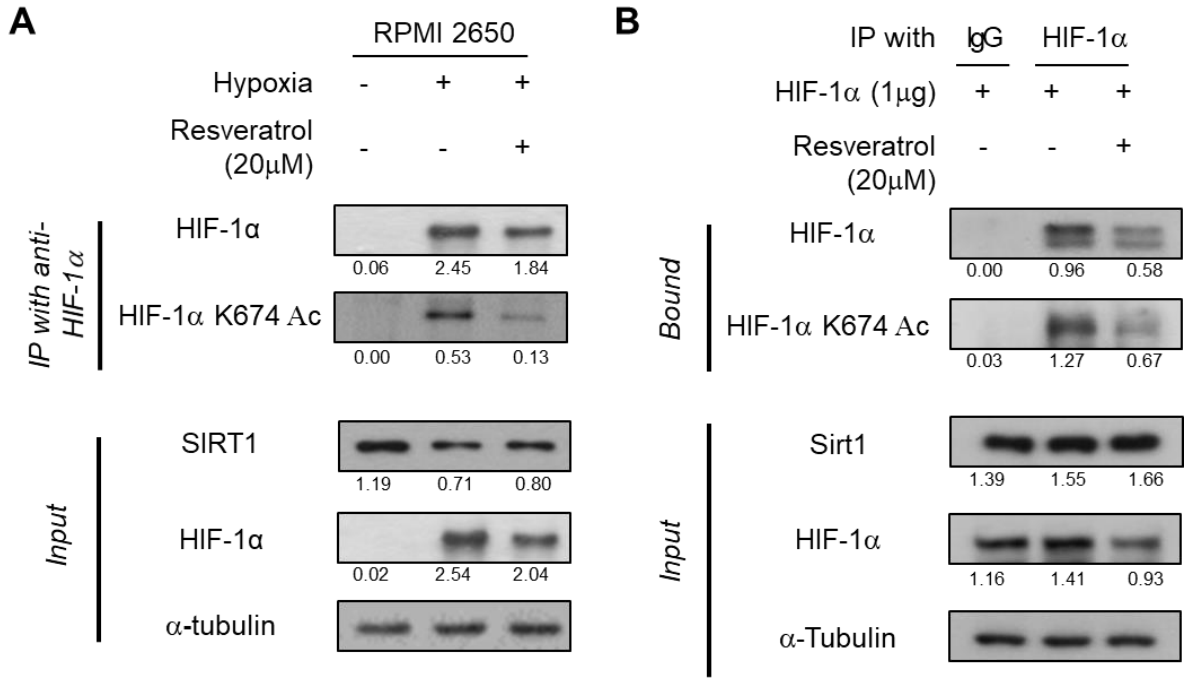

Figure 10. Resveratrol suppresses hypoxia-induced epithelial-to-mesenchymal transition (EMT) by de-acetylating HIF-1α. (A, B) RPMI 2650 cells were treated with resveratrol or vehicle in the HIF-1α-overexpressed or hypoxic conditions (24 h). Whole cell lysates and immune-precipitated proteins were immunoblotted with the indicated antibodies.

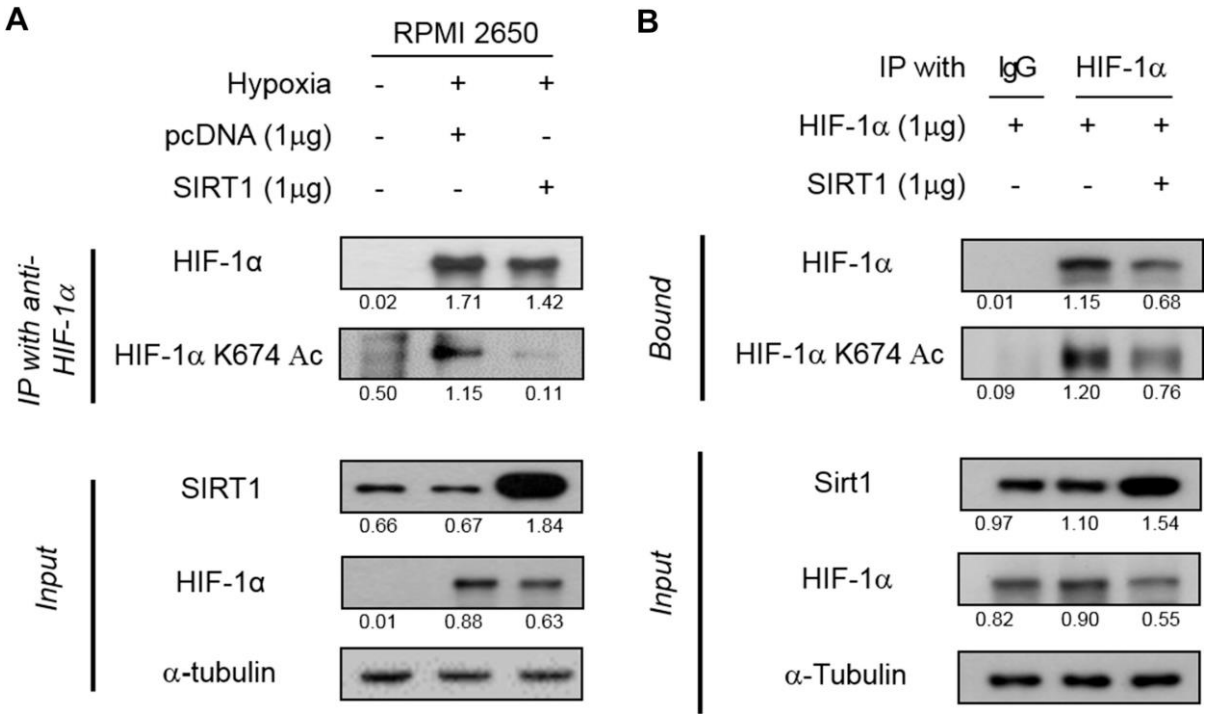

Figure 11. Effect of SIRT1 on HIF-1α de-acetylation. (A) RPMI 2650 cells were transfected with pcDNA or SIRT1 plasmids, followed by 24 hours of normoxic or hypoxic incubation. Whole cell lysates and immune-precipitated proteins were immunoblotted with the indicated antibodies. **(B)** RPMI 2650 cells were transfected with HIF-1α and SIRT1 plasmids, followed by 24 hours of normoxic incubation. Whole cell lysates were treated as mentioned above equally.

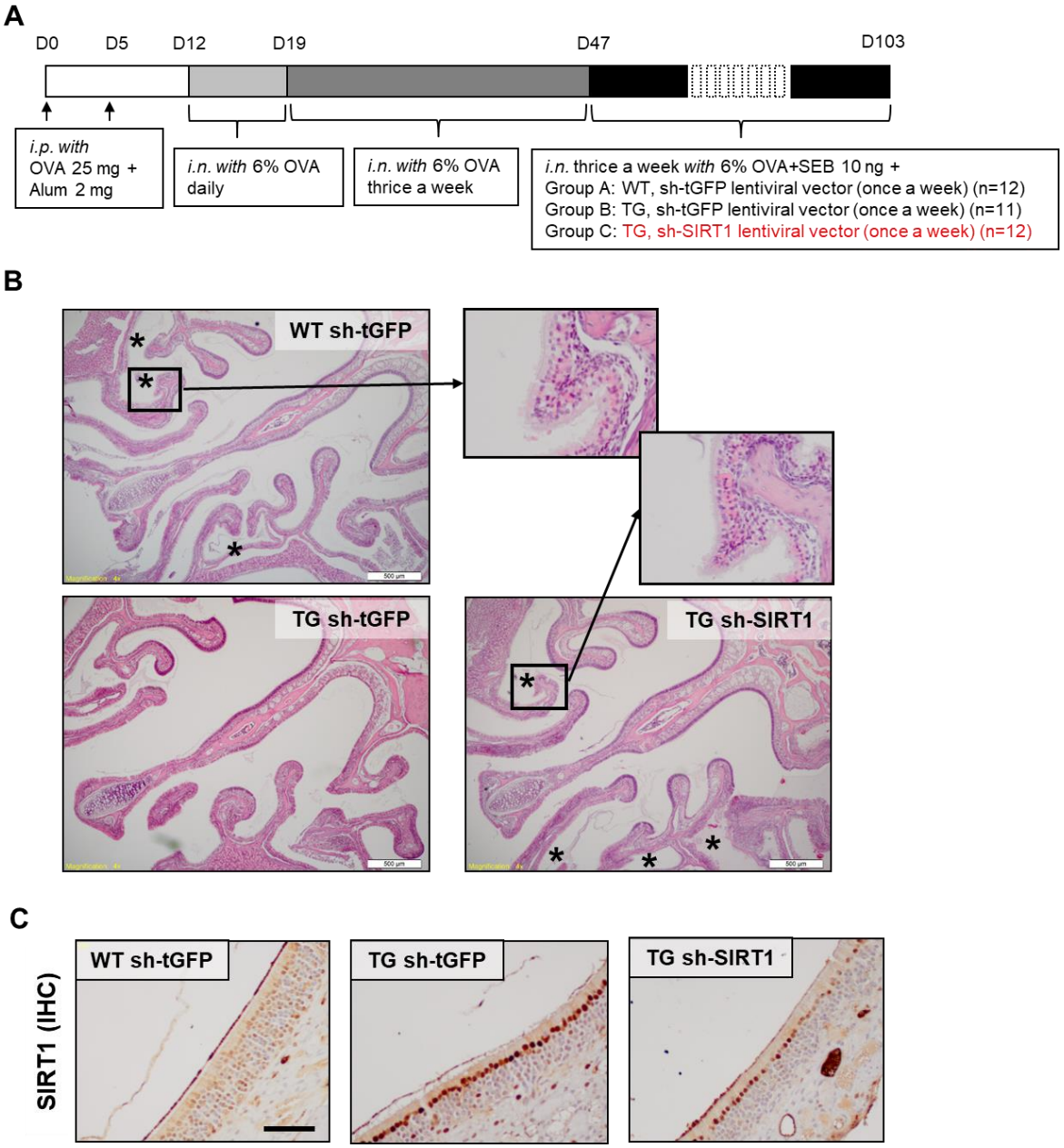

Figure 12. Tissue-specific knockdown of SIRT1 restores polyp formation in SIRT1 TG mice. (A) Protocol for the murine nasal polyp model. WT and SIRT1 TG mice were treated with OVA, SEB, and sh-tGFP or sh-SIRT1 lentiviral vectors. *i.p.*, intraperitoneal; *i.n.*, intranasal. **(B)** Photographs of representative polypoid lesions stained with H&E in the indicated groups. **(C)** Photographs of representative immuno-histochemical staining against SIRT1. Scale bar represents 100 μm.

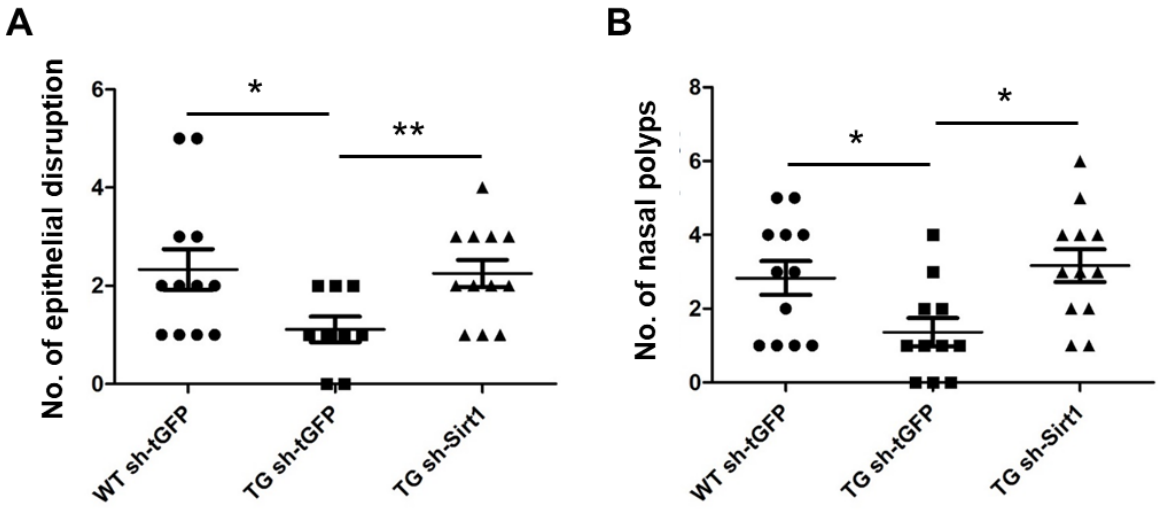

Figure 13. Tissue-specific knockdown of SIRT1 restores the number of epithelial disruptions and polyp formation in SIRT1 TG mice. (A, B) Numbers of epithelial disruptions and polypoid lesions were counted and then compared. * and ** denote $P < 0.05$ and $P < 0.01$, respectively, as determined using the Mann–Whitney U-test.

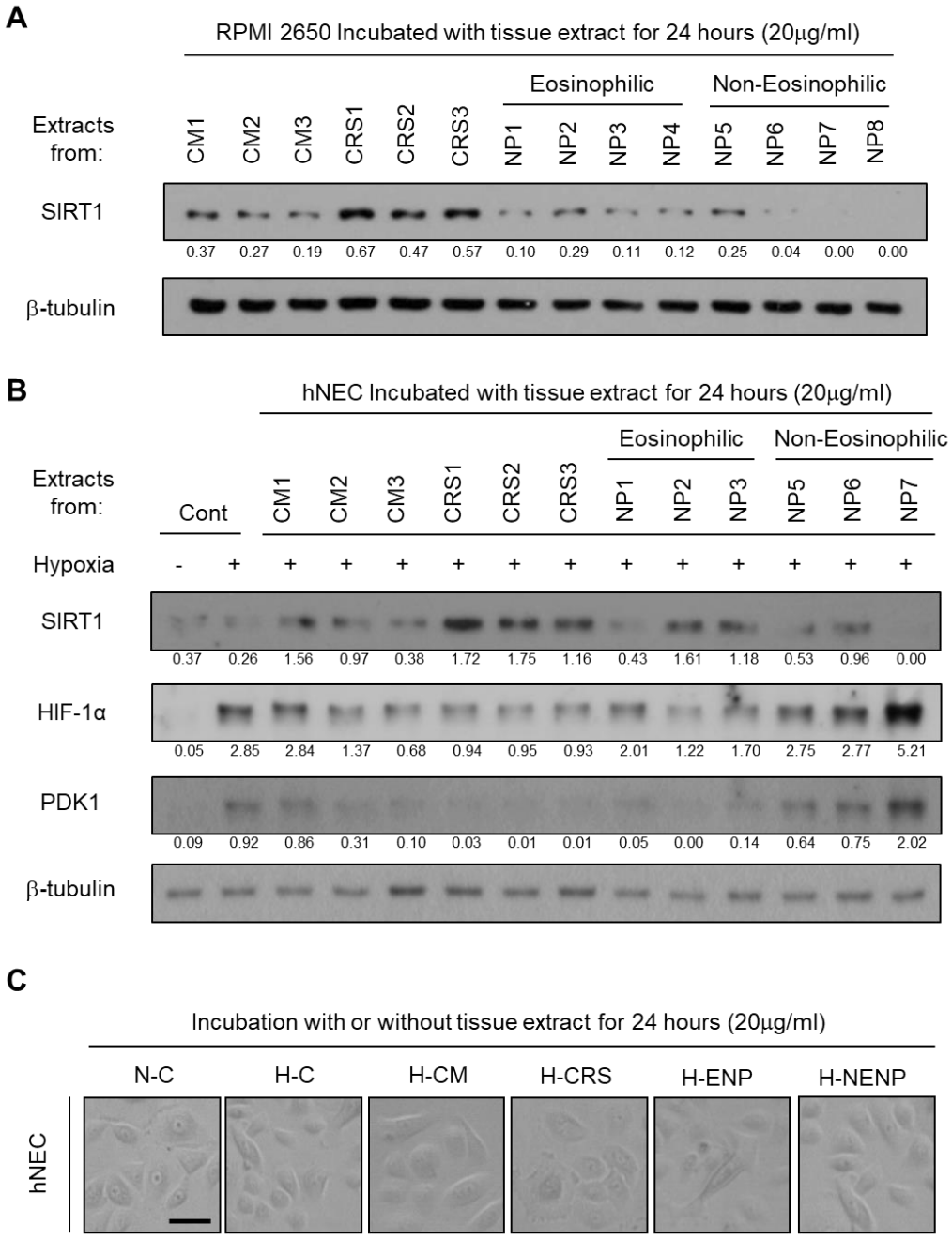

Figure 14. Increased expression of SIRT1 in nasal epithelial cells treated with mucosal extracts from CRSsNP, but not those from CRSwNP. (A) SIRT1 expression in RPMI 2650 cells treated with mucosal extracts from control UPs without nasal pathology, UPs of patients with CRS, or NP tissues from CRSwNP. The intensity values of bands were normalized by β-tubulin expression. **(B, C)** hNECs were incubated under N or H with mucosal extracts from UP, CRS, or NP. hNEC phase-contrast images were acquired. Scale bar represents 100 μm.

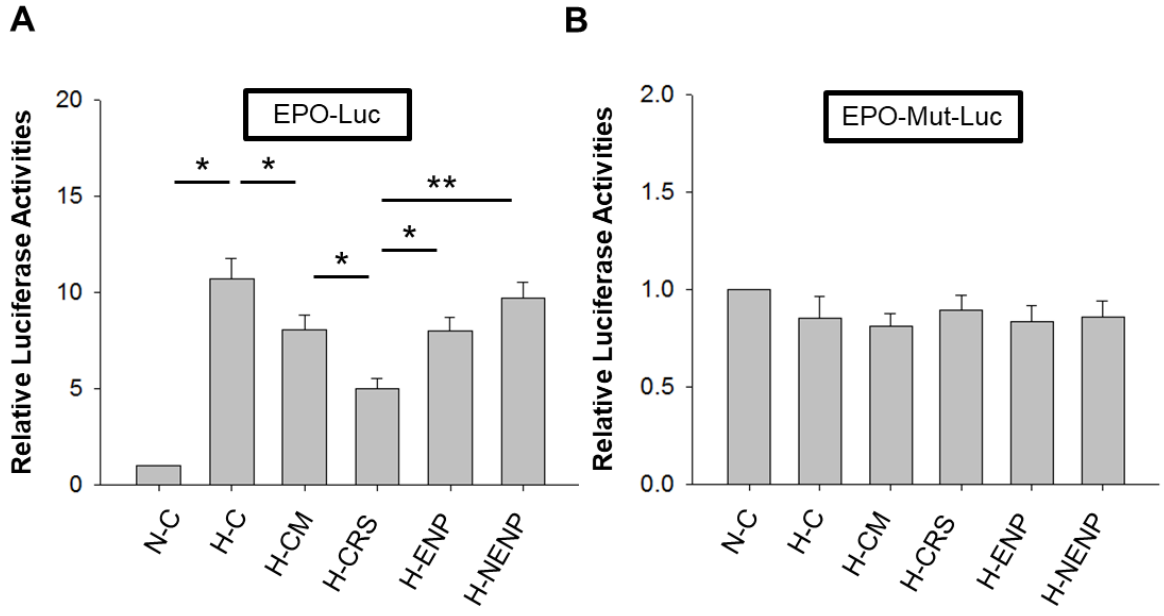

Figure 15. Attenuation of HIF-1α activity by the treatment of mucosal extracts from CRSsNP, but not those from CRSwNP. (A, B) Epo-luciferase and Epo-mutant luciferase activities with mucosal extracts (20 μg/mL) from UP, CRS, or NP as above. * and ** denote $P < 0.05$ and $P < 0.01$, respectively, as determined using the Mann–Whitney U-test.

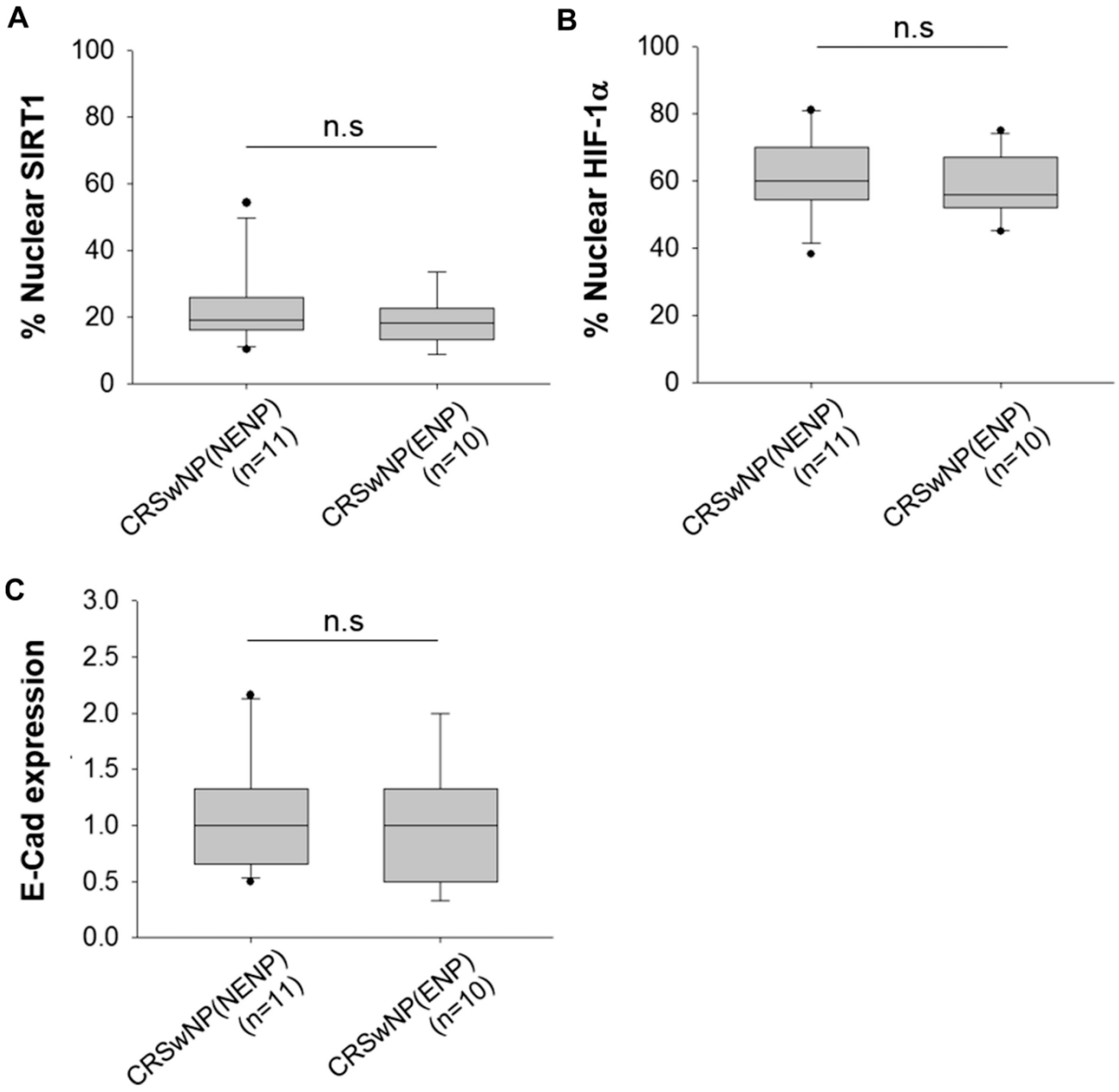

Figure 16. Comparison of SIRT1, HIF-1α, and E-cadherin (E-Cad) expression between ENPs and NENPs of patients with CRS. NP tissues from patients with CRSwNP were immuno-stained with SIRT1 **(A),** HIF-1α **(B),** and E-cadherin (E-Cad; **C**) antibodies. Comparison of nuclear HIF-1α, SIRT1, and E-cadherin expression in ENPs and NENPs of patients with CRS. E-cadherin expression was examined with an HPF (x400 magnification) and scored from 0 to3. The final score of each sample is presented as the average of scores from 3 HPFs. The detailed criteria for scoring are described in the Methods section. n.s., Not significant as determined by using the Mann-Whitney U test.

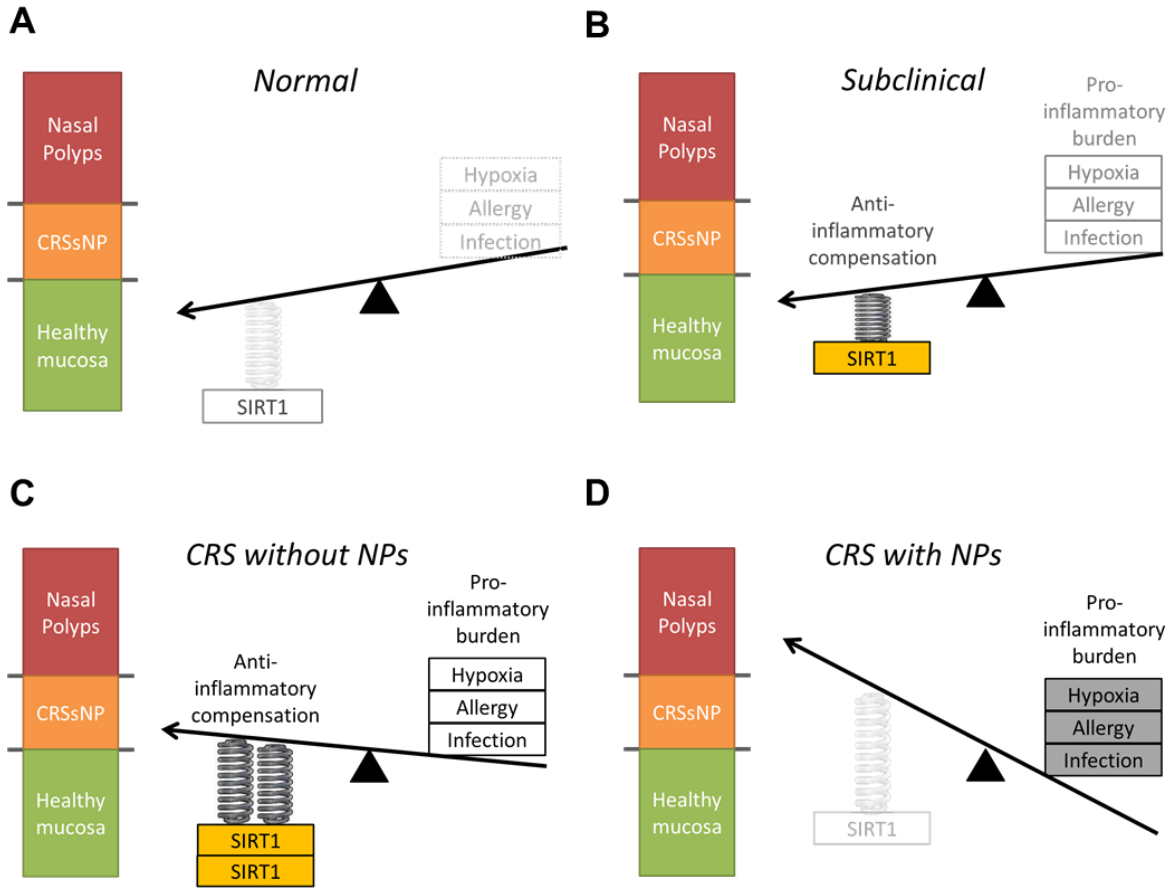

Figure 17. Schematic illustration of the role of SIRT1 in chronic rhinosinusitis with nasal polyps.

Table 1. Patient characteristics and methodologies used

	Control	CRSsNP	CRSwNP	
Total no. of subjects	N =11	N =15	N =10	N=21
Tissue used	UP	UP	UP	NP
Age (yr), mean (SD)	49 (20)	45 (15)	49 (14)	53 (13)
Atopy, N (%)	1 (9%)	2 (13%)	1 (10%)	3 (14%)
Asthma, N	0	1	0	2
Aspirin sensitivity, N	0	0	0	0
Lund-Mackay CT score, mean (SD)	0 (0)	9.3 (5.5)	12.7 (5.3)	13.1 (5.2)
Blood eosinophil (/mm^3)	67.9 (33.1)	139.7 (95.9)	163.6 (132.9)	150.7 (108.2)
Methodology used				
IHC	N= 8 (6 male)	N= 12 (6 male)	N= 10 (7 male)	N= 21 (17 male)
Tissue extracts	N= 3 (3 male)	N= 3 (1 male)	-	N= 8 (5 male)

Abbreviations: CRSwNP, chronic rhinosinusitis with nasal polyp; CRSsNP, chronic rhinosinusitis without nasal polyp; UP, uncinate process; NP, nasal polyp; CT, computed tomography; IHC, immunohistochemistry.

Table 2. List of antibodies used in this project

Antibody	Cat No.	Vendor	Application
α-SMA	ab5694	Abcam	WB, 1:2000
β-CTN	sc-7963	Santa Cruz	WB, 1:2000
β-tubulin	sc-9014	Santa Cruz	WB, 1:5000
E-cadherin	610181	BD	WB, 1:2000; IHC, 1:200
HIF-1α	Generated in our laboratory[94]		WB, 1:1000
HIF-1α	NB100-479	Novus	IHC, 1:50
HIF-1α (K674 Ac)	Generated in our laboratory[94]		WB, 1:1000
Ki-67	sc-15402	Santa Cruz	IHC, 1:500
PDK1	ADI-KAP-PK112-F	Stressgen	WB, 1:2000
SIRT1	07-131	Millipore	WB, 1:2000
SIRT1	NBP1-87038	Novus	IHC, 1:50
Snail	sc-28199	Santa Cruz	WB, 1:200
Twist	sc-15393	Santa Cruz	WB, 1:200
Vimentin	sc-7558	Santa Cruz	WB, 1:2000
ZEB1	Sc-515797	Santa Cruz	WB, 1:500
Rabbit IgG HRP	G21234	Invitrogen	WB, 1:5000
Mouse IgG HRP	G21040	Invitrogen	WB, 1:5000

1.3. DISCUSSION

Epithelial remodeling is a characteristic feature of chronic rhinosinusitis with nasal polyps. Specifically, remodeled CRSwNP tissues are frequently characterized by epithelial overgrowth and mesenchymal transition.[43, 44] Previous research showed that HIF-1α-mediated EMT under hypoxia might be an important mechanism involved in nasal polyp formation in CRS.[45] Here I found that SIRT1 suppressed this hypoxia-induced EMT and could inhibit nasal polypogenesis. *In vitro* mechanism studies revealed that SIRT1 activation, which inhibits HIF-1α transcriptional activity via de-acetylation (Figure 10 and Figure 11), reversed HIF-1α-mediated EMT (Figure 7 and Figure 9). Immuno-histochemical experiments showed that epithelial SIRT1 expression was elevated in CRSsNPs, and diminished or lost in CRSwNPs (Figure 3 and Figure 4). Thus, decreased SIRT1 expression may boost HIF-1α-mediated EMT in CRSwNPs. Taken together, my findings suggest that SIRT1 activation and maintenance is a plausible means of treating and preventing nasal polyp formation in CRS.

Emerging evidence indicates that airway epithelium may contribute to airway remodeling following environmental challenge via the EMT process.[39] EMT, a reversible process in which epithelial cells transdifferentiate into cells with mesenchymal characteristics, plays a crucial role in body plan formation and in the differentiation of multiple tissues and organs.[95] Growth factors as well as inflammatory cytokines and mediators, including transforming growth factor (TGF)-β, are known to weaken epithelial cell-to-cell adhesion and promote mesenchymal marker expression of extra domain A (EDA)-fibronectin, vimentin, and α-SMA.[39, 40] EMT not only plays crucial role in liver and kidney fibrosis as well as the asthmatic lung but also plays an important role in CRSwNPs.[44, 96] Epithelial dedifferentiation towards a mesenchymal phenotype was correlated with airway fibrosis and inflammation.[44]

In addition to TGF-β, hypoxia is another major EMT-inducing stimulus via HIF-1 activation.[45, 97] In particular, HIF-1 is a known key regulator of cellular responses to low oxygen status by trans-

activating various downstream genes. Human nasal polyps have higher HIF-1α expression than control nasal mucosa,[98, 99] which reportedly contributes to CRSwNP epithelial remodeling in diverse ways. For example, VEGF facilitates nasal polyp fibroblasts and leads to mucosal edema.[46, 100] HIF-1α is also a transcription factor that induces expression of a number of EMT-associated genes, such as *TGF-β*, *TWIST*, and lysyl oxidase (*LOX*).[101] In a mouse model, HIF-1 inhibitors suppressed polyp burden and EMT in diverse cells.[45] In addition, proprotein convertase (PC)1/3 overexpression induced morphological and phenotypic EMT changes in airway epithelial cells, and these changes may have contributed to the pathogenesis of nasal polyps.[102]

Sirtuins are highly conserved nicotinamide adenine dinucleotide (NAD)-dependent deacetylases that regulate lifespan in lower organisms[103] and affect aging-related pathology in mammals, such as diabetes, inflammation, and neurodegenerative disease.[56] In mammals, there are seven sirtuin homologs, SIRT1–7. Among them, SIRT1 has garnered the most attention. SIRT1 is known to deacetylate transcription factors that control the aging process[59] and suppress inflammation.[104, 105] SIRT1 deacetylates key histone residues involved in the regulation of transcription, including histone H3 lysine 9 (H3-K9), H4-K16, and H1-K26, and diverse non-histone protein targets, including p53, forkhead box protein O1/3 (FOXO1/3), peroxisome proliferator-activated receptor gamma coactivator 1a (PGC-1α), nuclear factor (NF)-kB, and HIFs.[55, 60]

In this study, I showed that SIRT1 inhibited hypoxia-induced EMT in nasal mucosa. This is to my knowledge the first report regarding the role of SIRT1 in nasal polypogenesis. Despite the lack of related literature, a few reports support my findings. Recently, Simic et al. showed that SIRT1 suppressed EMT in cancer metastasis and in organ fibrosis.[69] In addition, it was previously reported that resveratrol could be a novel drug against CRSwNP due to its action via the 5-lipoxygenase (5-LO) pathway.[68] The expression levels of interleukin (*IL)-4*, *IL-5*, prostaglandin-D synthase, and leukotriene C4 synthase genes were significantly decreased by administration of low- or high-dose resveratrol.[68] However, in these studies, the specific mechanism related to the effect of SIRT1 could not be elucidated due to the

systemic administration of resveratrol, which is also known to suppress inflammation by targeting peroxisome proliferator-activated receptor gamma (PPAR-γ) and NF-κB.[106] Given that SIRT1 is a critical negative regulator of both the innate and adaptive immune response in mice,[107] the effect of SIRT1 modulators should be investigated using site-specific treatment to exclude the systemic effect of SIRT1-targeting drugs. For this reason, I treated with SIRT1 modulators as well as lentiviral vectors intra-nasally, and confirmed the anti-polyp effect of SIRT1 *in vitro* and *in vivo* (Figure 12 and Figure 13).

Interestingly, the mucosal extracts from patients with CRS with or without NPs revealed differential SIRT1 expression in human nasal epithelial cells (Figures 14A and 14B). CRSsNP mucosal extract induced SIRT1 expression, but NP extract did not. Specifically, non-eosinophilic NPs suppressed SIRT1 expression compared to controls, indicating that different inflammatory milieu in patients could influence SIRT1 levels. Although I observed differential SIRT1 levels following treatment with different mucosal extracts, the underlying mechanism involved in extract-induced SIRT1 induction or suppression is still unknown. So far the regulation mechanism of SIRT1 expression is not fully understood. It has been reported that the SIRT1 protein could be suppressed by tumor repressor HIC1 (hyper-methylated in cancer 1) and microRNA miR-34a.[108, 109] It is noteworthy that the NF-κB complex could bind to the promoter of miR-34a, leading to SIRT1 downregulation.[110] Recently, Li et al demonstrated that interferon (IFN)-γ which is stimulated by NF-κB signaling could suppress the expression of SIRT1 in skeletal muscle cells.[111] My preliminary data also showed the possibility that IFN-γ might suppress SIRT1 and boost HIF-1α activity under hypoxia (Figures 8 and 9B). Given that the mucosal environment of NENP is characterized as higher IFN-γ and IL-17A rather than IL-5, the distinct cytokine milieu may contribute to the differential responses against the mucosa extracts of ENP or NENP. To further identify the relevance of inflammatory type of polyp to the SIRT1 regulation, I investigated SIRT1, HIF-1α and E-cadherin expressions between ENP and NENP tissues (Figure 16). Although the effect of NP extract on SIRT1 expression was different according to the inflammatory

types, there was no significant difference in SIRT1, HIF-1α and E-cadherin on IHC staining. It was possibly due to that the eosinophilic polyp extracts also could suppress the SIRT1 expression, so the difference of effects could not be seen. I currently could not determine exactly whether the SIRT1 suppression is dominant in non-eosinophilic NPs rather than eosinophilic ones. Further studies are required to clarify this characteristic feature and elucidate the underlying reason.

Taken together, SIRT1 might play a defensive role in CRS, and it seems that SIRT1 loss aggravates sino-nasal mucosa inflammation, finally leading to epithelial remodeling, including polypogenesis (Figure 17). My findings suggest that SIRT1 may be a reliable target for treating nasal polypogenesis via EMT suppression in mucosal epithelium. Moreover, SIRT1 activators could be a novel class of anti-polyp drug that modulates HIF-1 activity more delicately than do HIF-1 inhibitors. In addition, further investigation regarding the reason underlying loss of SIRT1 expression in nasal polyps could provide a molecular target for novel treatment strategies for nasal polyposis.

Chapter 2

Sinonasal Delivery of Resveratrol via Mucoadhesive Nanostructured Micro-particles in a Nasal Polyp Mouse Model

2.1. INTRODUCTION

Chronic rhinosinusitis with nasal polyps (CRSwNP) is a Th2-skewed heterogeneous inflammatory disease that is often accompanied by prominent eosinophilic infiltration, an increase in sub-epithelial thickness and the formation of micro-cavities in the mucosal epithelium.[14, 86] Even after treatment with the current optimal regimen of steroids or with functional endoscopic sinus surgery (FESS), the overall recurrence rates often exceed 25%, varying with history of allergy or asthma and age.[1, 112] Recent study presented that hypoxia-inducible factor-1alpha (HIF-1α) can induce the epithelial-to-mesenchymal transition (EMT) of the nasal polyp epithelium, leading to nasal polypogenesis.[45] Thereafter, I reported that Sirtuin 1 (SIRT1) can be considered a novel therapeutic target because of its suppression of HIF-1α-induced mucosal remodeling; thus, I proposed a SIRT1 activator, resveratrol, as a novel therapeutic agent.[113]

Resveratrol (RSV), a naturally occurring polyphenolic compound, has received great attention for its anti-carcinogenic, anti-inflammatory and anti-oxidant effects.[63-65] Despite its outstanding anti-polyp effects in mouse models, the bioavailability of RSV is low when it is locally delivered to the nasal cavity in solutions or suspensions.[70, 71] The utility of RSV is limited by its low aqueous solubility and its susceptibility to rapid clearance from the nasal cavity. Therefore, repeated intranasal administrations are often required to achieve a therapeutic effect for a prolonged period.[114, 115]

To overcome this limitation, I propose muco-adhesive micro-particles with a nanostructured surface as carriers for the nasal delivery of RSV. The micro-particles are mainly composed of poly (lactic-co-glycolic acid) (PLGA) to allow the sustained delivery of RSV.[73, 116] A muco-adhesive polymer, polyethylene glycol (PEG),[75, 76] was used as an additional constituent to increase micro-particle residence time in the mucosal layer of the nasal cavity.[117] Together with PEG, the nano-structuring of the surface of micro-particles, which provided an enlarged specific surface area, led to a synergistic increase in residence time. Therefore, I hypothesized that RSV-loaded micro-particles might reside in

the nasal cavity for a prolonged time and release RSV in a sustained manner, thereby enhancing its bioavailability and yielding a high potential for resolving the refractory clinical problems described above.

To my knowledge, this is the first study to report muco-adhesive, nanostructured micro-particles as sino-nasal delivery carriers for RSV and to evaluate RSV encapsulated micro-particles *in vivo* efficacy for the treatment of CRS in animal nasal polyp models. In the present study, muco-adhesive nanostructured micro-particles (PLGA/PEG NM) were fabricated based on the method reported in previous study,[77] wherein a solution containing both PLGA and PEG was electro-spun to produce a nano-fibrous sheet that was then freeze-milled to yield micro-particles with a nanostructured morphology. As controls, I also prepared three other distinct types of micro-particles: spherical micro-particles without muco-adhesion (i.e., spherical micro-particles with PLGA only; PLGA MS), spherical micro-particles with muco-adhesion (i.e., spherical micro-particles with a blend of PLGA and PEG; PLGA/PEG MS) and nanostructured micro-particles without muco-adhesion (i.e., nanostructured micro-particles with PLGA only; PLGA NM). The micro-particles were loaded with a fluorescent marker, diethylthiatricarbocyanine iodide (DTTCI) to examine their retention properties in the sino-nasal cavity; after nasal delivery, the quantity of remaining micro-particles was evaluated via in vivo fluorescence imaging. The RSV-loaded micro-particles were assessed via in vitro drug-release experiments to examine their sustained drug-release properties.

I used a mouse model of eosinophilic CRSwNP model to investigate the therapeutic effect in vivo.[71] The PLGA/PEG NM and RSV solutions were each delivered sino-nasally, and the degree of disease suppression was verified using Sirius red staining, Giemsa staining, Masson's Trichrome staining and Periodic Acid–Schiff (PAS) staining to evaluate eosinophils, goblet cells, collagen deposition and mast cells, respectively.

2.2 RESULTS

2.2.1. Micro-particle characterization

The micro-particles were first imaged with a scanning electron microscope (Figure 18). The MS prepared by the conventional emulsion method exhibited a spherical shape and a smooth surface, whereas the NM showed a rough nano-fibrous surface.[77, 78, 118] The overall morphologies of the MS and NM were not influenced by the presence of PEG, RSV or DTTCI, in accordance with previous study.[77, 78, 118] Here, the MS and NM were prepared so that they possessed a similar size distribution, which was measured to be 6.72 - 7.64 μm (Figure 19 and Table 3). The actual amount of PEG in the micro-particles was determined with a proton ^{1}H - nuclear magnetic resonance (^{1}H NMR) spectrometer; the PEG content was measured to be 9.95 and 10.17% for PLGA/PEG MS and PLGA/PEG NM, respectively (Table 3). According to CO_2 adsorption/desorption analysis, the specific surface area of the NM was more than 10 times larger than that of the MS because of the rough nanostructure on the surface of the NM. The specific surface areas were measured to be 291.23 m^2/g and 28.88 m^2/g for NM and MS, respectively. Regardless of micro-particle type, similar amounts of DTTCI and RSV were loaded, showing ranges of 7.93–8.87 μg/mg and 1.06–1.78 μg/mg, respectively (Table 3 and Table 4). I also examined the crystallinity of intact PLGA, intact PEG, RSV powder, and PLGA/PEG NM (Figure 20). PLGA was amorphous without any crystalline peaks,[119] while crystalline peaks were observed at 2θ = 19.2° and 22.3° with PEG[120] and at 6.6°, 13.2°, 16.4°, 19.2°, 22.3°, 23.6°, and 28.3° for RSV.[121] However, even with the presence of RSV, PLGA/PEG NM showed only two peaks at 2θ = 19.2° and 22.3°, both of which corresponded to PEG, suggesting that the RSV molecules were homogeneously distributed in PLGA/PEG NM without forming a crystalline structure.

2.2.2. In vitro release profile of RSV

For all micro-particle types, I examined the *in vitro* release profile of RSV in phosphate buffered

saline (PBS) at pH 7.4 and 37°C (Figure 21). RSV was released from all of the micro-particles in a sustained manner. For PLGA MS and PLGA/PEG MS, 87.7 and 76.6% of the loaded RSV was released, respectively, during the first 6 h; subsequently, 7-16.4% of the RSV was slowly released during the next 42 h. For PLGA NM and PLGA/PEG NM, 52.3 and 58.9% of the loaded RSV was released, respectively, during the first 6 h, while 28.7–44.3% of the RSV was released over the next 42 h. I also performed an in vitro release test in simulated nasal electrolyte solution (SNES) at pH 5.5, which is known to better mimic the condition in mouse nasal cavity. The release profile of RSV in the SNES (pH5.5) was similar to that in PBS (pH 7.4), where approximately 40, 55, and 69% of RSV was released in the first 6, 12, and 24 h, respectively (Figure 22). The remaining 8% of RSV was slowly released for the next 24 h at a rate of 0.33%/hour. The difference between the MS and NM in the size of the initial burst release may be ascribed to their different preparation methods. For the MS, much of the initially loaded RSV can be lost during the emulsion process, which would leave many pores or conduits inside the micro-particles that would enhance the release of the encapsulated RSV.[122, 123] Meanwhile, the NM were prepared under a dry environment via electrospinning and milling, possibly yielding a more dense polymer matrix structure in the micro-particles. This effect appeared to be more dominant than that of the specific surface area with respect to drug release.

Mucin adoption was measured in vitro to exhibit the ability of muco-adhesive PLGA/PEG NM to bind better to the mucosal nasal cavity as compared to non-muco-adhesive PLGA NM. The amount of mucin adsorbed to PLGA/PEG NM was measured to be 81.96 ± 1.86 μg/mg, which was significantly higher than that to PLGA NM only (70.13 ± 2.18 μg/mg), suggesting that PLGA/PEG NM is muco-adhesive due to the presence of muco-adhesive PEG, resulting in superior adherence to the nasal cavity.

2.2.3. In vivo sino-nasal retention properties

To examine the sino-nasal retention properties of the micro-particles, they were loaded with

DTTCI, a near-infrared fluorescent dye, instead of RSV and were administered intra-nasally to living animals. I measured the amount of micro-particles remaining in the nasal cavity over time using an *in vivo* imaging system (IVIS). DTTCI is known to be almost insoluble in water; thus, its release from the micro-particles was expected to be minimal under my experimental conditions. As shown in Figure 23, the MS were cleared relatively rapidly from the sino-nasal cavity. Regardless of the presence of PEG, 64 - 67% of the MS remained 6 h after administration, while less than 20% of the MS were observed after 24 h. Thus, the half-lives of micro-particle residence in the sino-nasal cavity were calculated as 10.5 ± 2.8 and 9.1 ± 0.3 h for PLGA MS and PLGA/PEG MS (Table 5), respectively. In contrast, the PLGA NM exhibited an apparent increase in sino-nasal retention. Of the initially administered PLGA NM, 87% remained at 6 h, 78% remained at 12 h and 48% remained 24 h after administration. The half-life of PLGA NM was 21.5 ± 2.5 h (Table 5), representing a more than 2-fold increase when compared with that of PLGA MS and PLGA/PEG MS. This increase in sino-nasal retention may be ascribed to van der Waals forces resulting from the enlarged specific area of the NM, which appeared to improve micro-particle adhesion to the surface of the sino-nasal space. Thus, the sino-nasal retention of PLGA NM was significantly different from that of PLGA MS and PLGA/PEG NM at 18 h and 36 h ($P < 0.05$).

PLGA/PEG NM, i.e., the micro-particles with both a nanostructured surface and muco-adhesiveness, exhibited the greatest sino-nasal retention. More than 96% of these micro-particles remained at 6 h, and their subsequent clearance occurred at a slow rate, as approximately 95, 75, and 56% of the micro-particles remained in the sino-nasal cavity at 12, 18, and 24 h, respectively. The half-life of PLGA/PEG NM was 23.5 ± 4.7 h (Table 5), which was the highest among the micro-particle types tested in this study. Compared with PLGA MS and PLGA/PEG MS, the retention of PLGA NM showed significant differences at 12, 18, 24 and 36 h ($P < 0.05$). This considerable improvement in sino-nasal retention may be attributed to synergistically improved muco-adhesiveness due to the enlarged specific surface area originating from the nanostructure.[77, 78, 118]; thus, the PLGA/PEG NM used here better adhered to the mucosal layer in the sino-nasal space.

2.2.4. In vivo effects on nasal polyps and epithelial disruption

Given the substantially improved intra-nasal retention and sustained drug release properties of PLGA/PEG NM, I sought to examine their *in vivo* efficacy as intranasal RSV delivery carriers. To do so, I applied the RSV-loaded PLGA/PEG NM to a previously established murine nasal polyp model (Figure 24A).[45, 71, 124, 125] The polyp model was generated by chronic administration of ovalbumin (OVA) and *Staphylococcus aureus* enterotoxin B (SEB) (Groups B-F). Group A consisted of animals that did not receive this treatment, representing the polyp-free control group. After the OVA and SEB treatments, I administered the different RSV formulations to examine their effects on the polyps in the model animals.

I first examined the number of polyps in the sino-nasal cavity. Group B was administered with the vehicle, i.e., PBS without RSV, and animals showed 5 or more nasal polyps in the sino-nasal cavity. However, upon intranasal delivery of RSV solution (Group C), there was an apparent reduction in polyp number compared to that of Group B, in accordance with previous results.[125] When the same amount of RSV was administered with PLGA/PEG NM (Group D), the number of polypoid lesions was further reduced compared to that of Group C (Figures 24B and 24 C). Notably, this reduction was also obvious with half the dose of RSV-loaded PLGA/PEG NM (also representing half the dose of RSV) (Group E). As expected, blank (no RSV) PLGA/PEG NM (Group F) showed almost no reduction in polypoid formation compared with Group B. I also counted the number of epithelial disruptions, as shown in Figure 24D. The animals treated with the formulations containing RSV (Groups C, D and E) exhibited a decreased number of epithelial disruptions compared with Groups B and F. Again, the reduction was greatest with RSV-loaded PLGA/PEG NM (Groups D and E).

2.2.5. In vivo evaluation of inflammatory surrogates

Next, I examined the anti-inflammatory effect of RSV when delivered in the various formulations tested in this study. As shown in Figure 25, in the absence of RSV (Groups B and F), prominent inflammation was observed in the nasal cavity and paranasal sinus. In contrast, the overall degree of inflammation was suppressed by administration of an RSV solution (Group C), while RSV-loaded PLGA/PEG NM (Groups D and E) showed an even greater effect. Again, even when of the dose of RSV delivered with PLGA/PEG NM was cut in half (Group E), its therapeutic effect on inflammation was comparable to that of the RSV solution (Group C), implying that the PLGA/PEG NM enhanced the therapeutic effect of sino-nasally delivered RSV on inflammation. The numbers of both mast cells and goblet cells were prominently decreased in Group D (Figures 25A and 25B). There was also a significant decrease in the number of mast cells, even with the half dose of RSV encapsulated with PLGA/PEG NM (Group E). As shown in Figure 25C, I also assessed the number of eosinophils, which play a critical role in the pathogenesis of human and murine nasal polyps.[126] The number of eosinophils was markedly decreased in all of the RSV-treated groups (Groups C, D and E). Notably, the greatest reduction in the number of eosinophils was observed in Group D. While total serum IgE levels increased in response to the OVA and SEB administration (Figure 25D), I observed that they decreased following RSV administration (Groups C, D and E). This effect was preserved with a half dose of RSV-loaded PLGA/PEG NM (Group E). Treatment with OVA and SEB induced prominent collagen accumulation in Groups B and F. Meanwhile, Groups C, D and E, which were treated with RSV, exhibited reduced collagen accumulation, as reported in previous study (Figures 25E and 25F).[127] Importantly, this effect was still evident with a half dose of RSV when delivered with PLGA/PEG NM (Group E). Representative histological images are shown in Figures 26A-D.

2.2.6. In vivo efficacy on E-cadherin restoration

RSV is known to activate SIRT1, which then attenuates HIF-1α activity in nasal epithelial cells through deacetylation.[60, 125] In this work, I assessed E-cadherin expression as a representative marker of

HIF-1α activity. E-cadherin loss in nasal epithelial cells was attributed to increased HIF-1α activity.[45] The nasal epithelium in Groups B and F showed markedly decreased E-cadherin expression compared to normal intact epithelium (Group A). However, upon administration of the RSV solution (Group C), E-cadherin expression remained high with respect to Groups B and F, indicating a marked reduction in polyp-formation capacity.[125] As anticipated, animals treated with RSV-loaded PLGA/PEG NM (Groups D and E) exhibited significantly greater E-cadherin expression. As in the other assays, a half dose of RSV-loaded PLGA/PEG NM still exhibited a notable result, blocking nasal epithelium remodeling as effectively as a full dose of the RSV solution. Even with continuous exposure to SEB and OVA, the RSV-loaded PLGA/PEG NM (Group D) could preserve the epithelium in nearly intact and healthy conditions resembling those in Group A (Figures 27A and 27B).

2.2.7. Biocompatibility evaluation

I then assessed the cytotoxicity of the formulations tested in this work using 2 different types of human nasal epithelial cells, i.e., nasal septum-derived carcinoma cells (RPMI 2650) and primary nasal epithelial cells (hNEC). As shown in Figure 28A, the viability and proliferation of cells treated with RSV solution, RSV-loaded PLGA/PEG NM or blank PLGA/PEG NM were all similar to that of cells treated with a nontoxic PBS+DMSO solution.[128, 129] However, resveratrol has known to be a have potent cytotoxicity in a high concentration.[130-132] To confirm this issue, I also performed the standard MTT-assay with RPMI 2650 cells in a concentration dependent manner. Similar to previous findings, I also found cytotoxicity of resveratrol in more than 50 μM. Given that I performed all the experiments nearly at 20 μM (0.88 μg/40 μl) of resveratrol, I concluded that the tested formulations are not cytotoxic (Figure 28B). For *in vivo* biocompatibility evaluation, I examined Ki-67, a marker for cell proliferation, in nasal mucosa samples obtained from the animals (Figures 29A and 29B). Ki-67 is a nuclear protein that is ubiquitously expressed in the G1, S and G2 phases of the cell cycle but not in G0 phase.[133, 134] Ki-67 expression was significantly increased relative to Group A in Groups B and F, which were not

treated with RSV. However, with RSV administration (Groups B, C and D), Ki-67 expression was reduced to a level similar to that of Group A, suggesting that cell proliferation was properly maintained. This effect was most apparent with RSV-loaded PLGA/PEG NM (Group D), and the effect of a half dose of RSV-loaded PLGA/PEG NM was comparable to that of a full dose of RSV solution (Group C).

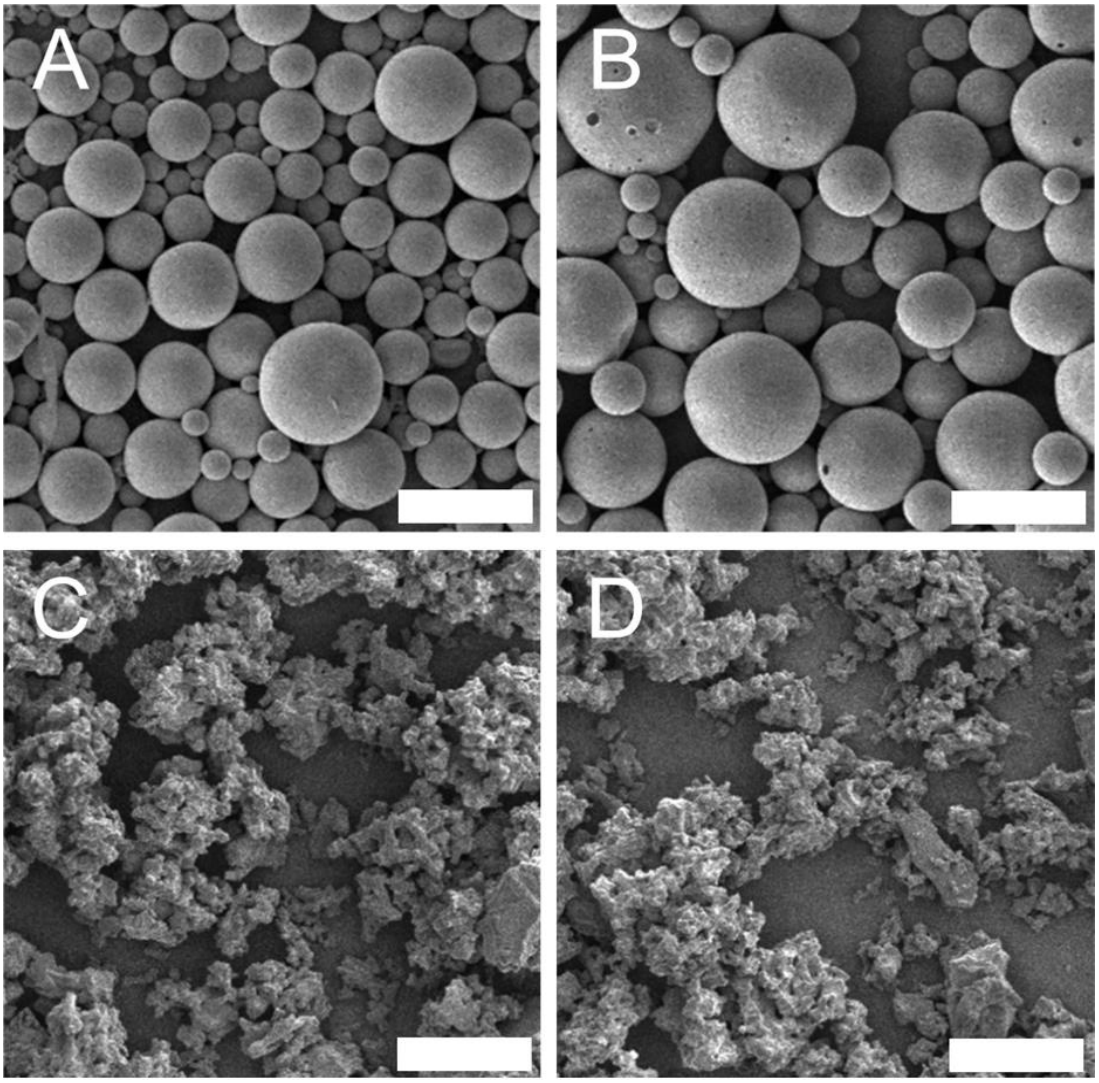

Figure 18. Representative scanning electron micrographs. (A) PLGA MS, **(B)** PLGA/PEG MS, **(C)** PLGA NM and **(D)** PLGA/PEG NM. The scale bars represent 50 μm.

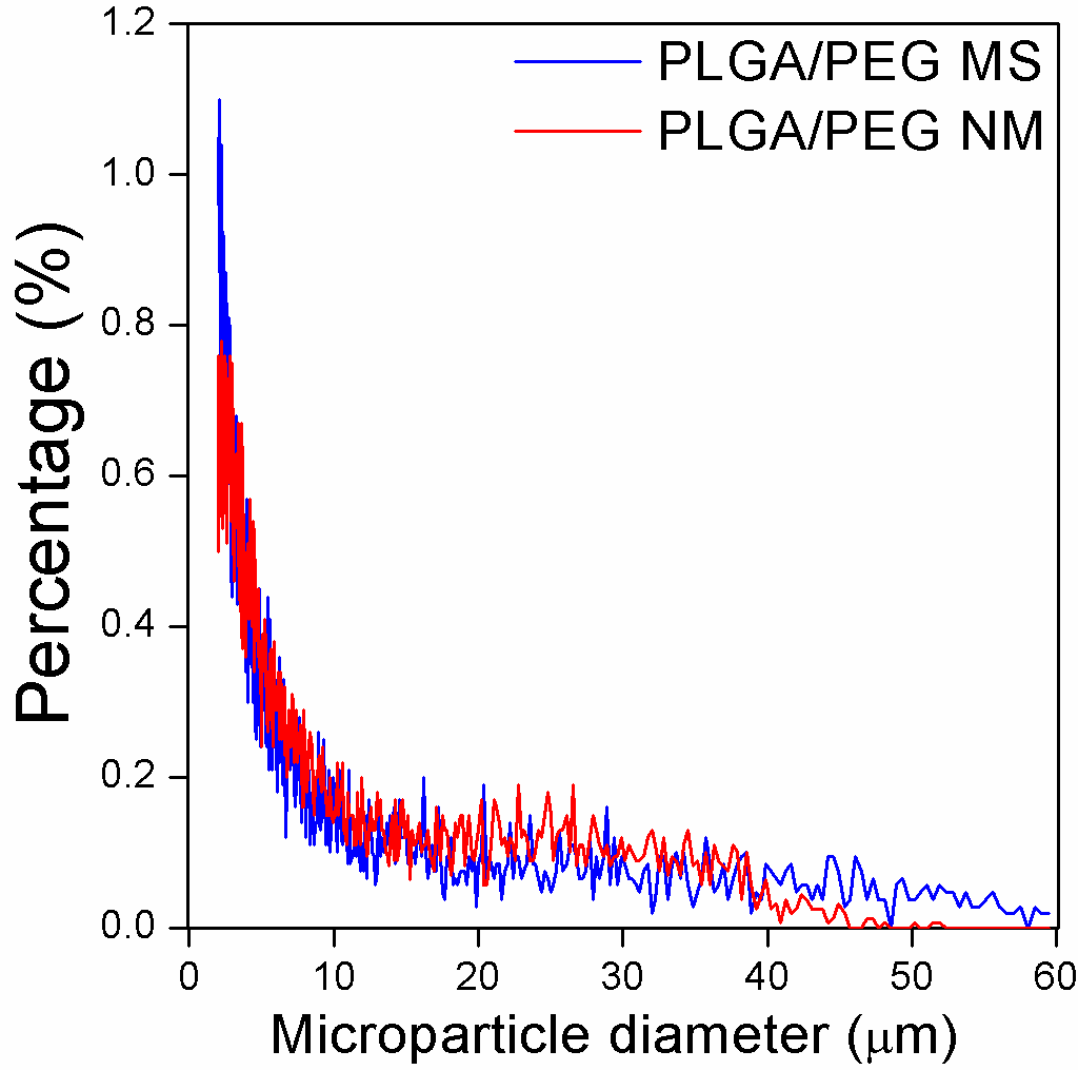

Figure 19. Size distribution profiles of PLGA/PEG MS (blue) and PLGA/PEG NM (red). Microparticle diameter was measured with a Coulter counter.

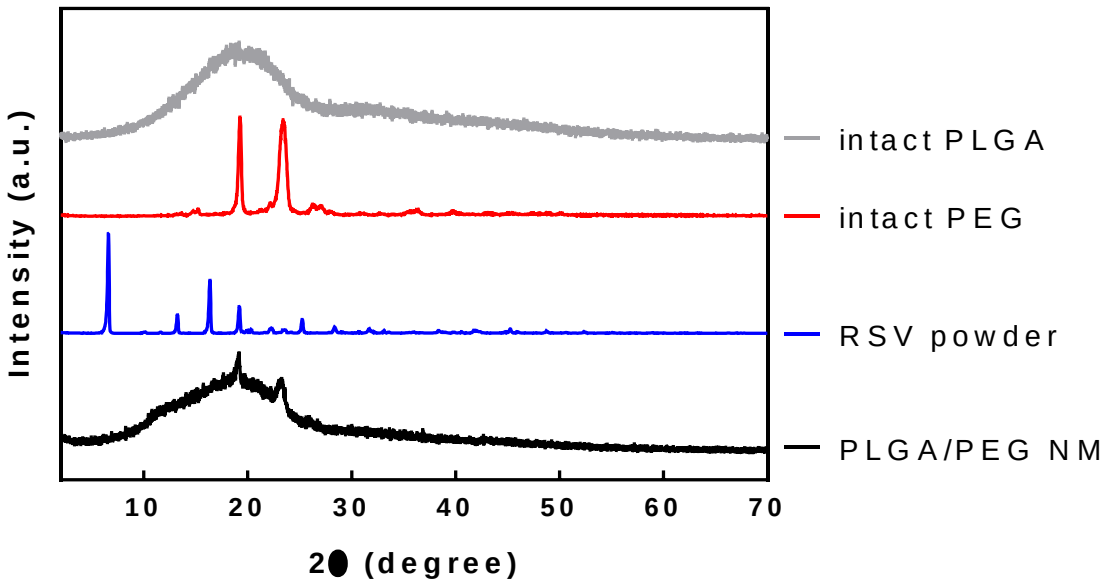

Figure 20. Powder X-ray diffraction (PXRD) patterns of intact PLGA, intact PEG, intact RSV and RSV loaded PLGA/PEG NM. The measurement was performed with an X-ray diffractometer (D/MAX RINT 2200-Ultima, Rigaku, Japan) that is equipped with Ni-filtered CuKα radiation (λ = 1.5418 Å). Each sample was deposited on a glass substrate and scanned continuously at a tube voltage and current of 40 kV and 30 mA, respectively. For intact PEG and RSV, distinct crystalline peaks were observed while intact PLGA did not exhibit any apparent peaks due to its amorphous structure. For the RSV loaded PLGA/PEG NM, the characteristic peaks originated from RSV were not observed but the distinct peaks originated from PEG were seen. This result suggested that unlike PEG, RSV was distributed in the PLGA/PEG NM without forming a crystalline structure.

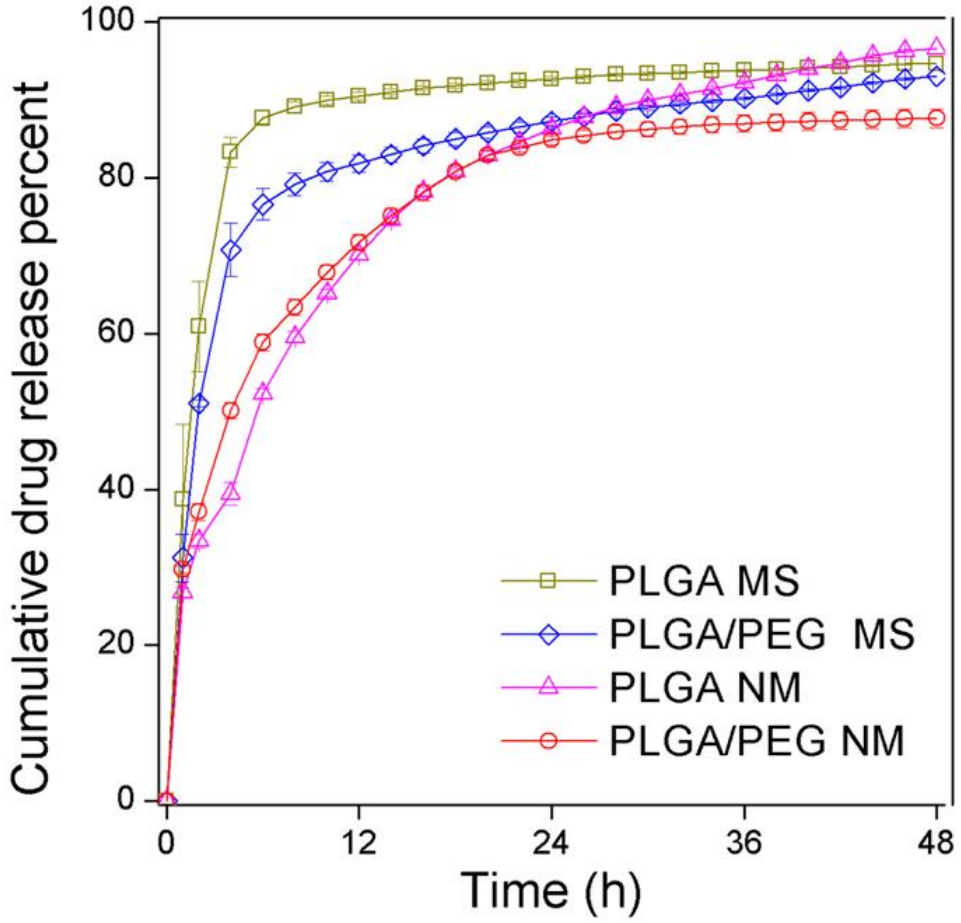

Figure 21. ***In vitro*** **release profiles of RSV from the micro-particles.** The experiment was performed in PBS (pH 7.4) containing 1% w/v Tween 20. At defined time points, the release medium was collected and measured by HPLC.

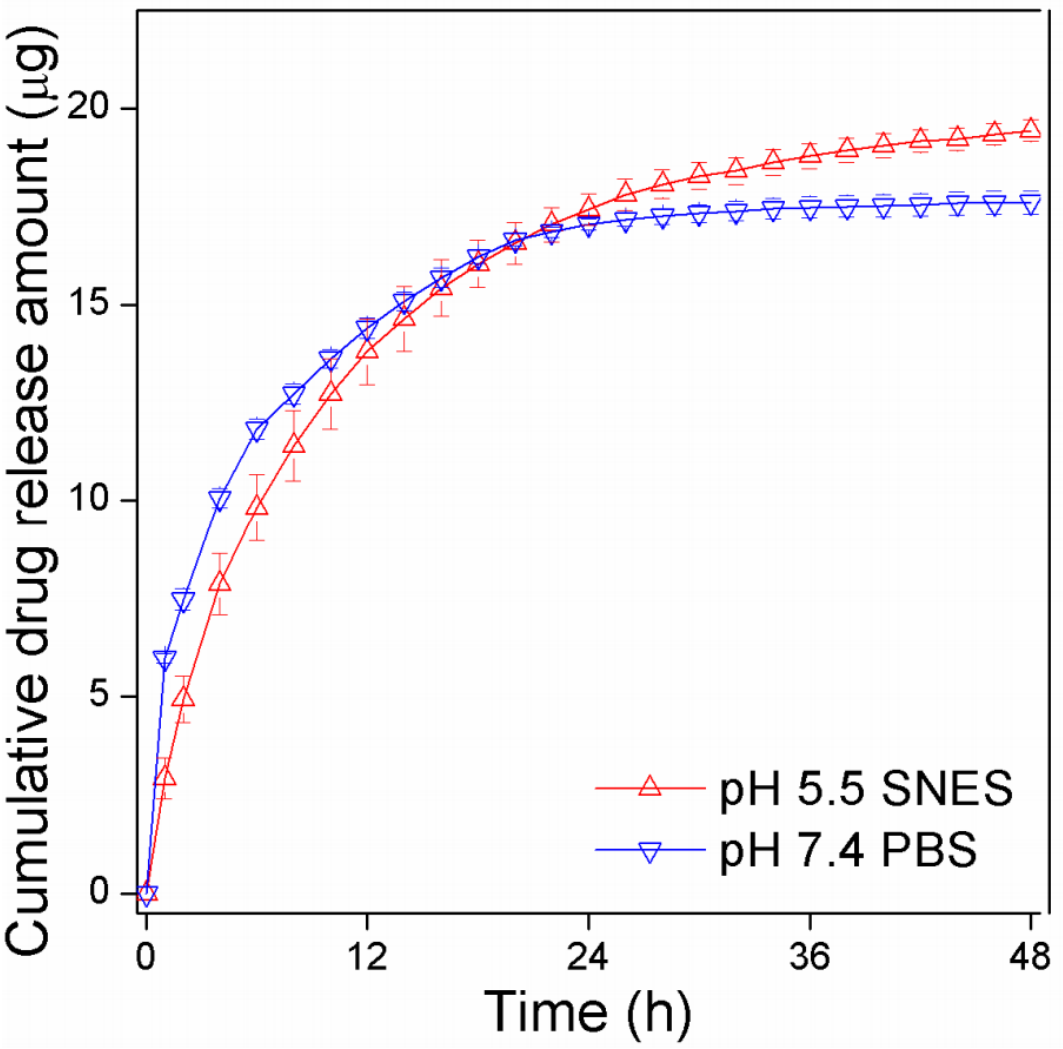

Figure 22. ***In vitro*** **release profiles of RSV from the PLGA/PEG NM obtained with pH 5.5 simulated nasal electrolyte solution containing 1% w/v Tween 20.** At defined time points, the release medium was collected and measured by HPLC, as depicted in the Methods section. The release profile obtained in pH 7.4 PBS (Figure 21) was replotted in the same graph for comparison. An overall release profile of RSV was not significantly different but a slightly higher release was observed at pH 5.5 compared with at pH 7.4. At pH 5.5, RSV is known to be more stable and thus, more effective RSV appeared to be available in the release medium.

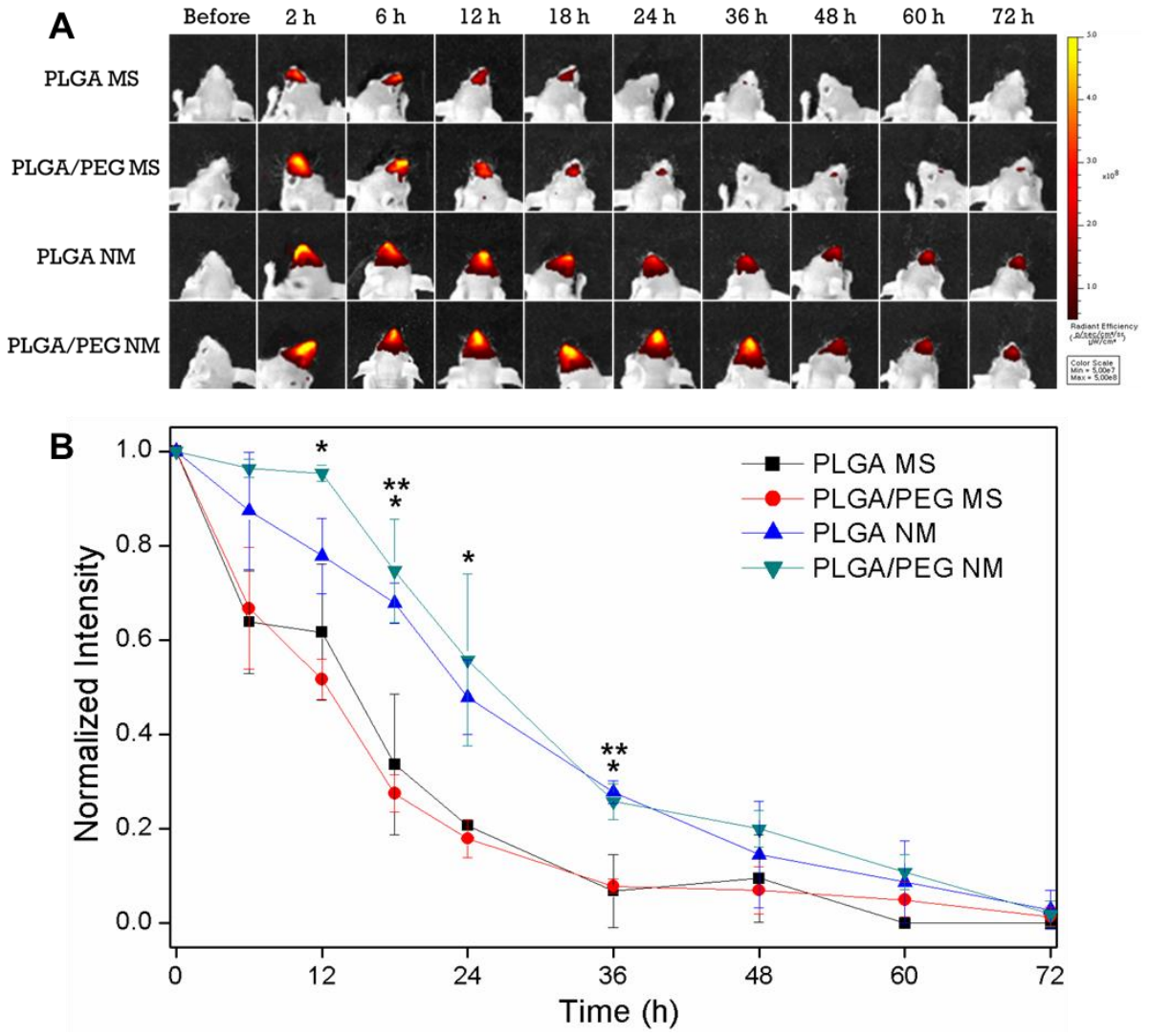

Figure 23. ***In vivo*** **sino-nasal retention profiles of micro-particles. (A)** Fluorescence images of the head were obtained using an *in vivo* imaging system at defined times after sinonasal administration of DTTCI-loaded micro-particle suspensions to male BALB/c mice. **(B)** The fraction of micro-particles remaining in the sino-nasal cavity was determined by measuring the intensity of the fluorescence signal in the nasal cavity in comparison to the maximal intensity obtained 2 h after administration. *At 12, 18, 24 and 36 h, PLGA/PEG NM were significantly different from PLGA MS and PLGA/PEG MS ($P < 0.05$). **At 18 and 36 h, PLGA NM were significantly different from PLGA MS and PLGA/PEG MS ($P < 0.05$).

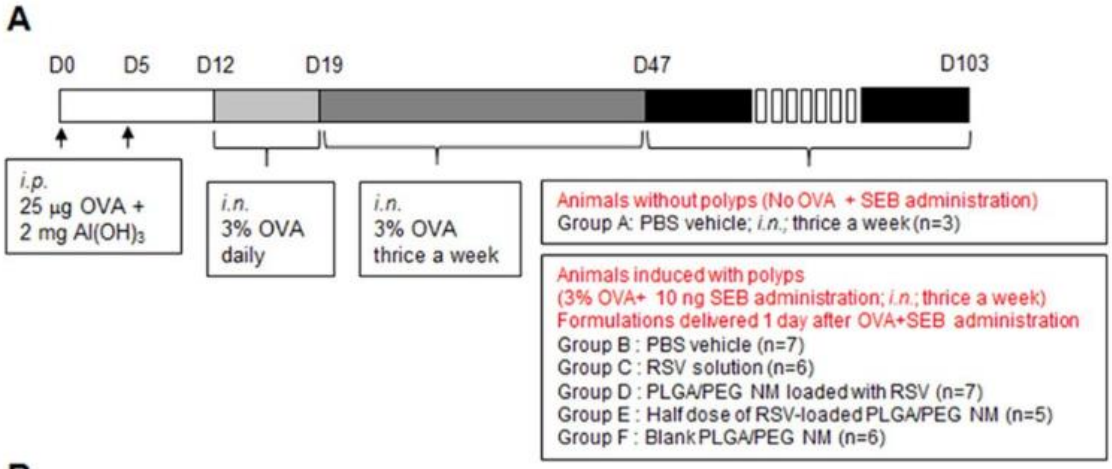
A
D0
D5
D12
D19
D47
D103
i.p.
25 μg OVA +
2 mg Al(OH)3
i.n.
3% OVA
daily
i.n.
3% OVA
thrice a week
Animals without polyps (No OVA + SEB administration)
Group A: PBS vehicle; i.n.; thrice a week (n=3)
Animals induced with polyps
(3% OVA+ 10 ng SEB administration; i.n.; thrice a week)
Formulations delivered 1 day after OVA+SEB administration
Group B : PBS vehicle (n=7)
Group C : RSV solution (n=6)
Group D : PLGA/PEG NM loaded with RSV (n=7)
Group E : Half dose of RSV-loaded PLGA/PEG NM (n=5)
Group F : Blank PLGA/PEG NM (n=6)

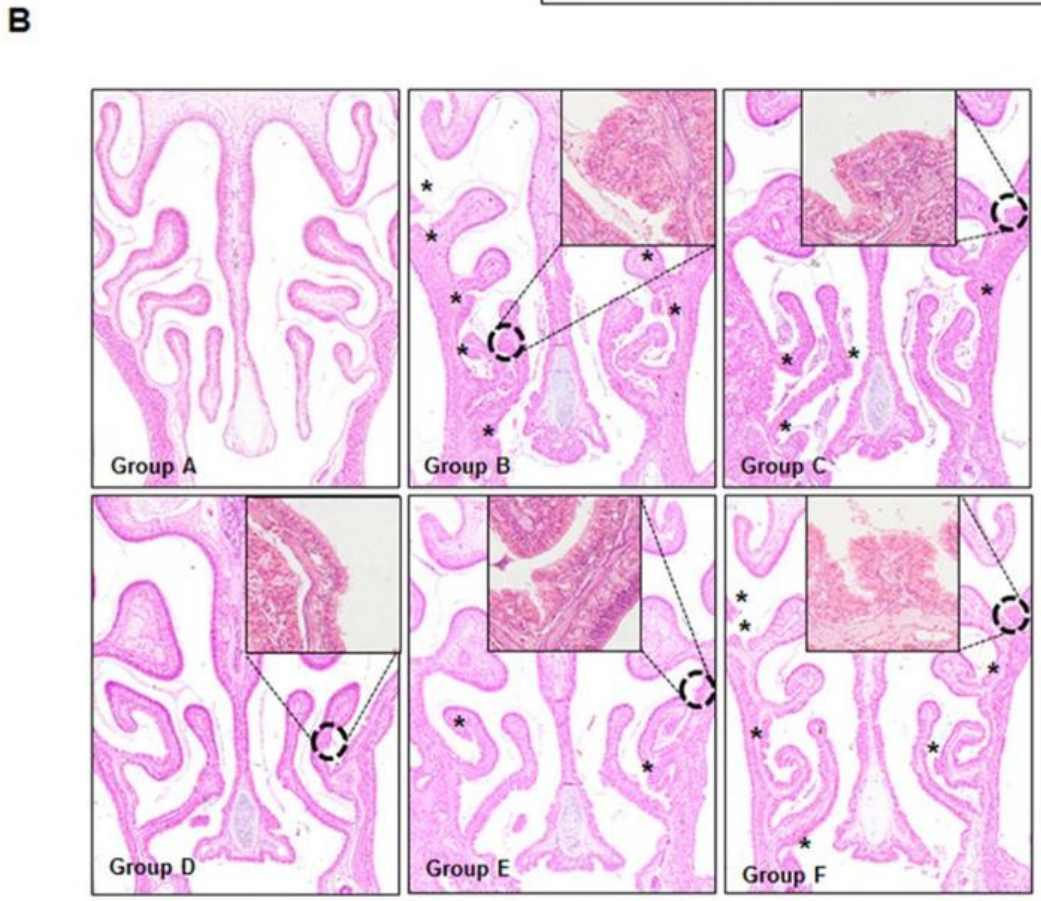
B
Group A
Group B
Group C
Group D
Group E
Group F

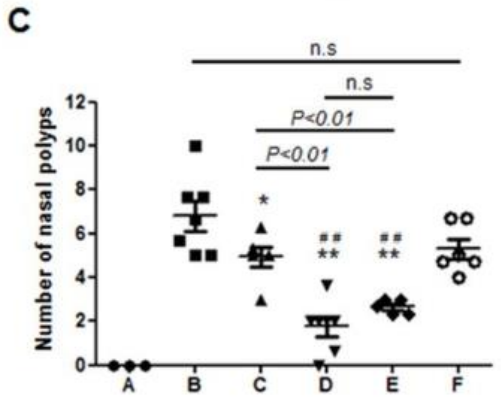
C
n.s
n.s
P<0.01
P<0.01
Number of nasal polyps
12
10
8
6
4
2
0
A
B
C
D
E
F

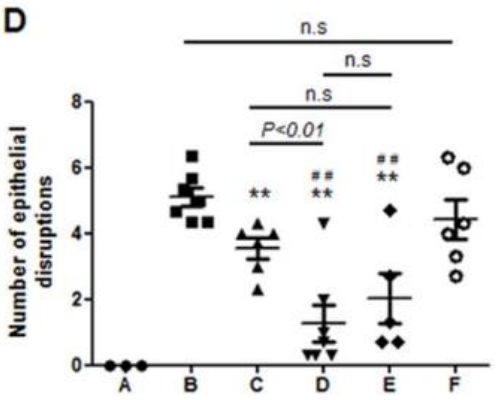
D
n.s
n.s
n.s
P<0.01
Number of epithelial disruptions
8
6
4
2
0
A
B
C
D
E
F

Figure 24. *In vivo* effects on nasal polyps and epithelial disruption. (A) Schematic illustration of the procedure for generating the murine nasal polyp (NP) animal model. To induce nasal polyps, mice were immunized with an intraperitoneal (i.p.) injection of 25 μg ovalbumin (OVA) in 2 mg of aluminum hydroxide gel on days 0 and 5, followed by daily intranasal (i.n.) administrations of 40 μl of a 3% OVA solution in phosphate-buffered saline (PBS; pH 7.4) at days 12 – 19. Subsequently, 40 μl of a 3% OVA solution was delivered intra-nsally 3 times per week until day 47. Finally, to maintain prolonged inflammation, 3% OVA solution (40 μl) and 10 ng of SEB (40 μl) were administered 3 times per week until the end point of the experiments. **(B)** Representative H&E-stained images of the posterior part of the nasal cavity. The inset, which is magnified from the dotted circle, shows a representative image of polyp formation. The asterisks indicate the locations of classical polypoid lesions. For each animal group, the numbers of **(C)** nasal polyps and **(D)** epithelial disruptions were counted and averaged in 3 distinct HPFs. Significant differences are denoted relative to Group B (PBS vehicle) (*$P < 0.05$, **$P < 0.01$) or to Group F (Blank PLGA/PEG NM) ($^{\#}P < 0.05$, $^{\#\#}P < 0.01$).

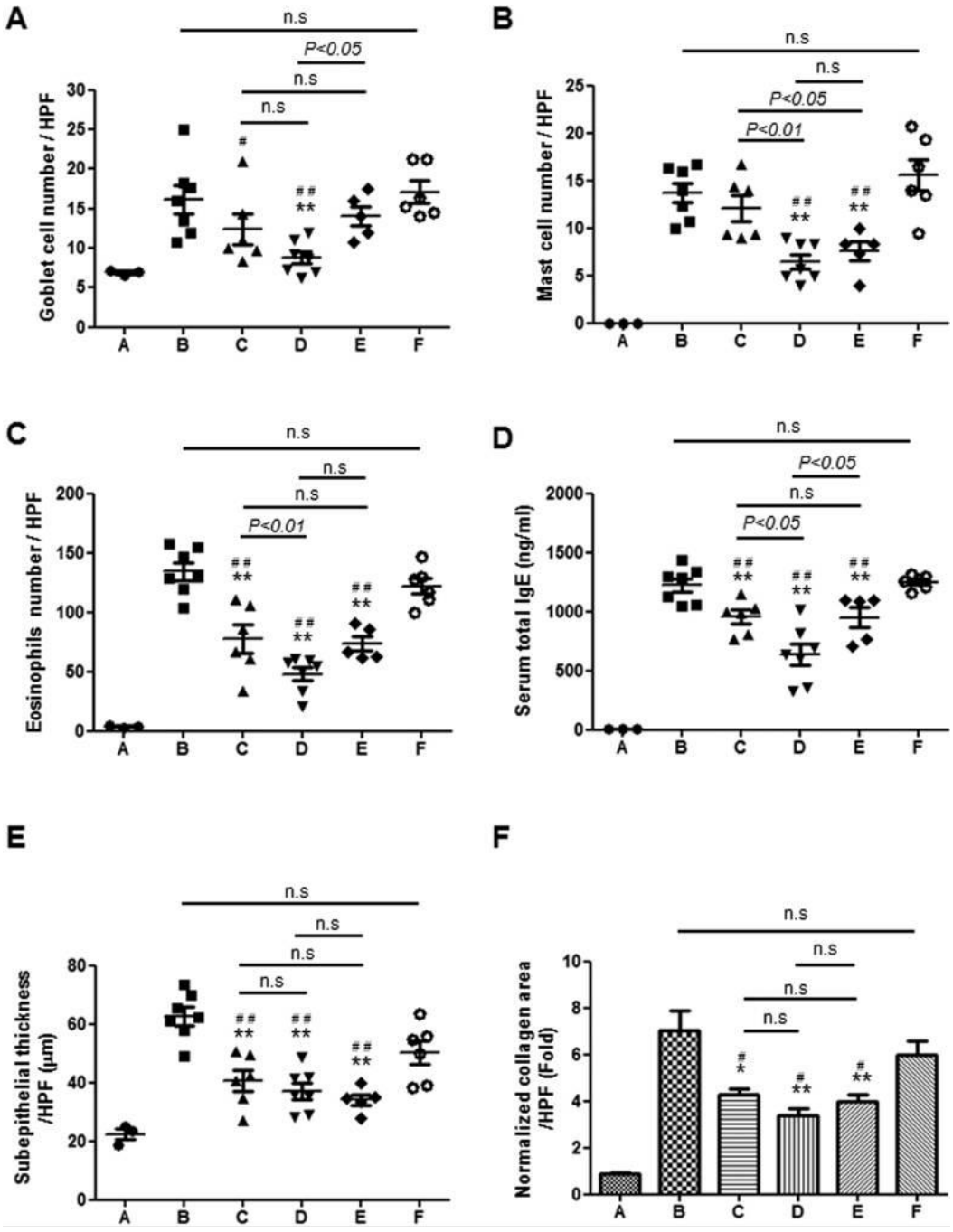

Figure 25. ***In vivo*** **evaluation of inflammatory markers.** For each animal group, the numbers of **(A)** goblet cells, **(B)** mast cells and **(C)** infiltrating eosinophils, **(D)** serum total IgE levels, **(E)** thickness of the sub-epithelial collagen layer and **(F)** areas of sub-epithelial collagen deposition were assessed and averaged from 3 distinct HPFs. Significant differences are denoted relative to Group B (PBS vehicle) ($*P < 0.05$, $**P < 0.01$) or to Group F (Blank PLGA/PEG NM) ($^{\#}P < 0.05$, $^{\#\#}P < 0.01$).

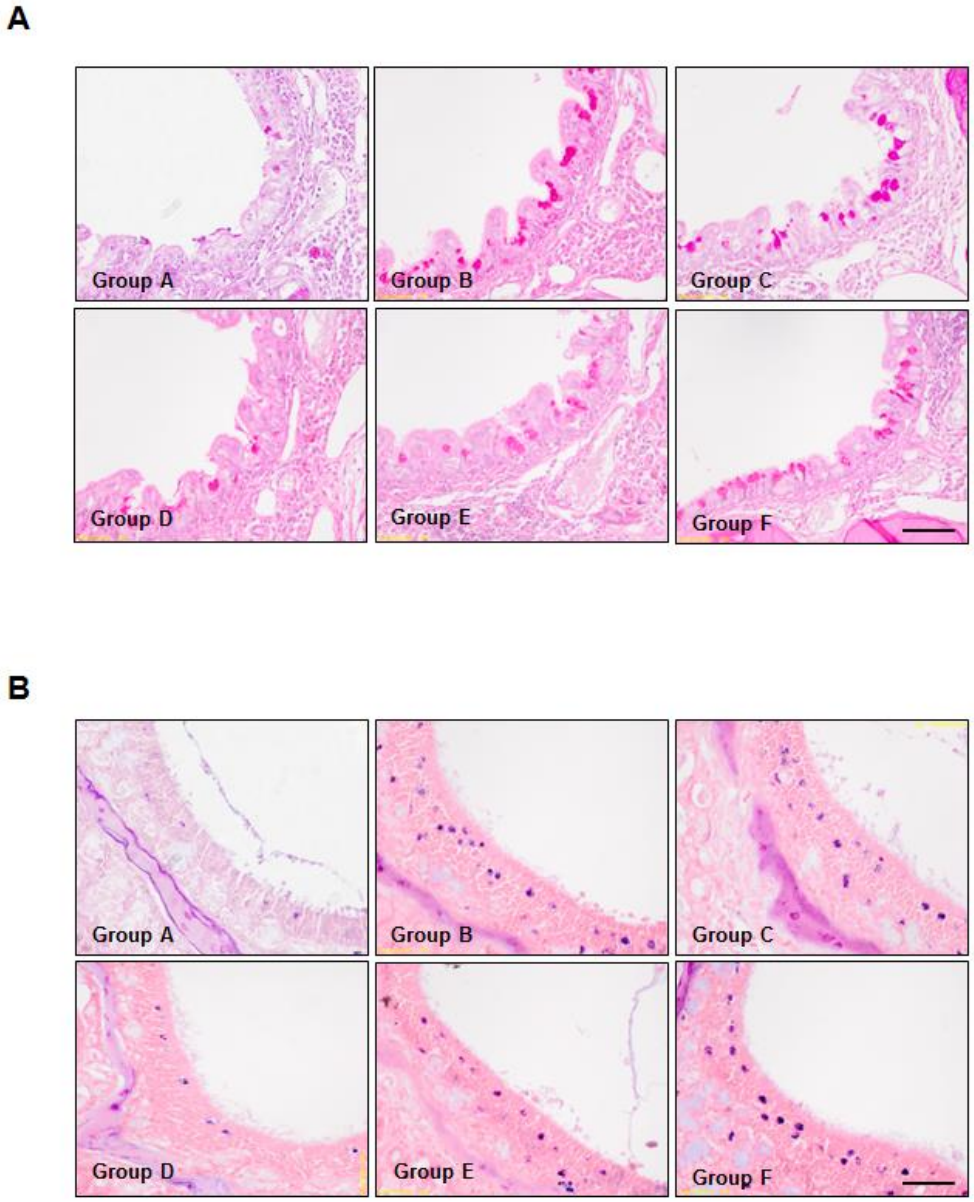

Figure 26. Representative photographs of sino-nasal tissues. (A) goblet cells, **(B)** mast cells, **(C)** eosinophils, and **(D)** collagen deposition.

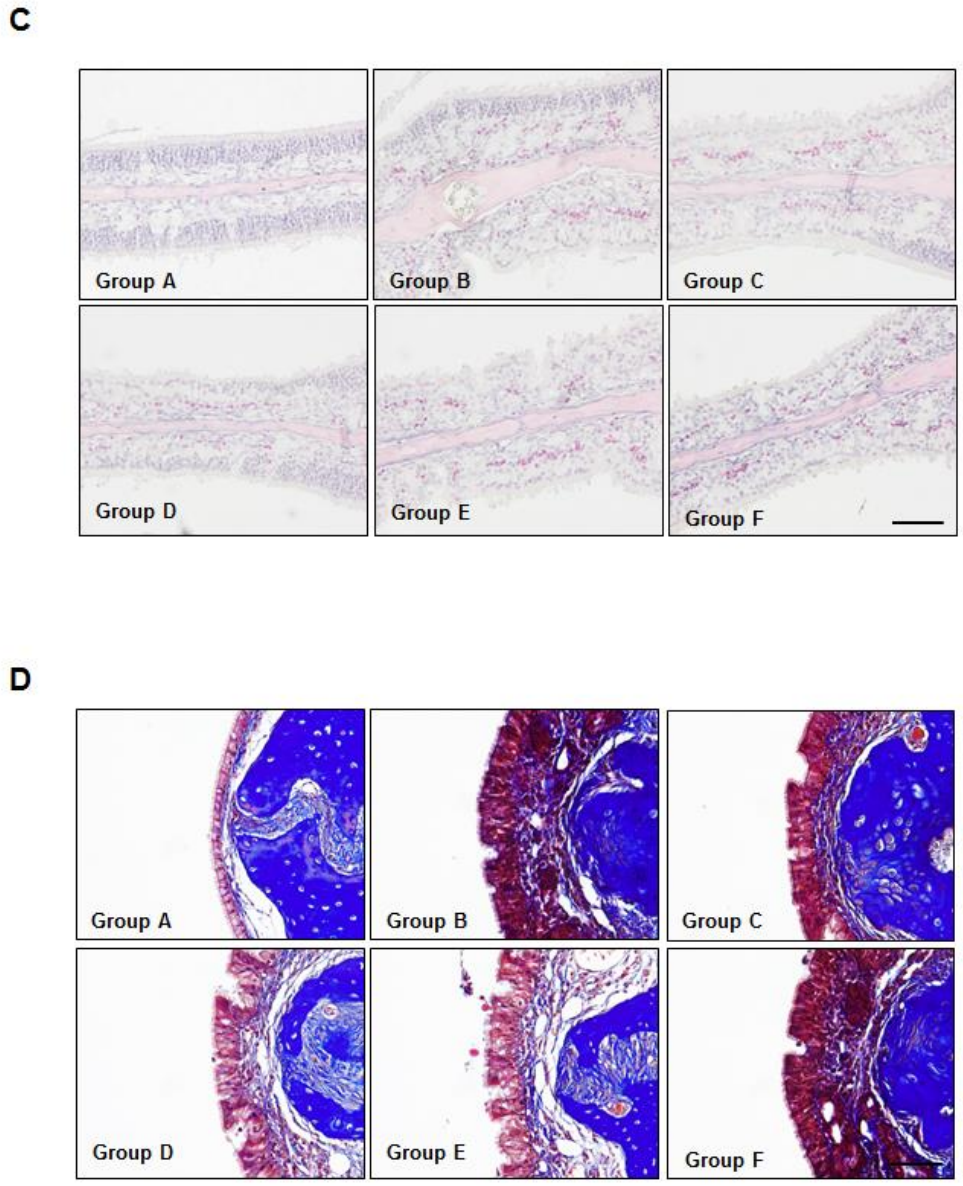

Figure 26. Representative photographs of sino-nasal tissues. **(A)** goblet cells, **(B)** mast cells, **(C)** eosinophils, and **(D)** collagen deposition.

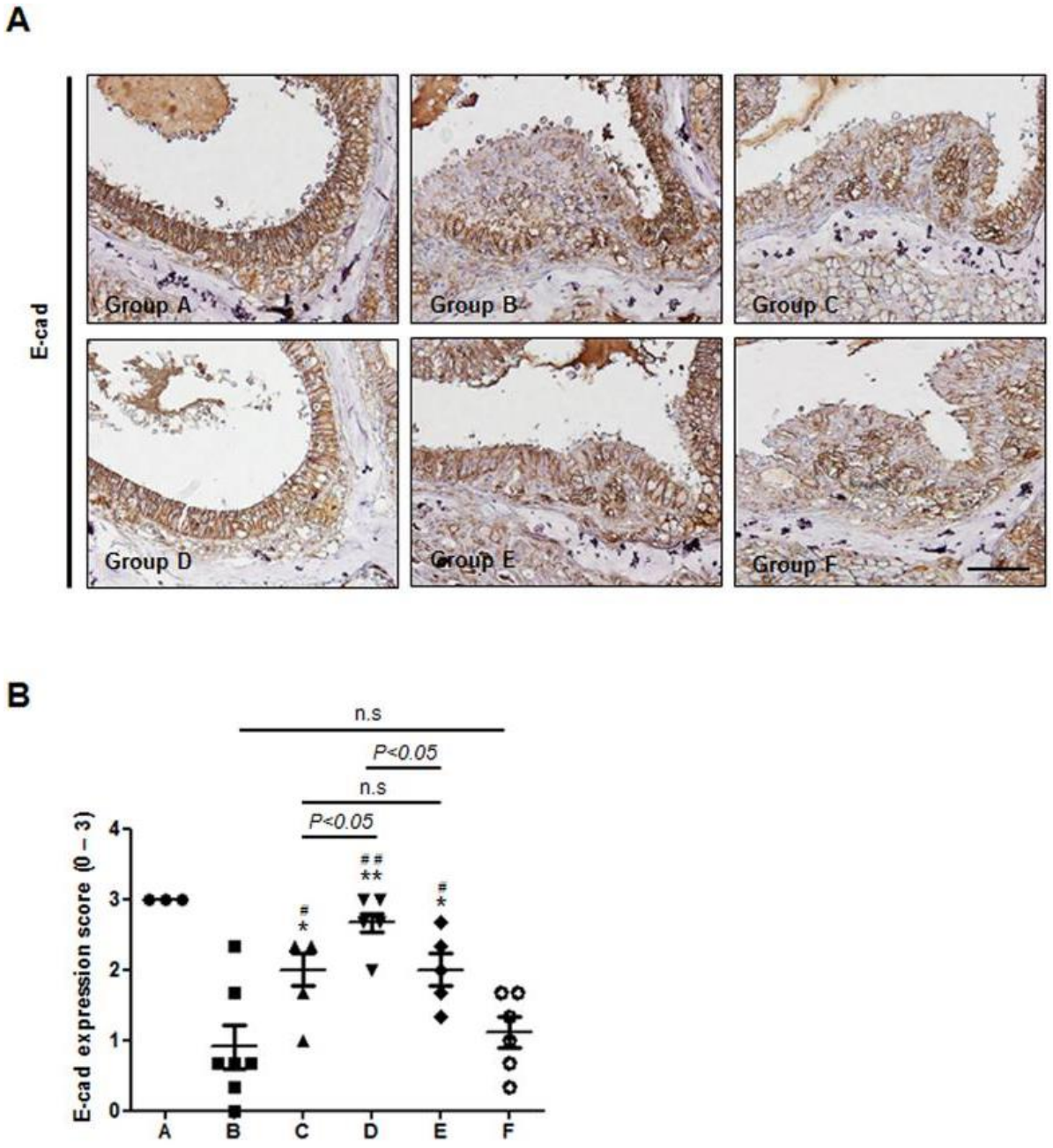

Figure 27. ***In vivo*** **efficacy of attenuating HIF-1α activity. (A)** Representative images of E-cadherin expression in the ethmoidal sinus mucosal epithelium. **(B)** Semi-quantitative score plots of E-cadherin expression. Significant differences are denoted relative to Group B (PBS vehicle) (*$P < 0.05$, **$P < 0.01$) or to Group F (Blank PLGA/PEG NM) ($^{\#}P < 0.05$, $^{\#\#}P < 0.01$).

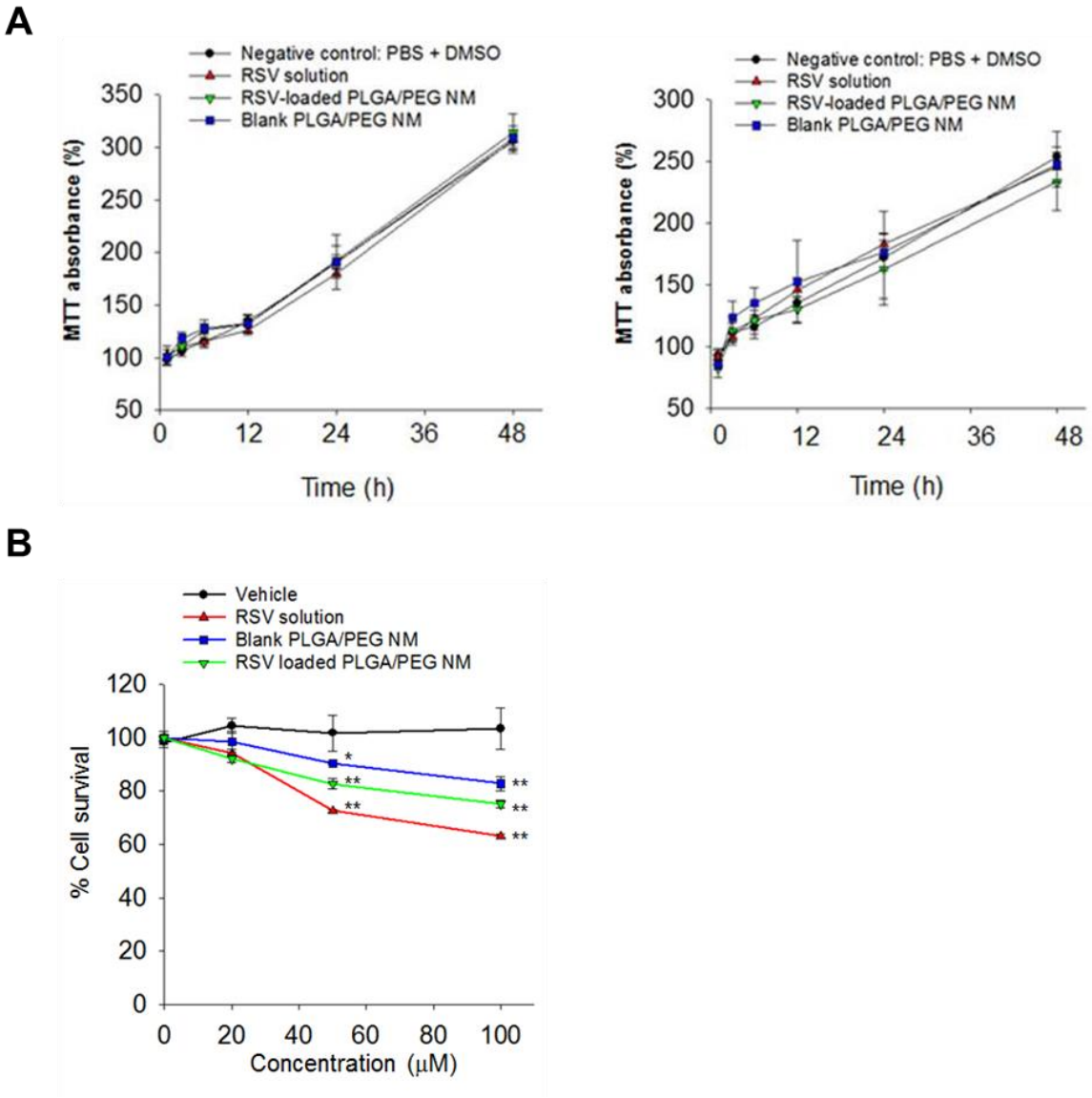

Figure 28. Evaluation of cytotoxicity of RSV, RSV-loaded PLGA/PEG NM and blank PLGA/PEG NM in cells. (A) The cytotoxicity of RSV, RSV-loaded PLGA/PEG NM and blank PLGA/PEG NM was evaluated with RPMI 2650 cells (nasal septum-derived squamous cell carcinoma, left) and with hNECs (human nasal epithelial cells, right). The relative cell viabilities at 48 h after treatment are expressed as percentages of the control (measured at 0 h). **(B)** Evaluation of the biocompatibility of RSV-loaded PLGA/PEG NM at varied concentrations. The cytotoxicity was evaluated with RPMI 2650 cells (nasal septum-derived squamous cell carcinoma). The cell viability was expressed as a percentage of the control (measured at 0 h).

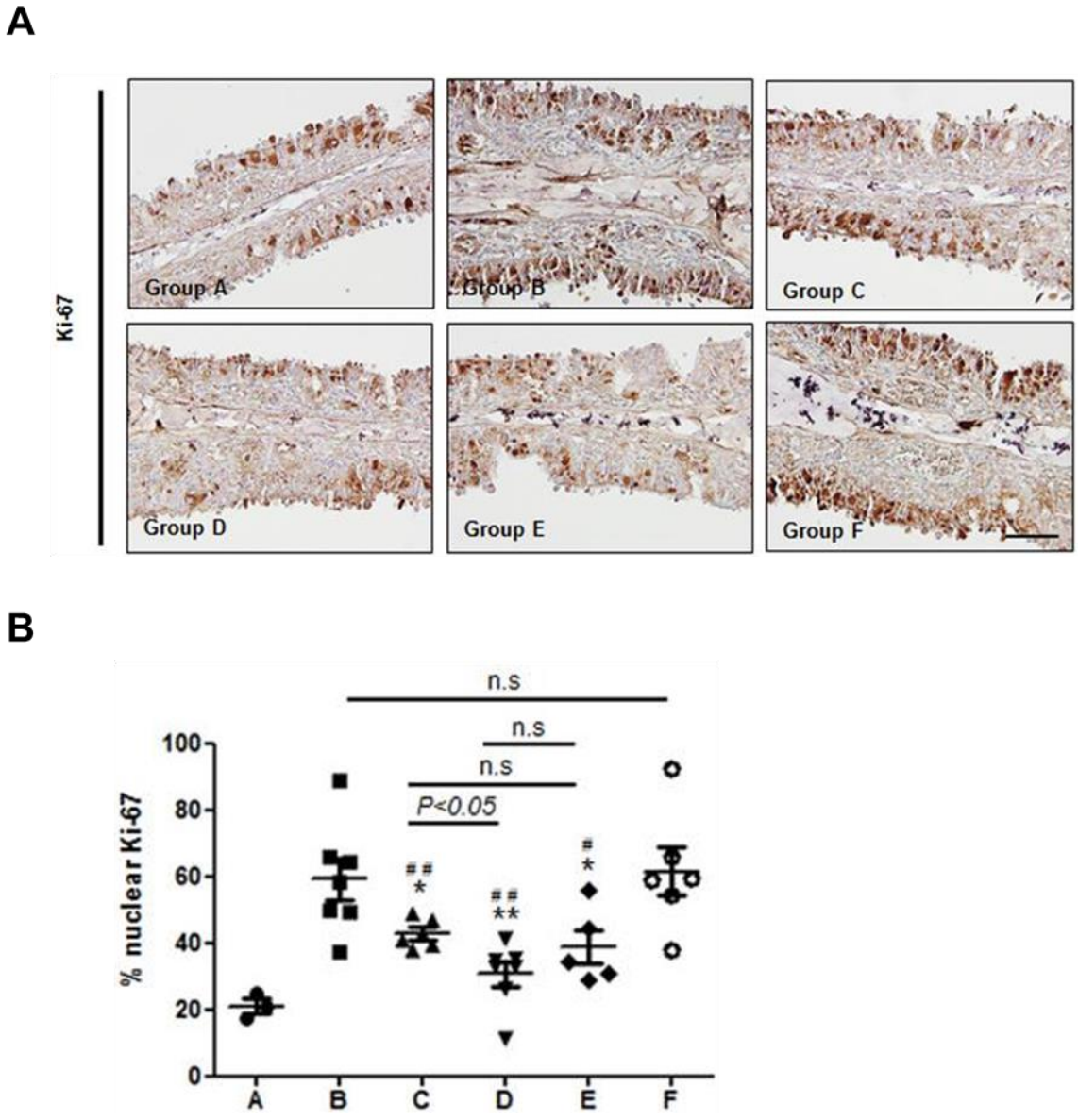

Figure 29. Evaluation of the biocompatibility of RSV-loaded PLGA/PEG NM. (A) Representative images of Ki-67 expression in the mucosal epithelium. **(B)** The numbers of Ki-67-positive nuclei within the nasal epithelium were counted in 3 different HPFs and averaged for each animal group. Significant differences are denoted relative to Group B (PBS vehicle) (**P* < 0.05, ***P* < 0.01) or to Group F (Blank PLGA/PEG NM) ($^{\#}P < 0.05$, $^{\#\#}P < 0.01$).

Table 3. Properties of the DTTCI-loaded micro-particles used in this work.

Micro-particle type	Mean size (μm)	PEG content (wt %)	Specific surface area (m^2/g)	DTTCI content (μg/mg)
PLGA MS	7.46 ± 1.32	0	N/D	8.87 ± 0.03
PLGA/PEG MS	7.64 ± 1.22	9.95	28.88	8.27 ± 0.11
PLGA NM	7.44 ± 0.98	0	N/D	8.16 ± 0.08
PLGA/PEG NM	6.72 ± 1.12	10.17	291.23	7.93 ± 0.05

N/D, not determined

Table 4. Properties of the RSV-loaded micro-particles used in this work.

Micro-particle Type	RSV Content (μg/mg)
PLGA MS	1.78 ± 0.10
PLGA/PEG MS	1.10 ± 0.03
PLGA NM	1.62 ± 0.03
PLGA/PEG NM	1.06 ± 0.02

Table 5. Half-lives of micro-particles administered to the sino-nasal cavity

Micro-particle type	Half-life (h)[†]
PLGA MS	10.5 ± 2.8
PLGA/PEG MS	9.1 ± 0.3
PLGA NM	21.5 ± 2.5
PLGA/PEG NM	23.5 ± 4.7

[†] Half-life was measured beginning 2 h after micro-particle administration.

2.3 DISCUSSION

RSV, which is abundant in red wine, grapes and blueberries, is known as a SIRT1 activator, and it is renowned for its anti-inflammatory, anti-oxidant and anti-cancer effects.[63, 64] Indeed, a large body of recent reports has verified the health-promoting bioactivity of RSV.[135-140] As one of its many effects, RSV has been reported to have a therapeutic effect on nasal polyps.[68, 125] However, the administration of RSV is limited by its very low aqueous solubility.[141, 142] Thus, when formulated in solution, the RSV concentration is so low that it is difficult for RSV to diffuse into the target tissue after administration. The RSV concentration can be increased by the use of an organic solvent as an additive in the formulation; however, this strategy may not be favorable for safety reasons.[143-145] Moreover, RSV in solution can be rapidly cleared from an administration site such as the sino-nasal cavity, further hampering drug absorption and thereby resulting in very low drug bioavailability.

Therefore, most recent studies have counteracted the low aqueous solubility of RSV by formulating it in nanoparticles, thereby increasing the specific surface area contacting the surrounding medium.[146-149] Nanoparticles also have the advantage of enhanced penetration through such delivery barriers as skin[150] or endothelial tissues.[151] However, the enhanced solubility of RSV may compensate for the relatively rapid release of RSV from the nanoparticles. In addition, previous approaches did not consider how well RSV was retained by carriers at the administration site, which is one of the important factors that determine local drug bioavailability.

The muco-adhesive nanostructured micro-particles described in this study have the advantage of a long residence time at the administration site in the sino-nasal cavity (Figure 23). My findings showed that the presence of a muco-adhesive substance alone (as in PLGA/PEG MS) appeared to improve micro-particle retention to some extent[152, 153]; however, a marked improvement was observed when muco-adhesion was synergistically enhanced by the enlarged specific surface area of the nanostructures in the PLGA/PEG NM (Table 3 and Figure 23). In addition to their improved adherence to the mucosal

layer in the sinonasal space, the PLGA/PEG NM released RSV in a sustained manner (Figure 21). After releasing 58.9% of the loaded RSV during the initial 6 h, RSV was slowly released at a rate of 1.14% per h throughout the half-life of PLGA/PEG NM (23.5 ± 4.7 h).

Therefore, the PLGA/PEG NM reported here can better mitigate polyp formation in an *in vivo* mouse model of eosinophilic rhinosinusitis with nasal polyps. My results showed a significant reduction in the number of nasal polyps with PLGA/PEG NM treatment compared with RSV solution treatment (Figure 24). This therapeutic effect may be ascribed to the enhanced anti-inflammatory effect of RSV (Figure 25) and to the more evident attenuation of HIF-1α expression due to higher SIRT1 activity (Figure 27).[125] Additionally, both the longer retention and sustained RSV-release properties of the PLGA/PEG NM in the sino-nasal cavity likely contribute to the improved therapeutic effects of RSV. An improvement in local RSV bioavailability is further suggested by the persistence of the effect, even with delivery of a half dose of the RSV-loaded PLGA/PEG NM.

Another advantage of the PLGA/PEG NM reported here is their good biocompatibility. PLGA is known to be highly biocompatible; thus it has already been used in a wide range of biomedical applications, such as biodegradable sutures, skin substitutes, and bio-absorbable bone fixation devices.[154-156] For the same reason, PEG has also been employed as a constituent of biological formulations[157] and has been widely researched as a bio-functional material.[76, 158, 159] In this work, I prepared PLGA/PEG NM by physically mixing the 2 biocompatible polymers. I attempted to enlarge the specific surface area of the PLGA/PEG NM to improve the muco-adhesive effect of the PEG additive (Figure 18 and Table 3). As the particles were of the order of microns in size, the PLGA/PEG NM would not be internalized by the cells, thereby minimizing the possibility of nanotoxicity.[160 161, 162] Accordingly, the PLGA/PEG NM were not cytotoxic to nasal septa or epithelial cells in my tests (Figure 28). Cell proliferation in the nasal mucosa was properly maintained when it was treated with RSV-loaded PLGA/PEG NM (Figure 29).

REFERENCES

1. Fokkens WJ, Lund VJ, Mullol J, Bachert C, Alobid I, Baroody F, et al. EPOS 2012: European position paper on rhinosinusitis and nasal polyps 2012. A summary for otorhinolaryngologists. Rhinology 2012; 50:1-12.

2. Slavin RG, Spector SL, Bernstein IL, Kaliner MA, Kennedy DW, Virant FS, et al. The diagnosis and management of sinusitis: a practice parameter update. J Allergy Clin Immunol 2005; 116:S13-47.

3. Hastan D, Fokkens WJ, Bachert C, Newson RB, Bislimovska J, Bockelbrink A, et al. Chronic rhinosinusitis in Europe--an underestimated disease. A GA(2)LEN study. Allergy 2011; 66:1216-23.

4. Pleis JR, Ward BW, Lucas JW. Summary health statistics for U.S. adults: National Health Interview Survey, 2009. Vital Health Stat 10 2010:1-207.

5. Kim YS, Kim NH, Seong SY, Kim KR, Lee GB, Kim KS. Prevalence and risk factors of chronic rhinosinusitis in Korea. Am J Rhinol Allergy 2011; 25:117-21.

6. Meltzer EO, Hamilos DL, Hadley JA, Lanza DC, Marple BF, Nicklas RA, et al. Rhinosinusitis: establishing definitions for clinical research and patient care. J Allergy Clin Immunol 2004; 114:155-212.

7. Rosenfeld RM, Piccirillo JF, Chandrasekhar SS, Brook I, Ashok Kumar K, Kramper M, et al. Clinical practice guideline (update): adult sinusitis. Otolaryngol Head Neck Surg 2015; 152:S1-

S39.

8. Senior BA, Kennedy DW, Tanabodee J, Kroger H, Hassab M, Lanza D. Long-term results of functional endoscopic sinus surgery. Laryngoscope 1998; 108:151-7.

9. Schleimer RP. Immunopathogenesis of Chronic Rhinosinusitis and Nasal Polyposis. Annu Rev Pathol 2017; 12:331-57.

10. Tan BK, Kern RC, Schleimer RP, Schwartz BS. Chronic rhinosinusitis: the unrecognized epidemic. Am J Respir Crit Care Med 2013; 188:1275-7.

11. Tan BK, Chandra RK, Pollak J, Kato A, Conley DB, Peters AT, et al. Incidence and associated premorbid diagnoses of patients with chronic rhinosinusitis. J Allergy Clin Immunol 2013; 131:1350-60.

12. Bhattacharyya N, Orlandi RR, Grebner J, Martinson M. Cost burden of chronic rhinosinusitis: a claims-based study. Otolaryngol Head Neck Surg 2011; 144:440-5.

13. Smith KA, Orlandi RR, Rudmik L. Cost of adult chronic rhinosinusitis: A systematic review. Laryngoscope 2015; 125:1547-56.

14. Casale M, Pappacena M, Potena M, Vesperini E, Ciglia G, Mladina R, et al. Nasal polyposis: from pathogenesis to treatment, an update. Inflamm Allergy Drug Targets 2011; 10:158-63.

15. Kakoi H, Hiraide F. A histological study of formation and growth of nasal polyps. Acta Otolaryngol 1987; 103:137-44.

16. Ishitoya J, Sakuma Y, Tsukuda M. Eosinophilic chronic rhinosinusitis in Japan. Allergol Int 2010; 59:239-45.

17. Hu Y, Cao PP, Liang GT, Cui YH, Liu Z. Diagnostic significance of blood eosinophil count in eosinophilic chronic rhinosinusitis with nasal polyps in Chinese adults. Laryngoscope 2012; 122:498-503.

18. Cao PP, Li HB, Wang BF, Wang SB, You XJ, Cui YH, et al. Distinct immunopathologic characteristics of various types of chronic rhinosinusitis in adult Chinese. J Allergy Clin Immunol 2009; 124:478-84, 84 e1-2.

19. Kim SJ, Lee KH, Kim SW, Cho JS, Park YK, Shin SY. Changes in histological features of nasal polyps in a Korean population over a 17-year period. Otolaryngol Head Neck Surg 2013; 149:431-7.

20. Kountakis SE, Arango P, Bradley D, Wade ZK, Borish L. Molecular and cellular staging for the severity of chronic rhinosinusitis. Laryngoscope 2004; 114:1895-905.

21. Snidvongs K, Chin D, Sacks R, Earls P, Harvey RJ. Eosinophilic rhinosinusitis is not a disease of ostiomeatal occlusion. Laryngoscope 2013; 123:1070-4.

22. Soler ZM, Sauer D, Mace J, Smith TL. Impact of mucosal eosinophilia and nasal polyposis on quality-of-life outcomes after sinus surgery. Otolaryngol Head Neck Surg 2010; 142:64-71.

23. Wang MJ, Zhou B, Li YC, Huang Q. [The role of peripheral blood eosinophil percentage in classification of chronic rhinosinusitis with nasal polyps]. Zhonghua Er Bi Yan Hou Tou Jing

Wai Ke Za Zhi 2013; 48:650-3.

24. Ikeda K, Shiozawa A, Ono N, Kusunoki T, Hirotsu M, Homma H, et al. Subclassification of chronic rhinosinusitis with nasal polyp based on eosinophil and neutrophil. Laryngoscope 2013; 123:E1-9.

25. Mori E, Matsuwaki Y, Mitsuyama C, Okushi T, Nakajima T, Moriyama H. Risk factors for olfactory dysfunction in chronic rhinosinusitis. Auris Nasus Larynx 2013; 40:465-9.

26. Kim JW, Hong SL, Kim YK, Lee CH, Min YG, Rhee CS. Histological and immunological features of non-eosinophilic nasal polyps. Otolaryngol Head Neck Surg 2007; 137:925-30.

27. Yoshimura K, Kawata R, Haruna S, Moriyama H, Hirakawa K, Fujieda S, et al. Clinical epidemiological study of 553 patients with chronic rhinosinusitis in Japan. Allergol Int 2011; 60:491-6.

28. Wen W, Liu W, Zhang L, Bai J, Fan Y, Xia W, et al. Increased neutrophilia in nasal polyps reduces the response to oral corticosteroid therapy. J Allergy Clin Immunol 2012; 129:1522-8 e5.

29. Jankowski R. Eosinophils in the pathophysiology of nasal polyposis. Acta Otolaryngol 1996; 116:160-3.

30. Mygind N, Dahl R, Bachert C. Nasal polyposis, eosinophil dominated inflammation, and allergy. Thorax 2000; 55 Suppl 2:S79-83.

31. Van Bruaene N, Perez-Novo CA, Basinski TM, Van Zele T, Holtappels G, De Ruyck N, et al. T-cell regulation in chronic paranasal sinus disease. J Allergy Clin Immunol 2008; 121:1435-41, 41 e1-3.

32. Van Zele T, Claeys S, Gevaert P, Van Maele G, Holtappels G, Van Cauwenberge P, et al. Differentiation of chronic sinus diseases by measurement of inflammatory mediators. Allergy 2006; 61:1280-9.

33. Mahdavinia M, Suh LA, Carter RG, Stevens WW, Norton JE, Kato A, et al. Increased noneosinophilic nasal polyps in chronic rhinosinusitis in US second-generation Asians suggest genetic regulation of eosinophilia. J Allergy Clin Immunol 2015; 135:576-9.

34. Zhang N, Van Zele T, Perez-Novo C, Van Bruaene N, Holtappels G, DeRuyck N, et al. Different types of T-effector cells orchestrate mucosal inflammation in chronic sinus disease. J Allergy Clin Immunol 2008; 122:961-8.

35. Stevens WW, Lee RJ, Schleimer RP, Cohen NA. Chronic rhinosinusitis pathogenesis. J Allergy Clin Immunol 2015; 136:1442-53.

36. Akdis CA, Bachert C, Cingi C, Dykewicz MS, Hellings PW, Naclerio RM, et al. Endotypes and phenotypes of chronic rhinosinusitis: a PRACTALL document of the European Academy of Allergy and Clinical Immunology and the American Academy of Allergy, Asthma & Immunology. J Allergy Clin Immunol 2013; 131:1479-90.

37. Van Bruaene N, Bachert C. Tissue remodeling in chronic rhinosinusitis. Curr Opin Allergy Clin Immunol 2011; 11:8-11.

38. Konnecke M, Burmeister M, Pries R, Boscke R, Bruchhage KL, Ungefroren H, et al. Epithelial-Mesenchymal Transition in Chronic Rhinosinusitis: Differences Revealed Between Epithelial Cells from Nasal Polyps and Inferior Turbinates. Arch Immunol Ther Exp (Warsz) 2017; 65:157-73.

39. Hackett TL. Epithelial-mesenchymal transition in the pathophysiology of airway remodelling in asthma. Curr Opin Allergy Clin Immunol 2012; 12:53-9.

40. Hackett TL, Warner SM, Stefanowicz D, Shaheen F, Pechkovsky DV, Murray LA, et al. Induction of epithelial-mesenchymal transition in primary airway epithelial cells from patients with asthma by transforming growth factor-beta1. Am J Respir Crit Care Med 2009; 180:122-33.

41. Lamouille S, Xu J, Derynck R. Molecular mechanisms of epithelial-mesenchymal transition. Nat Rev Mol Cell Biol 2014; 15:178-96.

42. Kalluri R, Neilson EG. Epithelial-mesenchymal transition and its implications for fibrosis. J Clin Invest 2003; 112:1776-84.

43. Lee HS, Myers A, Kim J. Vascular endothelial growth factor drives autocrine epithelial cell proliferation and survival in chronic rhinosinusitis with nasal polyposis. Am J Respir Crit Care Med 2009; 180:1056-67.

44. Hupin C, Gohy S, Bouzin C, Lecocq M, Polette M, Pilette C. Features of mesenchymal transition in the airway epithelium from chronic rhinosinusitis. Allergy 2014; 69:1540-9.

45. Shin HW, Cho K, Kim DW, Han DH, Khalmuratova R, Kim SW, et al. Hypoxia-inducible factor 1 mediates nasal polypogenesis by inducing epithelial-to-mesenchymal transition. Am J Respir Crit Care Med 2012; 185:944-54.

46. Lin SK, Shun CT, Kok SH, Wang CC, Hsiao TY, Liu CM. Hypoxia-stimulated vascular endothelial growth factor production in human nasal polyp fibroblasts: effect of epigallocatechin-3-gallate on hypoxia-inducible factor-1 alpha synthesis. Arch Otolaryngol Head Neck Surg 2008; 134:522-7.

47. van Uden P, Kenneth NS, Rocha S. Regulation of hypoxia-inducible factor-1alpha by NF-kappaB. Biochem J 2008; 412:477-84.

48. Palazon A, Goldrath AW, Nizet V, Johnson RS. HIF transcription factors, inflammation, and immunity. Immunity 2014; 41:518-28.

49. Giaccia A, Siim BG, Johnson RS. HIF-1 as a target for drug development. Nature Reviews Drug Discovery 2003; 2:803-11.

50. Semenza GL. Hypoxia-inducible factors in physiology and medicine. Cell 2012; 148:399-408.

51. Chang HC, Guarente L. SIRT1 and other sirtuins in metabolism. Trends Endocrinol Metab 2014; 25:138-45.

52. Michan S, Sinclair D. Sirtuins in mammals: insights into their biological function. Biochem J 2007; 404:1-13.

53. Yamamoto H, Schoonjans K, Auwerx J. Sirtuin functions in health and disease. Mol Endocrinol 2007; 21:1745-55.

54. Guarente L. Calorie restriction and sirtuins revisited. Genes Dev 2013; 27:2072-85.

55. Morris BJ. Seven sirtuins for seven deadly diseases of aging. Free Radic Biol Med 2013; 56:133-71.

56. Donmez G, Guarente L. Aging and disease: connections to sirtuins. Aging Cell 2010; 9:285-90.

57. Haigis MC, Guarente LP. Mammalian sirtuins--emerging roles in physiology, aging, and calorie restriction. Genes Dev 2006; 20:2913-21.

58. Pillarisetti S. A review of Sirt1 and Sirt1 modulators in cardiovascular and metabolic diseases. Recent Pat Cardiovasc Drug Discov 2008; 3:156-64.

59. Haigis MC, Guarente LP. Mammalian sirtuins - emerging roles in physiology, aging, and calorie restriction. Genes & Development 2006; 20:2913-21.

60. Lim JH, Lee YM, Chun YS, Chen J, Kim JE, Park JW. Sirtuin 1 modulates cellular responses to hypoxia by deacetylating hypoxia-inducible factor 1alpha. Mol Cell 2010; 38:864-78.

61. Yoon H, Shin SH, Shin DH, Chun YS, Park JW. Differential roles of Sirt1 in HIF-1alpha and HIF-2alpha mediated hypoxic responses. Biochem Biophys Res Commun 2014; 444:36-43.

62. Lavu S, Boss O, Elliott PJ, Lambert PD. Sirtuins--novel therapeutic targets to treat age-

associated diseases. Nat Rev Drug Discov 2008; 7:841-53.

63. Jang M, Cai L, Udeani GO, Slowing KV, Thomas CF, Beecher CW, et al. Cancer chemopreventive activity of resveratrol, a natural product derived from grapes. Science 1997; 275:218-20.

64. Baur JA, Sinclair DA. Therapeutic potential of resveratrol: the in vivo evidence. Nat Rev Drug Discov 2006; 5:493-506.

65. Kundu JK, Surh YJ. Cancer chemopreventive and therapeutic potential of resveratrol: mechanistic perspectives. Cancer Lett 2008; 269:243-61.

66. Chung S, Yao H, Caito S, Hwang JW, Arunachalam G, Rahman I. Regulation of SIRT1 in cellular functions: role of polyphenols. Arch Biochem Biophys 2010; 501:79-90.

67. Berman AY, Motechin RA, Wiesenfeld MY, Holz MK. The therapeutic potential of resveratrol: a review of clinical trials. NPJ Precis Oncol 2017; 1.

68. Kim SW, Kim DW, Khalmuratova R, Kim JH, Jung MH, Chang DY, et al. Resveratrol prevents development of eosinophilic rhinosinusitis with nasal polyps in a mouse model. Allergy 2013; 68:862-9.

69. Simic P, Williams EO, Bell EL, Gong JJ, Bonkowski M, Guarente L. SIRT1 suppresses the epithelial-to-mesenchymal transition in cancer metastasis and organ fibrosis. Cell Rep 2013; 3:1175-86.

70. Robinson K, Mock C, Liang D. Pre-formulation studies of resveratrol. Drug Dev Ind Pharm 2015; 41:1464-9.

71. Kim DW, Khalmuratova R, Hur DG, Jeon SY, Kim SW, Shin HW, et al. Staphylococcus aureus enterotoxin B contributes to induction of nasal polypoid lesions in an allergic rhinosinusitis murine model. Am J Rhinol Allergy 2011; 25:e255-61.

72. Zupancic S, Lavric Z, Kristl J. Stability and solubility of trans-resveratrol are strongly influenced by pH and temperature. Eur J Pharm Biopharm 2015; 93:196-204.

73. Hines DJ, Kaplan DL. Poly(lactic-co-glycolic) acid-controlled-release systems: experimental and modeling insights. Crit Rev Ther Drug Carrier Syst 2013; 30:257-76.

74. Makadia HK, Siegel SJ. Poly Lactic-co-Glycolic Acid (PLGA) as Biodegradable Controlled Drug Delivery Carrier. Polymers (Basel) 2011; 3:1377-97.

75. Salamat-Miller N, Chittchang M, Johnston TP. The use of mucoadhesive polymers in buccal drug delivery. Advanced Drug Delivery Reviews 2005; 57:1666-91.

76. Ludwig A. The use of mucoadhesive polymers in ocular drug delivery. Advanced Drug Delivery Reviews 2005; 57:1595-639.

77. Park CG, Kim YK, Kim MJ, Park M, Kim MH, Lee SH, et al. Mucoadhesive microparticles with a nanostructured surface for enhanced bioavailability of glaucoma drug. J Control Release 2015; 220:180-8.

78. Park CG, Kim MJ, Park M, Choi SY, Lee SH, Lee JE, et al. Nanostructured mucoadhesive microparticles for enhanced preocular retention. Acta Biomater 2014; 10:77-86.

79. Lee D-W, Shirley SA, Lockey RF, Mohapatra SS. Thiolated chitosan nanoparticles enhance anti-inflammatory effects of intranasally delivered theophylline. Respiratory research 2006; 7:1.

80. Slutter B, Bal S, Keijzer C, Mallants R, Hagenaars N, Que I, et al. Nasal vaccination with N-trimethyl chitosan and PLGA based nanoparticles: nanoparticle characteristics determine quality and strength of the antibody response in mice against the encapsulated antigen. Vaccine 2010; 28:6282-91.

81. Wang H, Lu X, Cao PP, Chu Y, Long XB, Zhang XH, et al. Histological and immunological observations of bacterial and allergic chronic rhinosinusitis in the mouse. Am J Rhinol 2008; 22:343-8.

82. Shin SH, Ponikau JU, Sherris DA, Congdon D, Frigas E, Homburger HA, et al. Chronic rhinosinusitis: an enhanced immune response to ubiquitous airborne fungi. J Allergy Clin Immunol 2004; 114:1369-75.

83. Spector SL, Bernstein IL, Li JT, Berger WE, Kaliner MA, Schuller DE, et al. Parameters for the diagnosis and management of sinusitis. J Allergy Clin Immunol 1998; 102:S107-44.

84. Bousquet J, Khaltaev N, Cruz AA, Denburg J, Fokkens WJ, Togias A, et al. Allergic Rhinitis and its Impact on Asthma (ARIA) 2008 update (in collaboration with the World Health Organization, GA(2)LEN and AllerGen). Allergy 2008; 63 Suppl 86:8-160.

85. Bachert C, Van Bruaene N, Toskala E, Zhang N, Olze H, Scadding G, et al. Important research questions in allergy and related diseases: 3-chronic rhinosinusitis and nasal polyposis - a GALEN study. Allergy 2009; 64:520-33.

86. Banerji A, Piccirillo JF, Thawley SE, Levitt RG, Schechtman KB, Kramper MA, et al. Chronic rhinosinusitis patients with polyps or polypoid mucosa have a greater burden of illness. Am J Rhinol 2007; 21:19-26.

87. Jin J, Chang DY, Kim SH, Rha KS, Mo JH, Shin EC, et al. Role of hypoxia-inducible factor-1alpha expression in regulatory T cells on nasal polypogenesis. Laryngoscope 2014; 124:E151-9.

88. Catrina SB, Okamoto K, Pereira T, Brismar K, Poellinger L. Hyperglycemia regulates hypoxia-inducible factor-1alpha protein stability and function. Diabetes 2004; 53:3226-32.

89. Taylor PC, Sivakumar B. Hypoxia and angiogenesis in rheumatoid arthritis. Curr Opin Rheumatol 2005; 17:293-8.

90. Rius J, Guma M, Schachtrup C, Akassoglou K, Zinkernagel AS, Nizet V, et al. NF-kappaB links innate immunity to the hypoxic response through transcriptional regulation of HIF-1alpha. Nature 2008; 453:807-11.

91. Houtkooper RH, Pirinen E, Auwerx J. Sirtuins as regulators of metabolism and healthspan. Nature Reviews Molecular Cell Biology 2012; 13:225-38.

92. Dali-Youcef N, Lagouge M, Froelich S, Koehl C, Schoonjans K, Auwerx J. Sirtuins: The

'magnificent seven', function, metabolism and longevity. Annals of Medicine 2007; 39:335-45.

93. Lavu S, Boss O, Elliott PJ, Lambert PD. Sirtuins - novel therapeutic targets to treat age-associated diseases (vol 7, pg 841, 2008). Nature Reviews Drug Discovery 2009; 8.

94. Shin HW, Cho CH, Kim TY, Park JW. Sunitinib deregulates tumor adaptation to hypoxia by inhibiting HIF-1alpha synthesis in HT-29 colon cancer cells. Biochem Biophys Res Commun 2010; 398:205-11.

95. Thiery JP, Acloque H, Huang RY, Nieto MA. Epithelial-mesenchymal transitions in development and disease. Cell 2009; 139:871-90.

96. Sun S, Ning X, Zhang Y, Lu Y, Nie Y, Han S, et al. Hypoxia-inducible factor-1alpha induces Twist expression in tubular epithelial cells subjected to hypoxia, leading to epithelial-to-mesenchymal transition. Kidney Int 2009; 75:1278-87.

97. Higgins DF, Kimura K, Bernhardt WM, Shrimanker N, Akai Y, Hohenstein B, et al. Hypoxia promotes fibrogenesis in vivo via HIF-1 stimulation of epithelial-to-mesenchymal transition. J Clin Invest 2007; 117:3810-20.

98. Chien CY, Tai CF, Ho KY, Kuo WR, Chai CY, Hsu YC, et al. Expression of hypoxia-inducible factor 1alpha in the nasal polyps by real-time RT-PCR and immunohistochemistry. Otolaryngol Head Neck Surg 2008; 139:206-10.

99. Hsu YC, Kuo WR, Chen YY, Tai CF, Tsai CJ, Wang LF. Increased expression of hypoxia-inducible factor 1alpha in the nasal polyps. Am J Otolaryngol 2007; 28:379-83.

100. Early SB, Hise K, Han JK, Borish L, Steinke JW. Hypoxia stimulates inflammatory and fibrotic responses from nasal-polyp derived fibroblasts. Laryngoscope 2007; 117:511-5.

101. Gonzalez DM, Medici D. Signaling mechanisms of the epithelial-mesenchymal transition. Sci Signal 2014; 7:re8.

102. Lee SN, Lee DH, Sohn MH, Yoon JH. Overexpressed proprotein convertase 1/3 induces an epithelial-mesenchymal transition in airway epithelium. Eur Respir J 2013; 42:1379-90.

103. Tissenbaum HA, Guarente L. Increased dosage of a sir-2 gene extends lifespan in Caenorhabditis elegans. Nature 2001; 410:227-30.

104. Wu L, Zhang A, Sun Y, Zhu X, Fan W, Lu X, et al. Sirt1 exerts anti-inflammatory effects and promotes steroidogenesis in Leydig cells. Fertil Steril 2012; 98:194-9.

105. Zhu X, Liu Q, Wang M, Liang M, Yang X, Xu X, et al. Activation of Sirt1 by resveratrol inhibits TNF-alpha induced inflammation in fibroblasts. PLoS One 2011; 6:e27081.

106. Xu F, Burk D, Gao Z, Yin J, Zhang X, Weng J, et al. Angiogenic deficiency and adipose tissue dysfunction are associated with macrophage malfunction in SIRT1-/- mice. Endocrinology 2012; 153:1706-16.

107. Kong S, Yeung P, Fang D. The class III histone deacetylase sirtuin 1 in immune suppression and its therapeutic potential in rheumatoid arthritis. J Genet Genomics 2013; 40:347-54.

108. Chen WY, Wang DH, Yen RC, Luo J, Gu W, Baylin SB. Tumor suppressor HIC1 directly

regulates SIRT1 to modulate p53-dependent DNA-damage responses. Cell 2005; 123:437-48.

109. Yamakuchi M, Ferlito M, Lowenstein CJ. miR-34a repression of SIRT1 regulates apoptosis. Proc Natl Acad Sci U S A 2008; 105:13421-6.

110. Li J, Wang K, Chen X, Meng H, Song M, Wang Y, et al. Transcriptional activation of microRNA-34a by NF-kappa B in human esophageal cancer cells. BMC Mol Biol 2012; 13:4.

111. Li P, Zhao Y, Wu X, Xia M, Fang M, Iwasaki Y, et al. Interferon gamma (IFN-gamma) disrupts energy expenditure and metabolic homeostasis by suppressing SIRT1 transcription. Nucleic Acids Res 2012; 40:1609-20.

112. Wynn R, Har-El G. Recurrence rates after endoscopic sinus surgery for massive sinus polyposis. Laryngoscope 2004; 114:811-3.

113. Lee M, Kim DW, Yoon H, So D, Khalmuratova R, Rhee CS, et al. Sirtuin 1 attenuates nasal polypogenesis by suppressing epithelial-to-mesenchymal transition. J Allergy Clin Immunol 2016; 137:87-98 e7.

114. Djupesland PG. Nasal drug delivery devices: characteristics and performance in a clinical perspective-a review. Drug Deliv Transl Res 2013; 3:42-62.

115. Illum L. Nasal drug delivery - recent developments and future prospects. J Control Release 2012; 161:254-63.

116. Makadia HK, Siegel SJ. Poly Lactic-co-Glycolic Acid (PLGA) as Biodegradable Controlled

Drug Delivery Carrier. Polymers 2011; 3:1377-97.

117. Ugwoke MI, Agu RU, Verbeke N, Kinget R. Nasal mucoadhesive drug delivery: background, applications, trends and future perspectives. Adv Drug Deliv Rev 2005; 57:1640-65.

118. Park CG, Kim E, Park M, Park J-H, Choy YB. A nanofibrous sheet-based system for linear delivery of nifedipine. Journal of Controlled Release 2011; 149:250-7.

119. Lee JE, Park S, Park M, Kim MH, Park CG, Lee SH, et al. Surgical suture assembled with polymeric drug-delivery sheet for sustained, local pain relief. Acta biomaterialia 2013; 9:8318-27.

120. Bolourchian N, Mahboobian MM, Dadashzadeh S. The effect of PEG molecular weights on dissolution behavior of simvastatin in solid dispersions. Iranian Journal of Pharmaceutical Research 2013; 12:11-20.

121. Lee C-W, Yen F-L, Huang H-W, Wu T-H, Ko H-H, Tzeng W-S, et al. Resveratrol nanoparticle system improves dissolution properties and enhances the hepatoprotective effect of resveratrol through antioxidant and anti-inflammatory pathways. Journal of agricultural and food chemistry 2012; 60:4662-71.

122. Yeo Y, Park K. Control of encapsulation efficiency and initial burst in polymeric microparticle systems. Arch Pharm Res 2004; 27:1-12.

123. Li M, Rouaud O, Poncelet D. Microencapsulation by solvent evaporation: State of the art for process engineering approaches. Int J Pharm 2008; 363:26-39.

124. Shin HW, Kim DK, Park MH, Eun KM, Lee M, So D, et al. IL-25 as a novel therapeutic target in nasal polyps of patients with chronic rhinosinusitis. J Allergy Clin Immunol 2015; 135:1476-85 e7.

125. Lee M, Kim DW, Yoon H, So D, Khalmuratova R, Rhee CS, et al. Sirtuin 1 attenuates nasal polypogenesis by suppressing epithelial-to-mesenchymal transition. J Allergy Clin Immunol 2015.

126. Mygind N, Dahl R, Bachert C. Nasal polyposis, eosinophil dominated inflammation, and allergy. Thorax 2000; 55:S79-S83.

127. Garcia P, Schmiedlin-Ren P, Mathias JS, Tang H, Christman GM, Zimmermann EM. Resveratrol causes cell cycle arrest, decreased collagen synthesis, and apoptosis in rat intestinal smooth muscle cells. Am J Physiol Gastrointest Liver Physiol 2012; 302:G326-35.

128. Da Violante G, Zerrouk N, Richard I, Provot G, Chaumeil JC, Arnaud P. Evaluation of the cytotoxicity effect of dimethyl sulfoxide (DMSO) on Caco2/TC7 colon tumor cell cultures. Biol Pharm Bull 2002; 25:1600-3.

129. Malinin TI, Perry VP. Toxicity of dimethyl sulfoxide on HeLa cells. Cryobiology 1967; 4:90-6.

130. Bernhard D, Schwaiger W, Crazzolara R, Tinhofer I, Kofler R, Csordas A. Enhanced MTT-reducing activity under growth inhibition by resveratrol in CEM-C7H2 lymphocytic leukemia cells. Cancer Lett 2003; 195:193-9.

131. Kotha A, Sekharam M, Cilenti L, Siddiquee K, Khaled A, Zervos AS, et al. Resveratrol inhibits Src and Stat3 signaling and induces the apoptosis of malignant cells containing activated Stat3 protein. Mol Cancer Ther 2006; 5:621-9.

132. Kang JH, Park YH, Choi SW, Yang EK, Lee WJ. Resveratrol derivatives potently induce apoptosis in human promyelocytic leukemia cells. Exp Mol Med 2003; 35:467-74.

133. Gerdes J, Lemke H, Baisch H, Wacker HH, Schwab U, Stein H. Cell cycle analysis of a cell proliferation-associated human nuclear antigen defined by the monoclonal antibody Ki-67. J Immunol 1984; 133:1710-5.

134. Schluter C, Duchrow M, Wohlenberg C, Becker MH, Key G, Flad HD, et al. The cell proliferation-associated antigen of antibody Ki-67: a very large, ubiquitous nuclear protein with numerous repeated elements, representing a new kind of cell cycle-maintaining proteins. J Cell Biol 1993; 123:513-22.

135. Lagouge M, Argmann C, Gerhart-Hines Z, Meziane H, Lerin C, Daussin F, et al. Resveratrol improves mitochondrial function and protects against metabolic disease by activating SIRT1 and PGC-1alpha. Cell 2006; 127:1109-22.

136. Howitz KT, Bitterman KJ, Cohen HY, Lamming DW, Lavu S, Wood JG, et al. Small molecule activators of sirtuins extend Saccharomyces cerevisiae lifespan. Nature 2003; 425:191-6.

137. Bradamante S, Barenghi L, Villa A. Cardiovascular protective effects of resveratrol. Cardiovasc Drug Rev 2004; 22:169-88.

138. Wang Q, Xu J, Rottinghaus GE, Simonyi A, Lubahn D, Sun GY, et al. Resveratrol protects against global cerebral ischemic injury in gerbils. Brain Res 2002; 958:439-47.

139. Jiang H, Zhang L, Kuo J, Kuo K, Gautam SC, Groc L, et al. Resveratrol-induced apoptotic death in human U251 glioma cells. Mol Cancer Ther 2005; 4:554-61.

140. Tsang SW, Zhang H, Lin Z, Mu H, Bian ZX. Anti-fibrotic effect of trans-resveratrol on pancreatic stellate cells. Biomed Pharmacother 2015; 71:91-7.

141. Amri A, Chaumeil JC, Sfar S, Charrueau C. Administration of resveratrol: What formulation solutions to bioavailability limitations? J Control Release 2012; 158:182-93.

142. Augustin MA, Sanguansri L, Lockett T. Nano- and micro-encapsulated systems for enhancing the delivery of resveratrol. Ann N Y Acad Sci 2013; 1290:107-12.

143. Mottu F, Laurent A, Rüfenacht DA, Doelker E. Organic solvents for pharmaceutical parenterals and embolic liquids: a review of toxicity data. PDA J Pharm Sci Technol 2000; 54:456-69.

144. Kelava T, Ćavar I, Čulo F. Biological actions of drug solvents. Period. Biol. 2011; 113:311-20.

145. Hanslick JL, Lau K, Noguchi KK, Olney JW, Zorumski CF, Mennerick S, et al. Dimethyl sulfoxide (DMSO) produces widespread apoptosis in the developing central nervous system. Neurobiol Dis 2009; 34:1-10.

146. Sanna V, Roggio AM, Siliani S, Piccinini M, Marceddu S, Mariani A, et al. Development of novel cationic chitosan-and anionic alginate-coated poly(D,L-lactide-co-glycolide)

nanoparticles for controlled release and light protection of resveratrol. Int J Nanomedicine 2012; 7:5501-16.

147. Narayanan NK, Nargi D, Randolph C, Narayanan BA. Liposome encapsulation of curcumin and resveratrol in combination reduces prostate cancer incidence in PTEN knockout mice. Int J Cancer 2009; 125:1-8.

148. Basavaraj S, Betageri GV. Improved oral delivery of resveratrol using proliposomal formulation: investigation of various factors contributing to prolonged absorption of unmetabolized resveratrol. Expert Opin Drug Deliv 2014; 11:493-503.

149. Singh G, Pai RS. Recent advances of resveratrol in nanostructured based delivery systems and in the management of HIV/AIDS. J Control Release 2014; 194:178-88.

150. Hu C, Wang Q, Ma C, Xia Q. Non-aqueous self-double-emulsifying drug delivery system: A new approach to enhance resveratrol solubility for effective transdermal delivery. Colloids Surf A Physicochem Eng Asp 2016; 489:360-9.

151. Carletto B, Berton J, Ferreira TN, Dalmolin LF, Paludo KS, Mainardes RM, et al. Resveratrol-loaded nanocapsules inhibit murine melanoma tumor growth. Colloids Surf B Biointerfaces 2016; 144:65-72.

152. Chun M-K, Sah H, Choi H-K. Preparation of mucoadhesive microspheres containing antimicrobial agents for eradication of H. pylori. Int J Pharm 2005; 297:172-9.

153. Tao Y, Lu Y, Sun Y, Gu B, Lu W, Pan J. Development of mucoadhesive microspheres of

acyclovir with enhanced bioavailability. Int J Pharm 2009; 378:30-6.

154. Hines DJ, Kaplan DL. Poly (lactic-co-glycolic) acid− controlled-release systems: experimental and modeling insights. Crit Rev Ther Drug Carrier Syst 2013; 30.

155. Middleton JC, Tipton AJ. Synthetic biodegradable polymers as orthopedic devices. Biomaterials 2000; 21:2335-46.

156. Gentile P, Chiono V, Carmagnola I, Hatton PV. An overview of poly (lactic-co-glycolic) acid (PLGA)-based biomaterials for bone tissue engineering. Int J Mol Sci 2014; 15:3640-59.

157. Murube J, Paterson A, Murube E. Classification of artificial tears. In: Lacrimal gland, tear film, and dry eye syndromes 2: Springer; 1998. p. 693-704.

158. Salamat-Miller N, Chittchang M, Johnston TP. The use of mucoadhesive polymers in buccal drug delivery. Adv Drug Deliv Rev 2005; 57:1666-91.

159. Harris JM. Poly (ethylene glycol) chemistry: biotechnical and biomedical applications: Springer Science & Business Media; 2013.

160. Paolicelli P, de la Fuente M, Sánchez A, Seijo B, Alonso MJ. Chitosan nanoparticles for drug delivery to the eye. Expert Opin Drug Deliv 2009; 6:239-53.

161. Elsabahy M, Wooley KL. Design of polymeric nanoparticles for biomedical delivery applications. Chem Soc Rev 2012; 41:2545-61.

162. Dobrovolskaia MA, McNeil SE. Immunological properties of engineered nanomaterials. Nat Nanotechnol 2007; 2:469-78.

국문 초록

코 폴립은 만성 부비동염 환자에서 관찰되는 현상으로 고질적인 질환 이다. 일전의 연구에서, 비강 내 용종 이 hypoxia-inducible factor (HIF)에 의한 상피-간엽 전환 현상에 의해 매개 됨을 확인 하였다. 현재까지 저산소와 관련된 질환을 치료하기 위해 많은 HIF 타겟 약물들이 소개되었지만 대부분 함암제로서 개발되어 세포에 독성이 매우 강하고, 그래서 코 폴립과 같은 질환에 사용하기 에는 적합 하지 않았다. 한편, 최근 보고에서 히스톤 탈 아세틸화 효소인 Sirtuin 1 (SIRT1) 이 HIF1와 결합하여 HIF1의 전사 능력을 억제 시킬 수 있다는 사실이 규명 되었다. 따라서 본 연구에서는 SIRT1에 의한 HIF1 매개 상피-간엽 전환 능력의 감소가 코 폴립 형성을 억제 할 수 있는지 평가 하고자 하였다. 먼저, SIRT1이 과 발현 된 마우스의 비강 상피에서 코 폴립의 숫자와 상피세포의 결손이 감소하는 것을 관찰 하였다. 또한 SIRT1의 활성을 증가 시킬 수 있는 약물인 resveratrol (RSV)을 마우스 비강 내에 전달 하였 을 때 코 폴립의 숫자가 감소하는 반면, SIRT1의 활성을 억제하는 약물인 sirtinol을 처리하였을 때는 코 폴립 형성 능력이 다시 증가하는 것을 관찰 하였다. 실제로 SIRT1의 발현은 코 폴립을 동반한 만성 부비동염 환자의 상피 세포에서 크게 감소해 있었다. 코 상피세포에서 SIRT1을 과 발현 하거나 SIRT1의 활성을 증가 시켰을 때, HIF 매개 상피-간엽 전환 현상이 다시 회복 되는 것을 관찰 할 수 있었다. SIRT1이 과 발현 된 마우스의 비강 내에 SIRT1 small hairpin RNA (shRNA)를 탑재한 lentivirus를 주입 하게 되면 코 폴립의 숫자가 증가하는 것을 확인 할 수 있었다. 무엇보다도, 코 폴립을 동반한 환자의 조직 추출물을 코 상피세포에 처리 하였 을 때 SIRT1의 발현이 감소하고 그에 따라 HIF 의 활성이 증가 하는 현상을 볼 수 있었다. 이처럼, RSV는 만성 부비동염을 동반한 코 폴립 설치류 모델 에서 효과적으로 코 폴립의 형성을 억제 할 수 있다. 하지만, RSV 의 낮은 용해성과 비강내에서의 빠른 소실 때문에 RSV 의 생체 이용률은 매우 제한적이었고, 이러한 한계점을 극복하기 위해 접착 능력을 가진 나노 구조 입자의 파티클 (poly lactic-co-glycolic acid/polyethylene glycol nanostructured microparticle; PLGA/PEG NM)을 RSV 를 전달하는 재료로서 활용 해 보기로 하였다. PLGA/PEG NM는 장시간 동안 지속적으로 RSV를 방출 할 수 있었다. 나노 구조

입자 파티클의 확장된 표면 접착 부분 때문에 점막에 잔존 하는 시간이 크게 증가 하였고, 결과적으로 비강내 점막에서 PLGA/PEG NM이 오랜 시간 동안 제거되지 않고 남아 있는 것을 관찰 할 수 있었다. RSV의 증가된 약물 전달 능력을 설치류에서 평가하기 위해 코 폴립 마우스 모델을 활용 하였고, 이 때 RSV를 탑재한 PLGA/PEG NM의 마우스 비강 내 전달은 그렇지 않은 마우스에 비하여 코 폴립 형성 능력을 현저히 감소 시켰으며, 상피-간엽 전환을 다시 회복 시킬 수 있었다. 이러한 효과는 사용한 RSV 용량의 절반만 탑재한 PLGA/PEG NM를 전달 하였을 때도 관찰 할 수 있었다. 종합 하여 볼 때, SIRT1과 PLGA/PEG에 탑재된 RSV의 처리는 효과적으로 HIF 매개 상피-간엽 전환 현상을 억제하여 코 폴립 형성을 효과적으로 감소 시킬 수 있었고, 이는 SIRT1이 코 폴립의 치료 타겟으로서 가능성을 나타낸다고 할 수 있다. 그러므로, PLGA/PEG NM은 RSV의 생체 이용률을 향상시킬 수 있는 잠재력 높은 재료로서 활용 될 수 있을 것이며, 더 나아가 코 폴립의 치료에 활용 될 수 있을 것으로 기대한다.

주요어: SIRT1, HIF-1, Resveratrol, 코 폴립, 아세틸화, 상피-간엽 전환, PLGA/PEG NM, 점막 부착성, 나노 구조, 마이크로입자

학번: 2014-22013